Magnetic and lattice heat capacity of some pseudo one-dimensional systems

MAGNETIC AND LATTICE HEAT CAPACITY OF SOME PSEUDO ONE-DIMENSIONAL SYSTEMS

K. KOPINGA

MAGNETIC AND LATTICE HEAT CAPACITY OF SOME PSEUDO ONE-DIMENSIONAL SYSTEMS

PROEFSCHRIFT

TER VERKRIJGING VAN DE GRAAD VAN DOCTOR IN DE TECHNISCHE WETENSCHAPPEN AAN DE TECHNISCHE HOGESCHOOL EINDHOVEN, OP GEZAG VAN DE RECTOR MAGNIFICUS, PROF.DR. P. VAN DER LEEDEN, VOOR EEN COMMISSIE AANGEWEZEN DOOR HET COLLEGE VAN DEKANEN IN HET OPENBAAR TE VERDEDIGEN OP VRIJDAG 3 SEPTEMBER 1976 TE 16.00 UUR

DOOR

KLAAS KOPINGA

GEBOREN TE EINDHOVEN

DRUK: WIBRO HELMOND

Dit proefschrift is goedgekeurd door de promotoren
Prof. Dr. P. van der Leeden en Prof. Dr. S.A. Friedberg

Aan mijn ouders

Aan Ine

TABLE OF CONTENTS

CHAPTER I

INTRODUCTION

The thermodynamic properties of an infinite three-dimensional ensemble of interacting magnetic moments have not yet been solved exactly. Therefore, a growing number of both theoretical and experimental investigations have been devoted to ensembles of spins which interact mainly in one or two dimensions. In this thesis we will confine ourselves to pseudo one-dimensional magnetic systems, i.e. systems which can be described by a purely one-dimensional model system over a wide range of temperatures, and our main interest will be devoted to their magnetic heat capacity. Even for linear chain model systems, exact solutions for the heat capacity are available only in a very few cases, but suitable approximation procedures may often provide a satisfactory description. A survey of some relevant results will be presented in Chapter II.

In order to analyse the experimental data, it is necessary to separate the magnetic contribution (C_M) and the lattice contribution (C_L) to the total specific heat. For the compounds of interest a fairly accurate description of the lattice heat capacity is required, since one-dimensional magnetic correlations are still important at higher temperatures, where $C_L >> C_M$. Unfortunately, the usual three-dimensional Debye model fails to give a correct description of the lattice heat capacity, because the majority of substances which display one-dimensional magnetic characteristics are also rather anisotropic from a lattice dynamical point of view. An exact calculation of C_L is impossible, since it would require a detailed knowledge of all interatomic force constants. Therefore, various attempts have been made to modify the conventional Debye theory in such a way, that it would give an appropriate description of the lattice heat capacity of rather anisotropic media. The reported results, however, drastically oversimplify the actual dynamical behaviour or rely to a large extent on the characteristic properties of a certain compound. In Chapter III we shall present a model which, starting from continuum elasticity theory, offers a suitable description of the lattice heat capacity of both layered and chainlike compounds.

As already mentioned above, several approximation procedures have been used in the calculation of the magnetic heat capacity of most one-

dimensional model systems. It would therefore be worthwhile to confront the predicted behaviour with some experimental results on magnetically one-dimensional systems. In practice, such systems may consist of chains of strongly coupled magnetic ions, which are separated from each other by intermediate non-magnetic alkali ions, H_2O groups or organic complexes. One should bear in mind, however, that in any real system small interactions between the chains will be present, giving rise to deviations from the "unperturbed" one-dimensional behaviour, especially at low temperatures, where they may produce three-dimensional ordering. Although this ordered region - in principle - obscures the low temperature behaviour of the one-dimensional model system, it generally offers additional information about the character and the magnitude of the magnetic interactions, which is often necessary to judge the applicability of a certain theoretical model system.

After a description of the calorimeter, which is given in Chapter IV, we shall present the results of an investigation on the series of isomorphic compounds $(CH_3)_4NXCl_3$, with X = Cd, Mn, Ni. The analysis of the heat capacity of these substances, which is outlined in Chapter V, served several purposes. First, by examining the diamagnetic cadmium isomorph the model describing the lattice heat capacity, presented in Chapter III, could be tested directly. Secondly, the manganese compound (TMMC) is an almost ideal approximation of an S = 5/2 antiferromagnetic Heisenberg linear chain system, and therefore the results on this isomorph are a good check on the corresponding theoretical prediction for the magnetic heat capacity. Finally, from the analysis of the heat capacity the intrachain interaction in both magnetic isomorphs has been determined.

Chapter VI will be devoted to the series of isomorphic manganese compounds $CsMnCl_3.2H_2O$, $\alpha RbMnCl_3.2H_2O$ and $CsMnBr_3.2H_2O$. These substances can all be considered as pseudo one-dimensional S = 5/2 antiferromagnetic Heisenberg systems, and - in principle - offer a possibility to study the influence of both the intermediate alkali ion as well as the halide ions on the various magnetic interactions. Apart from an analysis of of the heat capacity in the paramagnetic region, from which the intrachain interaction was determined, the influence of the - relatively small - interchain interactions on the magnetic behaviour in the ordered state will be studied. For this purpose we performed a spin-wave analysis of the magnetic properties of $CsMnCl_3.2H_2O$. Next we shall consider the

compounds $CsCoCl_3.2H_2O$ and $RbFeCl_3.2H_2O$, which are isomorphic with the series presented above. The magnetic interactions in these two substances are very anisotropic, and a direct relation with a particular magnetic model system is not obvious. In Chapter VII the experimental data on both isomorphs will be presented. For each compound we shall propose a model which explains the main features of the observed magnetic behaviour. In Chapter VIII the magnetic heat capacity of these compounds near the three-dimensional ordering temperature will be compared with that of the three manganese isomorphs.

CHAPTER II

SPECIFIC HEAT OF SOME LOW-DIMENSIONAL MAGNETIC MODEL SYSTEMS

2.1. Introduction

The thermodynamic properties of pseudo low-dimensional magnetic systems have received considerable interest both theoretically and experimentally. Because a detailed analysis is generally precluded by the complexity of the system, the dominant characteristics of the magnetic behaviour are often confronted with the properties of a simplified model system. Such a model system may consist of isolated layers or chains of equivalent magnetic ions, involving nearest neighbour exchange interactions only. These interactions are represented by the hamiltonian

$$H = -2 \sum_{<ij>} \vec{S}_i \vec{\vec{J}}_{ij} \vec{S}_j, \qquad (1)$$

where the indices <ij> refer to pairs of neighbouring sites. A further simplification of the model is introduced by assuming that the principal axes of all exchange tensors coincide and by restricting the number of independent elements $J_{ij}^{\alpha\alpha}$. This results in the following classification of the type of interaction:

Ising $\quad (J_{ij}^{xx} = J_{ij}^{yy} = 0,\ J_{ij}^{zz} = J_{ij})$,

XY $\quad (J_{ij}^{xx} = J_{ij}^{yy} = J_{ij},\ J_{ij}^{zz} = 0)$, or

Heisenberg $\quad (J_{ij}^{xx} = J_{ij}^{yy} = J_{ij}^{zz} = J_{ij})$.

Despite these simplifications, an exact calculation of the specific heat has been possible in a very few cases only. Well-known examples are the Ising linear chain for arbitrary spin-value [1], the S = 1/2 linear chain with XY interaction [2], and the S = 1/2 rectangular array with Ising interactions [3].

For many one-dimensional model systems, however, suitable extrapolation procedures may provide a satisfactory description. At high and intermediate temperatures the heat capacity can be calculated from high temperature series expansions [4], which may be extended with a Padé approximant method. This method will be considered in more detail in the follow-

ing section. Secondly, the heat capacity of the infinite ensemble may be obtained from extrapolation of the exact results for finite chains with increasing numbers of spins. For $S \leq 5/2$ a combination of the results from both procedures has been found [5] to give a rather accurate estimate over a large temperature interval. For Heisenberg exchange, the low-temperature region may be approximated phenomenologically by expressing the heat capacity in a suitable polynomial series of the reduced temperature kT/J. The coefficients are found by matching the series to some suitably chosen boundary conditions, as will be pointed out in the following section.

2.2. *Linear chains with Heisenberg exchange for $S \leq 5/2$*

A very general method for the calculation of high temperature series for the specific heat of infinite ensembles of interacting spins has been presented by Rushbrooke and Wood [4]. If the ensemble is described by a hamiltonian H, the partition function Z of the system is given by

$$Z = \text{Trace } [\exp(-H/kT)] \tag{2}$$

for any matrix representation of H.
Since the magnetic heat capacity of the system can be written as

$$C = \frac{\partial}{\partial T} \left[kT^2 \frac{\partial}{\partial T} (\ln Z)\right], \tag{3}$$

it may be calculated rather straightforwardly by expanding ln Z in inverse powers of the reduced temperature. The result is

$$C/R = \frac{4}{3} S^2(S+1)^2\beta^2 \sum_{i=0}^{n} c_i\beta^i, \qquad \beta = J/kT. \tag{4}$$

For general spin, the coefficients c_i have been calculated up till n = 6. For small values of S, additional information may be obtained from an exact calculation of the eigenvalues of the hamiltonian for finite chains [6], which yields the constants c_i up till n = 20, 12, 10, 8, 8 for S = 1/2 to 5/2, respectively [5].

The series given by equation (4), however, appears to be rather poorly convergent. An improved description has been found to be possible by extending the radius of convergence of the series with a Padé approximant method [6]. Application of this method is based upon the assumption that the radius of convergence of the series (4) is determined by two complex conjugated poles β_o and β_o^* of the order γ situated in the complex β plane. To correct for this singularity the original series is transformed into

$$C/R = \frac{4}{3} S^2(S+1)^2\beta^2 \frac{\sum_{i=0}^{m} r_i \beta^i}{(\beta-\beta_o)^\gamma(\beta-\beta_o^*)^\gamma} \quad . \tag{5}$$

The latter series is found to provide an accurate estimate for the heat capacity at temperatures down to $kT \sim 0.4JS(S+1)$ for $S = 5/2$.

An alternative method for the calculation of the heat capacity of an infinite chain is based upon extrapolation of the results for finite chains with increasing numbers of spins [7]. A suitable procedure has been found to extrapolate the specific heat per site $C_N(T)/N$ as a function of $1/N$ [5, 8, 9]. This method has been shown to give an exact result in the limit $\beta \to 0$ [5]. At lower temperatures, however, the uncertainty in the extrapolation gradually increases, due to the fact that at these temperatures the heat capacity is dominated by the low energy part of the eigenvalue spectrum, which is rather sensitive to the number of spins N, especially for antiferromagnetic coupling. Secondly, the dimension of the eigenvalue problem rapidly increases with increasing S, and therefore the number of chains that can be solved numerically is rather limited. Fortunately, this is partly compensated by the fact that C_N/N varies more smoothly for larger values of S [5]. For antiferromagnetic chains the extrapolation procedure yielded reliable results at temperatures down to $kT/|J|S(S+1) \sim 0.4$–0.8. For ferromagnetic coupling, this temperature range extends down to $kT/JS(S+1) \sim 0.2$–0.5. The inferred heat capacity appeared to agree very well with the prediction from high temperature series expansions outlined above, the difference being less than 1 % for $kT \sim |J|S(S+1)$.

The low temperature heat capacity may be inferred from classical spin-wave theory [10, 11] to be proportional to $T^{1/2}$ for ferromagnetic and

proportional to T for antiferromagnetic interaction. The predicted constants of proportionality, however, are found to be somewhat too high [7, 12], and the discrepancy seems to increase for decreasing values of S. Therefore, the spin-wave prediction is only used to select a suitable power series of the reduced temperature kT/J, by which the heat capacity in the low temperature region is approximated. For the ferromagnetic problem, the expression

$$C(T) = \sum_{i=0}^{n} a_i (kT/J)^{i+\frac{1}{2}} \tag{6}$$

is chosen, while the antiferromagnetic case is described by

$$C(T) = \sum_{i=0}^{n} b_i (kT/J)^{i+1}. \tag{7}$$

The constants a_i or b_i may be obtained by matching the series to some suitably chosen boundary conditions. If we require, for instance, that

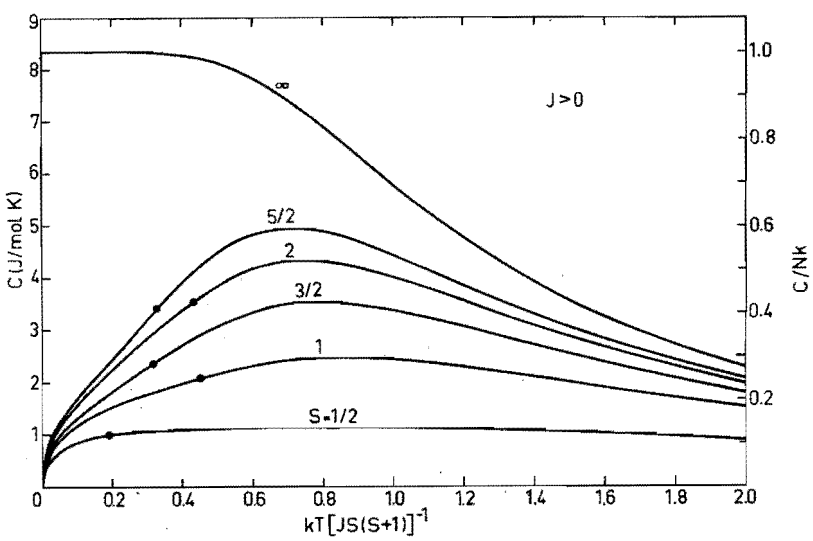

FIG. 2.1. Specific heat of infinite ferromagnetic Heisenberg linear chains as a function of the reduced temperature for several values of the spin quantum number. The dot on each curve indicates the temperature where the low-temperature polynomial is fitted to the estimate obtained from direct extrapolation of the heat capacity of finite chains. (after [5]).

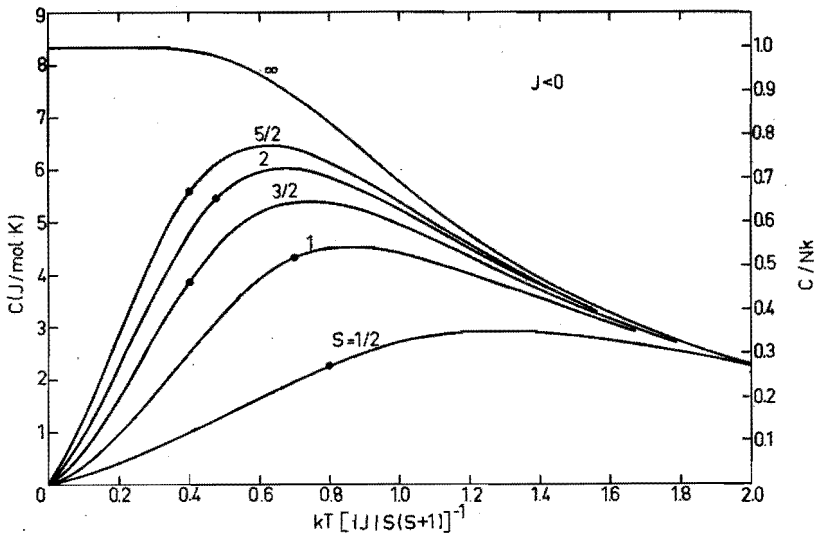

FIG. 2.2. Specific heat of infinite antiferromagnetic Heisenberg linear chains as a function of the reduced temperature for several values of the spin quantum number. The dots are explained in the caption of Figure 2.1. (after [5]).

the series correctly predicts the heat capacity C(T*) and the derivative with respect to temperature $(\partial C/\partial T)_{T^*}$ at an intermediate "take-over" temperature T*, and that the total magnetic entropy increase amounts to R ln(2S+1), equation (6) or (7) is determined uniquely for n = 2.

It is evident, that the low-temperature behaviour obtained from this procedure will be a phenomenological description only. A truncation of the series after n = 2 might be physically meaningful if a rapid convergence is observed, but this has been found to occur only for large values of S. The error of the description in the low-temperature region may be estimated somewhat indirectly by considering the variations of the predicted heat capacity arising from variations of the "take-over" temperature T*. This yields an error of $\sim$ 4 % for S = 5/2 and somewhat larger errors for decreasing S.

To check the actual accuracy, however, it would be very useful to confront the theoretical prediction with some experimental results for kT < |J|. We will return to this subject in Chapter V in more detail.

The overall behaviour of the heat capacity has been calculated as a function of the reduced temperature $kT/|J|S(S+1)$ for $S \leqslant 5/2$. In Figure 2.1 and 2.2 the results are plotted for ferromagnetic and antiferromagnetic exchange interaction, respectively. The curve marked " ∞ " is the result from an exact calculation for $S = \infty$ given by Fisher [13].

2.3. *S = 1 linear chain with Heisenberg exchange and single-ion anisotropy*

For a large number of Ni^{++} (S = 1) compounds, the single-ion anisotropy appears to be more or less axial in character. Since, on the other hand, the exchange interaction is found to be largely isotropic, it seems not unrealistic to represent the magnetic properties of a linear chain of equivalent Ni^{++} ions by the hamiltonian

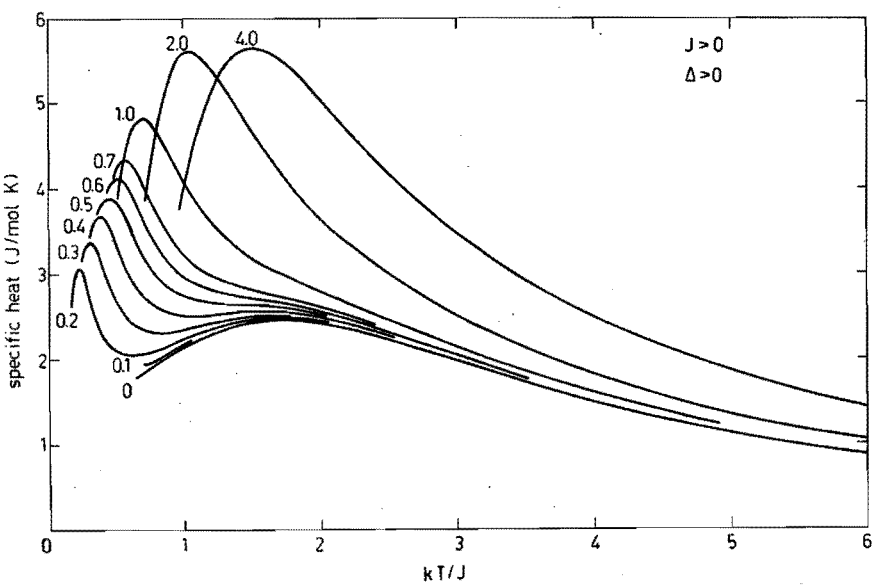

FIG. 2.3. Estimated specific heat of an S = 1 infinite linear chain with Heisenberg exchange and uniaxial single-ion anisotropy. The curves are plotted only for temperatures at which the estimated error is less than 4 % and are characterized by the ratio $D/|J|$ (after [5]).

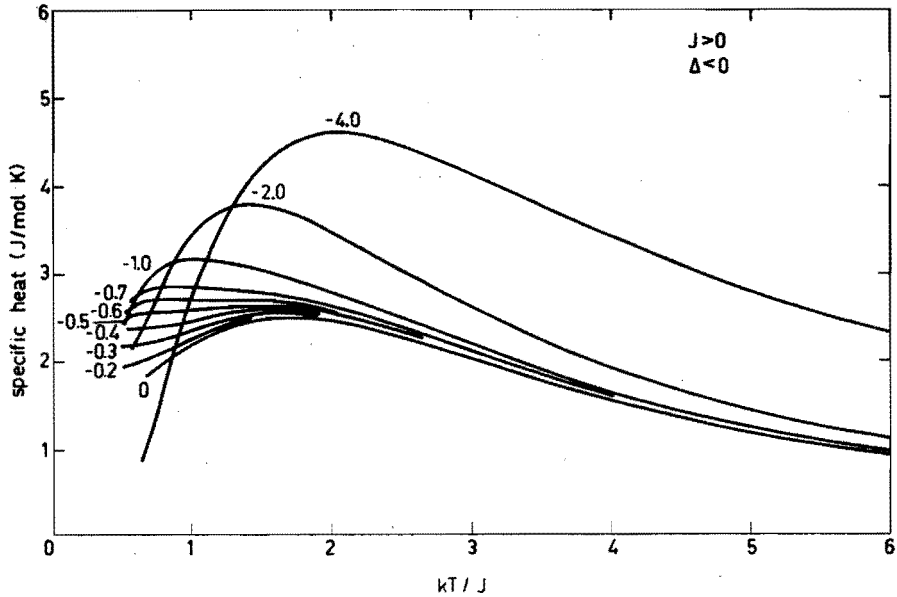

FIG. 2.4. Estimated specific heat of an S = 1 infinite linear chain with Heisenberg exchange and uniaxial single-ion anisotropy. The comment of Figure 2.3 applies.

$$H = -2J \sum_{i=1}^{N-1} \vec{S}_i . \vec{S}_{i+1} - D \sum_{i=1}^{N} [S_{iz}^2 - \tfrac{1}{3} S(S+1)]. \qquad (8)$$

In principle, the heat capacity for $N \to \infty$ may be obtained by direct extrapolation of the numerical results for finite N.

The presence of axial symmetry offers the possibility to reduce the matrix representing the hamiltonian (8) into blocks that can be diagonalized separately, because the z component of the total spin is still a good quantum number. The problem could be handled numerically up till N = 7 [14]. Extrapolated results are shown in Figure 2.3, 2.4, 2.5 and 2.6 for all sign combinations of Δ (=D) and J. The curves are drawn in the temperature region where the estimated uncertainty is less than 4 %. As mentioned before, the error rapidly decreases with increasing temperature, and amounts to $\sim$ 0.5 % at $kT/|J| \sim 2$.

In fitting experimental data, the procedure outlined above has the disadvantage that for each value of D/J the complete eigenvalue-problem has to be solved, which is extremely laborious. A representation of the heat capacity with a high temperature series expansion is therefore preferred. A suitable starting point has been found [5] to express the heat capacity C(J,D) as:

$$C(J,D) = C(J,0) + C(0,D) + \sum_{i,j} a_{ij} J^i D^j \beta^{i+j} / 3^{i+j} (i+j)!$$

$$C(0,D) = 2\beta^2 D^2 e^{D\beta} / (1+2e^{D\beta})^2 \qquad (9)$$

$$C(J,0) = 96 \sum_{i\geq 2} c_i J^i \beta^i / 3^i i! \quad (\beta = 1/kT).$$

The constants a_{ij} have been calculated up till i+j = 8 [15]. For any combination of D and J, it is possible to construct a power series, whose

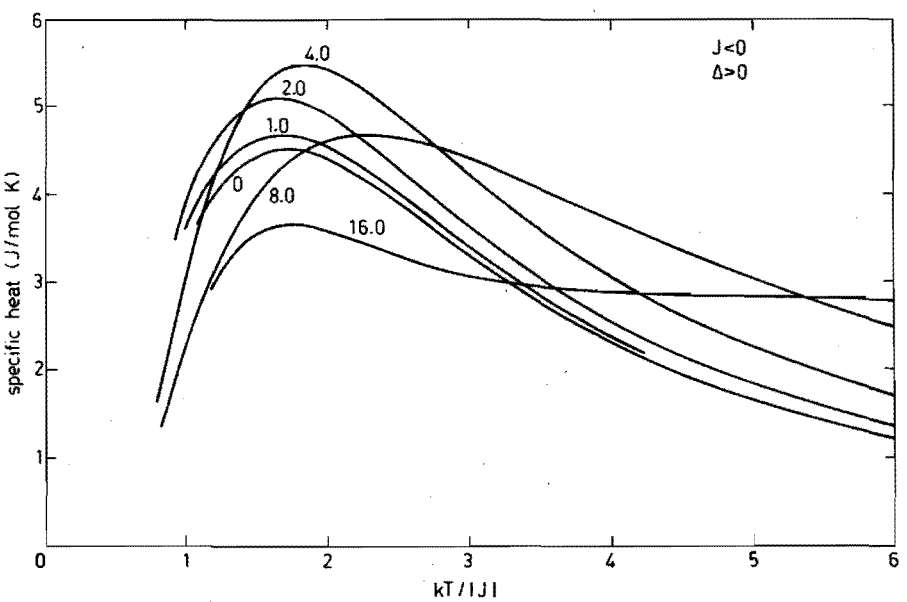

FIG. 2.5. Estimated specific heat of an S = 1 infinite linear chain with Heisenberg exchange and uniaxial single-ion anisotropy. The comment of Figure 2.3 applies.

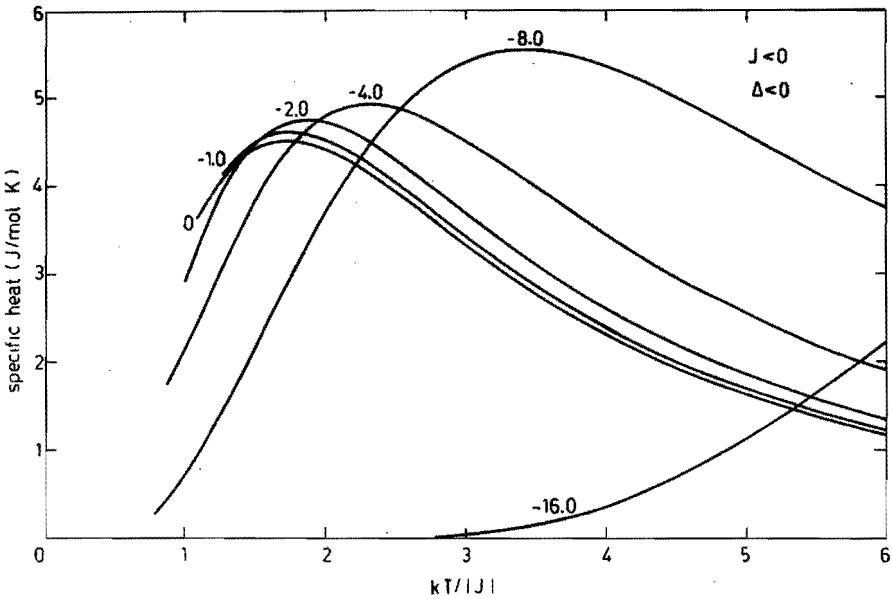

FIG. 2.6. Estimated specific heat of an S = 1 infinite linear chain with Heisenberg exchange and uniaxial single-ion anisotropy. The comment of Figure 2.3 applies.

coefficients are obtained by summation of the corresponding powers in equation (9). The radius of convergence of the series may be extended with a Padé approximant method, generally resulting in a fair description at temperatures down to $kT/|J| \sim 2$.

The low temperature heat capacity has not been examined in detail. Firstly, the presence of single ion anisotropy complicates the determination of the qualitative behaviour at T = 0. In contrast to a behaviour proportional to $T^{1/2}$ or T, exponential terms may be present, as is obvious from the heat capacity in the limit J/D = 0, which can be solved exactly. Furthermore, at this moment the available experimental results [16, 17] do not show any need for a phenomenological description of the low-temperature behaviour as given in the preceeding section, since in this temperature region they display considerable deviations from pure linear chain characteristics [18].

2.4. *S = 1/2 linear chains with Ising or XY exchange*

2.4.1. *Ising exchange*

An elegant way to solve the one-dimensional Ising problem is the use of the transfer matrix method [19], which will be briefly outlined below. We consider the Ising hamiltonian

$$H = -2J \sum_{i=1}^{N} S_i^z S_{i+1}^z \tag{10}$$

For S = 1/2, m_i can be either + 1/2 or - 1/2. Because the interaction involves only the z component of the spins, all functions characterized by $|m_1, m_2, \ldots\ldots, m_N\rangle$ are eigenfunctions of the hamiltonian (10). We have chosen the cyclic boundary condition $S_{N+1} \equiv S_1$, for reasons that will become clear below.

The interaction between a pair of spins S_i and S_{i+1} will give rise to an energy $U(m_i, m_{i+1}) = -\frac{1}{2} J$ if both spins are parallel and to an energy $+\frac{1}{2} J$ if they are antiparallel. If we define a transfer function f by

$$f(m_i, m_{i+1}) = \exp[-U(m_i, m_{i+1})/kT], \tag{11}$$

the partition function can be written as

$$Z_N(T) = \sum_{m_1=-\frac{1}{2}}^{+\frac{1}{2}} \sum_{m_2=-\frac{1}{2}}^{+\frac{1}{2}} \cdots \sum_{m_N=-\frac{1}{2}}^{+\frac{1}{2}} f(m_1, m_2) f(m_2, m_3) \cdots f(m_N, m_1). \tag{12}$$

Next we define a transfer matrix T, given by

$$T \equiv \begin{pmatrix} f(+1/2,+1/2) & f(+1/2,-1/2) \\ f(-1/2,+1/2) & f(-1/2,-1/2) \end{pmatrix}, \tag{13}$$

in terms of which the partition function $Z_N(T)$ can be expressed as

$$Z_N(T) = \mathrm{Trace}(T^N), \tag{14}$$

since the off-diagonal elements of T^N contain all combinations of spins for which $S_{N+1} \neq S_1$. Those combinations vanish under cyclic boundary conditions. Now the trace of the Nth power of the transfer matrix is equal to $\lambda_+^N + \lambda_-^N$, where λ_+ and λ_- are the eigenvalues of T, determined

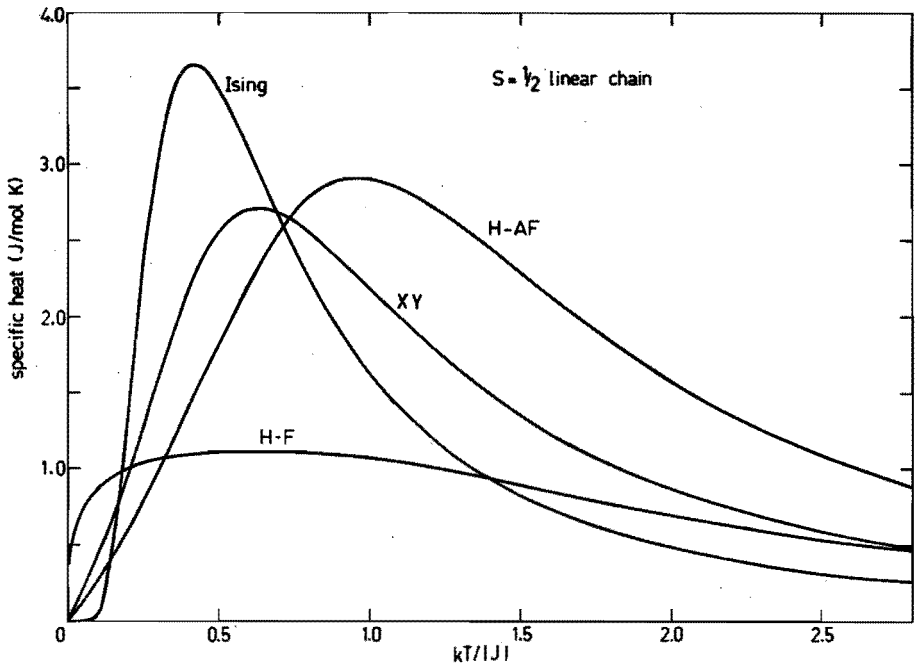

FIG. 2.7. Specific heat of infinite S = 1/2 linear chains as a function of the reduced temperature for Ising, XY and Heisenberg interaction. The ferromagnetic and antiferromagnetic case are - if different - indicated by F and AF, respectively.

by

$$\begin{vmatrix} e^{J/kT} - \lambda & e^{-J/2kT} \\ e^{-J/2kT} & e^{J/kT} - \lambda \end{vmatrix} = 0. \qquad (15)$$

This yields the solution

$$\lambda_+ = 2\cosh(J/2kT), \quad \lambda_- = 2\sinh(J/2kT), \qquad (16)$$

and the partition function is given by

$$Z_N(T) = 2^N[\cosh^N(J/2kT) + \sinh^N(J/2kT)]. \qquad (17)$$

In the thermodynamic limit, the Gibbs potential per spin can be obtained from

$$G(T) = -kT \lim_{N\to\infty} \frac{1}{N} \ln Z_N(T) =$$

$$-kT \lim_{N\to\infty} \frac{1}{N} \ln \{2^N \cosh^N(J/2kT)[1 + \tanh^N(J/2kT)]\} =$$

$$-kT \ln[2\cosh(J/2kT)], \tag{18}$$

since the last term vanishes for $N \to \infty$.
The heat capacity is related to the Gibbs potential by

$$C = -T \frac{\partial^2 G}{\partial T^2}, \tag{19}$$

and a straightforward calculation yields a molar heat capacity

$$C/R = (J/2kT)^2 [1-\tanh^2(J/2kT)] . \tag{20}$$

Inspection of this equation shows that the specific heat does not depend on the sign of J, as might already have been conjectured from the symmetry of the eigenvalue-spectrum. The result is plotted in Figure 2.7 as a function of the reduced temperature $kT/|J|$.

2.4.2. XY exchange

The S = 1/2 chain with XY exchange has been treated by Katsura [2]. The thermodynamic properties of the infinite ensemble are evaluated analytically with the aid of creation and annihilation operators. Since we are not primarily interested in details of the calculation, which is straightforward but rather complicated, only the result will be presented here. If the system is described by the hamiltonian

$$H = -2J \sum_{i=1}^{N} (S_i^x S_{i+1}^x + S_i^y S_{i+1}^y), \tag{21}$$

the molar heat capacity is given by

$$C/R = \frac{4}{\pi} (J/2kT)^2 \int_0^{\pi} \frac{\cos^2\omega \, d\omega}{\cosh^2[(J/kT)\cos\omega]} \, . \qquad (22)$$

An analytic evaluation of the integral in this equation is not possible, but since the integrand varies rather smoothly, the heat capacity may be approximated numerically with a very high degree of accuracy. Like the Ising-problem, the specific heat is independent of the sign of the exchange interaction. The result is plotted in Figure 2.7 as a function of the reduced temperature $kT/|J|$. For comparison, the heat capacity of the Heisenberg S = 1/2 linear chain is plotted in the same figure.

2.5. S = 1/2 rectangular lattice with Ising exchange

The specific heat of an infinite rectangular array of spins with two interaction strengths, i.e. an interaction J between neighbouring sites in the x direction and an interaction J' between neighbouring sites in the y direction, has been calculated rigorously by Onsager [3]. The molar heat capacity is expressed in Onsager's notation as

$$\begin{aligned} C/R = \frac{4}{\pi} \{ & -iK(k)Z(ia,k)[H'/\sinh(2H')]^2 \\ & -iK(k)Z[iK(k')-ia,k][H/\sinh(2H)]^2 \\ & + 2[K(k)-E(k)][\mathrm{sn}(ia,k)/i\sinh(2H')]\, HH'\}, \end{aligned} \qquad (23)$$

where H and H' denote J/2kT and J'/2kT, respectively. K and E are elliptic integrals of the first and second kind, defined by the set of equations

$$\begin{aligned} & u = F(\mathrm{am}\ u,k) = \int_0^{\mathrm{am}\ u} (1-k^2\sin^2\varphi)^{-1/2} d\varphi, \\ & K(k) = F(\pi/2,k), \qquad k' = (1-k^2)^{1/2}, \\ & E(\mathrm{am}\ u,k) = \int_0^{\mathrm{am}\ u} (1-k^2\sin^2\varphi)^{1/2} d\varphi, \quad E(k) = E(\pi/2,k). \end{aligned} \qquad (24)$$

The variables a and k are functions of H and H', and will be treated below.

For an actual calculation, it is necessary to express the Jacobian elliptic functions appearing in equation (23) as combinations of elliptic integrals of the first and second kind with real arguments, for which accurate numerical procedures are available [20]. This has been achieved as follows.

The function Z[iK(k')-ia,k] can be written as

$$Z[iK(k')-ia,k] = -dn(ia,k)cs(ia,k) - i\pi/2K(k) - Z(ia,k), \tag{25}$$

while Z(ia,k) may be transformed to a Z function with real argument as follows:

$$Z(ia,k) = dn(ia,k)sc(ia,k) - iZ(a,k') \\ -i\pi\, F(a,k)/[2K(k)K(k')]. \tag{26}$$

For a further evaluation of equation (23) we have to distinguish the region above and below the critical temperature T_c, given by

$$\sinh(J/kT_c)\,\sinh(J'/kT_c) = 1. \tag{27}$$

With the expressions for the various Jacobian functions given in [3] we arrive for $T \gtrsim T_c$ at

$$\begin{aligned} C/R = \frac{4}{\pi}\{&[K(k)\cosh(J'/kT)/\cosh(J/kT) - K(k)Z(a,k') \\ &- \tfrac{\pi}{2}F(a,k)/K(k')](J'/kT)^2/[2\sinh(J'/kT)]^2 \\ &+ [K(k)\cosh(J'/kT)\cosh(J/kT) - K(k)\cosh(J'/kT)/\cosh(J/kT) \\ &+ K(k)Z(a,k') + \tfrac{\pi}{2}F(a,k)/K(k') - \tfrac{\pi}{2}](J/kT)^2/[2\sinh(J/kT)]^2 \\ &+ \tfrac{1}{2}[K(k)-E(k)](J/kT)(J'kT)/[\sinh(J/kT)\sinh(J'/kT)]\}, \end{aligned} \tag{28}$$

with $a = \arctan[1/\sinh(J/kT)]$ and $k = \sinh(J/kT)\sinh(J'/kT)$.

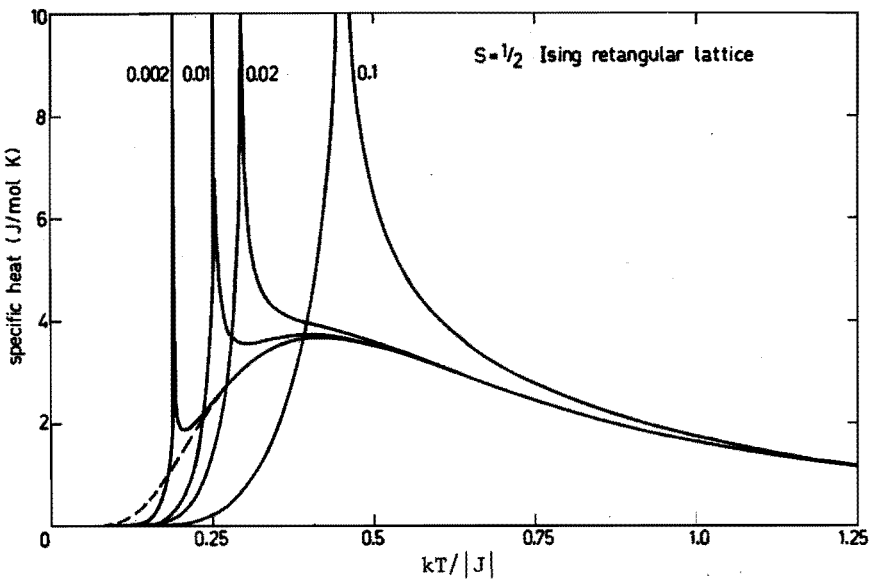

FIG. 2.8. Specific heat of a S = 1/2 rectangular array with Ising interactions as a function of the reduced temperature. The curves are identified by the ratio $|J'/J|$.

For $T \leqslant T_c$ we obtain

$$
\begin{aligned}
C/R = \frac{4}{\pi}\{ & [K(k)\coth(J/kT)\tanh(J'/kT) - K(k)Z(a,k') \\
& - \tfrac{\pi}{2}F(a,k)/K(k')](J'/kT)^2/[2\sinh(J'/kT)]^2 \\
& + [K(k)\coth(J'/kT)\coth(J/kT) - K(k)\coth(J/kT)\tanh(J'/kT) \\
& + K(k)Z(a,k') + \tfrac{\pi}{2}F(a,k)/K(k') - \tfrac{\pi}{2}](J/kT)^2/[2\sinh(J/kT)]^2 \\
& + \tfrac{1}{2}[K(k)-E(k)](J/kT)(J'/kT)\},
\end{aligned}
\tag{29}
$$

with $a = \arctan[\sinh(J'/kT)]$ and $k = 1/[\sinh(J/kT)\sinh(J'/kT)]$. With the aid of the equation

$$
Z(a,k) = E(a,k) - F(a,k)E(k)/K(k) \tag{30}
$$

the Z function may finally be expressed as a combination of complete and incomplete elliptic integrals of the first and second kind.

The heat capacity, inferred from equation (28) and (29) is plotted in Figure 2.8 as a function of the reduced temperature $kT/|J|$ for various values of J'/J. As may be seen from this figure, the chainlike behaviour at intermediate temperatures is obscured by the ordering already for $|J'/J| \sim 0.02$. It is evident, that the Ising-like anisotropy has a very dramatic effect in the two-dimensional case, since the pure 2-d Heisenberg and XY models have been reported to display no long-range order [21].

REFERENCES CHAPTER II

1. M. Suzuki, B. Tsujiyama, and S. Katsura, J. Math. Phys. 8, 124 (1967).
2. S. Katsura, Phys. Rev. 127, 1508 (1962).
3. L. Onsager, Phys. Rev. 65, 117 (1944).
4. G.S. Rushbrooke and P.J. Wood, Mol. Phys. 1, 257 (1958).
5. T. de Neef, Ph.D. Thesis, Eindhoven (1975).
6. For a general review see, for instance, *"Phase transitions and critical phenomena"*, Vol. 3, Edited by C. Domb and M.S. Green, Acad. Press, London (1974).
7. J.C. Bonner and M.E. Fisher, Phys. Rev. A135, 640 (1964).
8. T. de Neef, A.J.M. Kuipers and K. Kopinga, J. Phys. A7, L171 (1974).
9. H.W.J. Blöte, Physica 79B, 427 (1975).
10. R. Kubo, Phys. Rev. 87, 568 (1952).
11. J. van Kranendonk and J.H. van Vleck, Rev. Mod. Phys. 30, 1 (1958).
12. E. Rhodes and S. Scales, Phys. Rev. B8, 1994 (1973).
13. M.E. Fisher, Am. J. Phys. 32, 343 (1964).
14. T. de Neef and W.J.M. de Jonge, Phys. Rev. B11, 4402 (1975).
15. T. de Neef, to be published.

16. M. Hurley and B.C. Gerstein, J. Chem. Phys. 59, 6667 (1973).

17. J.V. Lebesque et al., to be published.

18. K. Kopinga, T. de Neef, W.J.M. de Jonge and B.C. Gerstein, Phys. Rev. B13, 3953 (1976).

19. See, for instance, H.E. Stanley, *"Introduction to phase transitions and critical phenomena"*, Clarendon Press, Oxford (1971).

20. M. Abramowitz and I.A. Stegun, *"Handbook of mathematical Functions"*, Chapter 16 and 17, N.B.S. 55 (1964).

21. N.D. Mermin and H. Wagner, Phys. Rev. Lett. 17, 1133 (1966).

CHAPTER III

LATTICE HEAT CAPACITY OF PSEUDO LOW-DIMENSIONAL COMPOUNDS [1]

3.1. Introduction

The analysis of the thermodynamic properties of a substance generally requires a separation of the lattice heat capacity from the other contributions. Although in principle the lattice specific heat of pseudo low-dimensional systems with a simple crystallographic structure may be calculated rather straightforwardly, the majority of the low-dimensional compounds have rather complex chemical structures, which precludes a rigorous calculation of the frequency distribution of the lattice vibrations.

Fortunately, the lattice heat capacity appears to be rather insensitive to the detailed structure of the vibrational spectrum, and approximate spectrum calculations may provide a very satisfactory description in many cases. This is demonstrated by the fact that the overall lattice heat capacity of a large number of compounds with a small anisotropy (e.g. cubic) can be successfully described by a linear superposition of suitably normalized three-dimensional Debye functions [2].

General and simple expressions for the lattice heat capacity of layered and chainlike structures have been proposed by Tarasov [3]. Although his theory, in which the heat capacity is expressed as a linear combination of Debye functions of suitable dimensionality, contains a number of rather drastic simplifications, it correctly predicts some qualitative features of the overall heat capacity. However, in general the accuracy is not sufficient to enable a reliable separation of the magnetic and the lattice contribution to the heat capacity [4, 5]. In fact, his description is somewhat oversimplified, especially concerning the "in plane" and "out of plane" or, alternatively, the "in chain" and "out of chain" modes of vibration, which are not treated separately, although they give rise to rather different restoring forces.

In several cases the experimental data within a limited temperature region can be represented by a linear superposition of suitably normalized one-, two- and three-dimensional Debye functions. In this kind of procedure, however, the Debye functions are merely used as mathematical basis functions, the normalization factors and Θ-values being inferred

from a least-squares fit to the experimental data. Apart from the fact, that such a procedure lacks a physical background, an accurate description over a large temperature interval requires a rather large number of adjustable parameters. On the other hand, the experimental data on several pseudo low-dimensional systems [5, 6, 7] indicate that at lower temperatures the lattice heat capacity should be represented by higher order terms than just T^3. This behaviour cannot be described by a linear superposition of Debye functions, unless one admits rather unphysical values of the parameters.

Detailed calculations on the vibrational spectrum and thermal properties of strongly anisotropic compounds have been performed only in a few special cases, mostly dealing with layered structures, particularly graphite [8]. Most of the results, however, cannot be applied to other substances, since they strongly depend on the characteristic lattice structure and the ratio of the atomic force constants. In this chapter we will present a rather general description of the lattice heat capacity of both layered and chainlike compounds, involving only a minimum of adjustable parameters. The theory will be based upon an elastic approach, in which only the most dominant dispersion effects will be taken into account.

For a large variety of layered or chainlike compounds, the elastic anisotropy within the layers or perpendicular to the chains appears to be small compared to the anisotropy in a plane perpendicular to the layers or parallel to the chains. We assume that a fair integral description of the most essential features of the long wavelength behaviour of such compounds can be obtained by approximating them by a system with purely uniaxial elastic anisotropy, such as a hexagonal 6/mmm structure. To a certain extent, such an assumption is supported by the results reported by Hofmann et al. [2]. They described the lattice heat capacity C_L of a number of binary compounds by a model involving two three-dimensional Debye functions

$$C_L = \frac{1}{3}\,[D_3(\Theta_\ell) + 2D_3(\Theta_t)]. \qquad (1)$$

For a completely isotropic continuum, Θ_ℓ and Θ_t would be associated with the longitudinal and transverse modes of vibration, respectively. Even for cubic structures, however, a certain amount of anisotropy is present

between - for instance - the {100} and the {111} direction, which is not taken into account explicitly by equation (1). Nevertheless, this expression appeared to give a very good description of various sets of experimental data on this type of compounds [2] over a wide range of temperatures.

The organization of this chapter is as follows. The dynamical behaviour of media with uniaxial elastic anisotropy will be considered in section 3.2, while in section 3.3 the frequency distribution function for the different modes of vibration will be calculated. In section 3.4 the heat capacity of layered structures will be considered, while section 3.5 will be devoted to the heat capacity of chainlike structures. The discussion given in section 3.6 will conclude this chapter.

3.2. Lattice dynamics in uniaxial compounds

3.2.1. Introduction

One of the best-known nearly two-dimensional compounds is graphite. It has a hexagonal structure with space group $P6_3/mmc$, built up from honey-comb net planes of carbon atoms, which are spaced at a distance of ~ 3.40 Å. The distance between two carbon atoms within a layer amounts to ~ 1.42 Å. The rather unusual temperature dependence of the specific heat of this compound was explained by Komatsu [9, 10, 11] by considering it as a system of loosely coupled layers. His basic idea was that, since the covalent binding forces within the honey-comb net planes are very strong compared to the interlayer interactions, dispersion effects in a direction perpendicular to the layers might already be important for a wide range of frequencies, in which waves propagating within the layers still could be treated in the elastic or small-k approximation. In the calculation of the heat capacity, dispersion effects due to the discrete nature of the layers would therefore be negligible, and the substance might be treated as a system consisting of thin elastic plates spaced at a distance d. He described the restoring forces due to the intra-layer interactions by the elastic constants c_{11}, c_{12} and c_{66} $(= \frac{1}{2}(c_{11}-c_{12}))$, and apart from these a bending modulus K. The restoring forces due to the interaction between the layers were represented by a compressional constant c_{33} and a shearing constant c_{44}. For relatively

small values of c_{44}, the following dispersion relations were obtained:

$$\rho\omega_1^2 = c_{11}\,(k_x^2 + k_y^2) + \frac{c_{44}}{d^2}\sin^2(k_z d)\,, \tag{2a}$$

$$\rho\omega_2^2 = c_{66}\,(k_x^2 + k_y^2) + \frac{c_{44}}{d^2}\sin^2(k_z d)\,, \tag{2b}$$

$$\rho\omega_3^2 = c_{44}\,(k_x^2 + k_y^2) + \frac{c_{33}}{d^2}\sin^2(k_z d) + K^2\,(k_x^2 + k_y^2)^2\,, \tag{2c}$$

where z denotes the direction perpendicular to the layers, and $\vec{k} = \frac{2\pi}{\lambda}\vec{e}_k$, a wave vector in the direction of the unit propagation vector $\vec{e}_k$. Because in graphite purely two-dimensional layers are present, which have strong covalent internal forces and hence a large resistance against bending, the fourth power term in equation (2c) may give rise to dispersion effects already for acoustic frequencies. For most layered structures, however, Komatsu's theory may not be used without some serious modifications, since the majority of these compounds do not display such an extreme crystallographic anisotropy as graphite. In fact, the constant c_{33} may be of the same order of magnitude as the constants c_{11} and c_{12}. On the other hand, the "layers" in the compounds of interest are often built up from rather complicated clusters of atoms and hence the influence of K will be relatively small at acoustic wavelengths.

In compounds with a large number of atoms per unit cell (r), the acoustic modes of vibration only account for a rather small fraction of the total number of degrees of freedom. It has been suggested to describe only the acoustic mode spectrum by a Debye-like approximation and to describe the optical mode spectrum by 3r-3 suitably normalized delta-functions located at some "average" optical mode frequencies. However, apart from the fact that a large number of unknown parameters would be introduced, experimental evidence indicates that the optical mode spectrum often appears to be rather "smeared out" [12]. Moreover, the assignment of the different branches of the dispersion relation of the lattice vibrations to "optical" and "acoustical" modes is unimportant for the calculation of the heat capacity. Therefore we shall approximate the 3r branches of the dispersion relation within the first Brillouin zone by three "pseudo-elastic" branches, which are located within a *modified Brillouin zone* (MBZ).

The general problem will be treated as follows. Firstly, we will describe the system by continuum elasticity theory, following a procedure somewhat analoguous to the treatment of Bowman and Krumhansl [13]. Next, the most dominating dispersion effects will be included by some suitably chosen MBZ boundaries. The dispersion at long wavelengths due to the intrinsic stiffness of layers or chains will be briefly considered in section 3.2.4. For sake of clarity, the calculation below will be performed assuming a layered structure. The majority of the results, however, may be applied to chainlike compounds also, which will be pointed out in section 3.4.

3.2.2. Small k-approximation

The equations of motion of elastic waves in a continuum with hexagonal anisotropy are given by

$$\rho \frac{\partial^2 u}{\partial t^2} = c_{11}\frac{\partial^2 u}{\partial x^2} + c_{66}\frac{\partial^2 u}{\partial y^2} + (c_{12}+c_{66})\frac{\partial^2 v}{\partial x \partial y} + c_{44}\frac{\partial^2 u}{\partial z^2} + (c_{13}+c_{44})\frac{\partial^2 w}{\partial x \partial z}, \quad (3a)$$

$$\rho \frac{\partial^2 v}{\partial t^2} = c_{66}\frac{\partial^2 v}{\partial x^2} + c_{11}\frac{\partial^2 v}{\partial y^2} + (c_{12}+c_{66})\frac{\partial^2 u}{\partial x \partial y} + c_{44}\frac{\partial^2 v}{\partial z^2} + (c_{13}+c_{44})\frac{\partial^2 w}{\partial y \partial z}, \quad (3b)$$

$$\rho \frac{\partial^2 w}{\partial t^2} = c_{33}\frac{\partial^2 w}{\partial z^2} + c_{44}\left(\frac{\partial^2 w}{\partial x^2} + \frac{\partial^2 w}{\partial y^2}\right) + (c_{13}+c_{44})\left(\frac{\partial^2 u}{\partial x \partial z} + \frac{\partial^2 v}{\partial y \partial z}\right), \quad (3c)$$

where $\vec{x} = (x,y,z)$, and u, v and w are the displacements in the x, y and z direction, respectively. Consider waves propagating in an infinite medium:

$$\begin{pmatrix} u \\ v \\ w \end{pmatrix} = \begin{pmatrix} \xi \\ \eta \\ \zeta \end{pmatrix} e^{\,i(\vec{k}.\vec{x} - \omega t)}. \quad (4)$$

Substitution in equation (3) yields the eigenvalue problem

$$\begin{vmatrix} c_{11}k_x^2 + c_{66}k_y^2 + c_{44}k_z^2 - \rho\omega^2 & (c_{12}+c_{66})k_x k_y & (c_{13}+c_{44})k_x k_z \\ (c_{12}+c_{66})k_x k_y & c_{66}k_x^2 + c_{11}k_y^2 + c_{44}k_z^2 - \rho\omega^2 & (c_{13}+c_{44})k_y k_z \\ (c_{13}+c_{44})k_x k_z & (c_{13}+c_{44})k_y k_z & c_{44}(k_x^2 + k_y^2) + c_{33}k_z^2 - \rho\omega^2 \end{vmatrix} \begin{vmatrix} \xi \\ \eta \\ \zeta \end{vmatrix} = 0. \quad (5)$$

As a consequence of the hexagonal symmetry it is possible to separate out a solution corresponding to

$$\rho\omega_2^2 = c_{66}(k_x^2 + k_y^2) + c_{44}k_z^2. \tag{6}$$

This mode of vibration has a displacement in the xy plane "transverse" with respect to $\vec{k}$. The remaining eigenvalue-problem is

$$\begin{pmatrix} c_{11}(k_x^2 + k_y^2) + c_{44}k_z^2 - \rho\omega^2 & (c_{13}+c_{44})\, k_z\sqrt{k_x^2 + k_y^2} \\ (c_{13}+c_{44})\, k_z\sqrt{k_x^2 + k_y^2} & c_{44}(k_x^2 + k_y^2) + c_{33}k_z^2 - \rho\omega^2 \end{pmatrix} \begin{pmatrix} \xi' \\ \zeta \end{pmatrix} = 0. \tag{7}$$

ξ' is located in the xy plane at a direction perpendicular to the eigenvector that corresponds to equation (6). If the off-diagonal elements

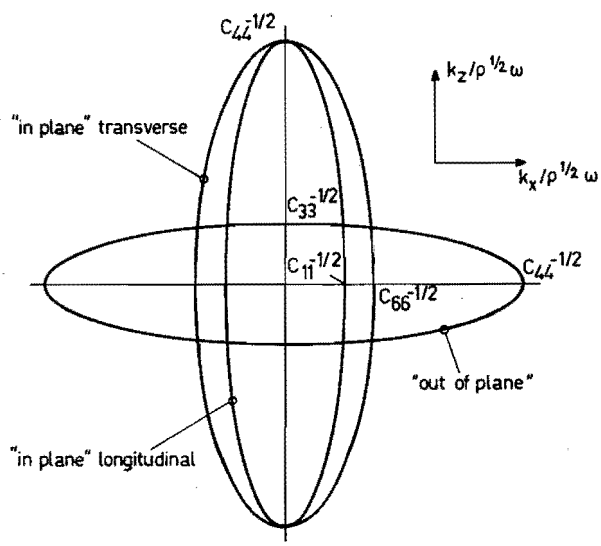

FIG. 3.1. Constant frequency contours in the $\vec{k}$ space, which result from the diagonal-approximation of the eigenvalue problem describing the equations of motion of elastic waves in a hexagonal layered structure. The meaning of the different vibrational modes is explained in the text.

in equation (7) are completely ignored, we obtain the approximate solutions

$$\rho\omega_1^2 = c_{11}(k_x^2 + k_y^2) + c_{44}k_z^2, \tag{8a}$$

$$\rho\omega_3^2 = c_{44}(k_x^2 + k_y^2) + c_{33}k_z^2. \tag{8b}$$

The mode of vibration denoted by ω_1 has a displacement in the xy plane "longitudinal" with respect to in-plane component of $\vec{k}$, while the mode denoted by ω_3 has a displacement perpendicular to the xy plane. The constant frequency contours of the solutions (6) and (8) are ellipsoids in the $\vec{k}$ space, which have rotational symmetry around the k_z axis. For a large number of layered compounds the constant c_{44} appears to be relatively small, and hence the curves presented in Figure 3.1 may be fairly representative.

If the off-diagonal elements in equation (7) are taken into account, a rigorous calculation of the eigenvalues and eigenvectors shows that the two solutions given by equation (8) are coupled. First, each mode of vibration does no longer correspond to one particular direction of polarization and, secondly, both ω versus k relations are somewhat modified. The effect of this modification is shown in Figure 3.2 for some representative values of the elastic constants. The drawn curves denote the constant frequency contours in the diagonal-approximation, while the dots represent the results obtained from a numerical calculation of the eigenvalues. The effect of the coupling is rather pronounced in the region where the two drawn curves intersect, which corresponds to a cone in the $\vec{k}$ space given by

$$(k_x^2 + k_y^2) \;/\; k_z^2 = (c_{33}-c_{44})/(c_{11}-c_{44}). \tag{9}$$

It can be seen from Figure 3.2, however, that the correction is much smaller for most of the $\vec{k}$ space. Of course, the direction of polarization is very sensitive to the direction of the $\vec{k}$ vector, but this has no consequence for the calculation of the heat capacity, and we feel that the diagonal approximation (8) provides a fair overall description of the dynamical behaviour of the model.

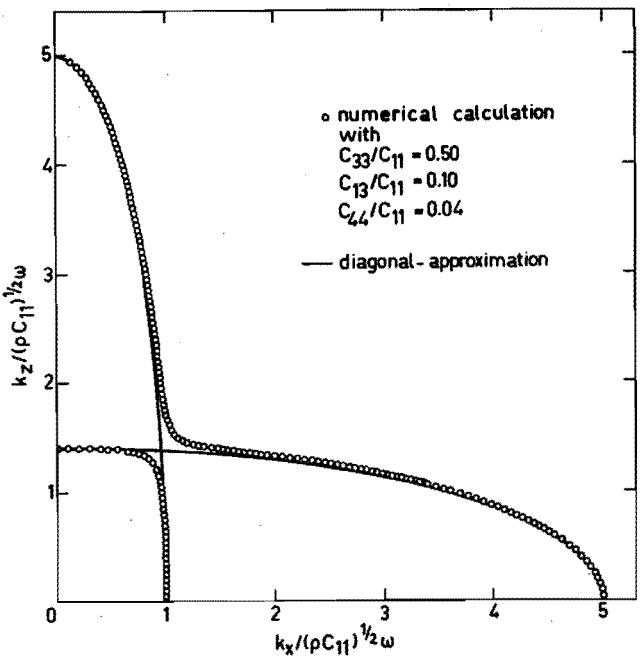

FIG. 3.2. An example of the effect of the introduction of the non-diagonal elements in the eigenvalue-problem describing the elastic waves in a hexagonal medium.

3.2.3. Dispersion effects

As can be seen from Figure 3.1 relatively small $\vec{k}$ vectors are associated with the "in plane" modes propagating in the xy plane. In the neighbourhood of the z direction, where the $\vec{k}$ vector is relatively large, the elastic continuum approximation may very likely be incorrect, since the contours will reach the MBZ boundary already for moderate values of ω, which may give rise to rather drastic dispersion effects. In order to describe these effects we assert that for this mode of vibration, waves propagating in the layers may be considered as purely elastic, while dispersion effects near the z direction may be taken into account by a MBZ boundary parallel to the xy plane located at $k_z = \pm \pi/2d$. One should note, that this assumption is only correct if c_{44} is relatively small, and hence

the validity range of the present theory is limited to substances which have a fair amount of elastic anisotropy. We will return to this subject in section 3.4. "Truncation" at the MBZ boundary will occur if k_z in the equations (6) and (8a) is modified to $d^{-1}\sin(k_z d)$, while k_x and k_y remain unchanged. This modification yields the set of equations

$$\rho\omega_1^2 = c_{11}(k_x^2 + k_y^2) + \frac{c_{44}}{d^2}\sin^2(k_z d), \tag{10a}$$

$$\rho\omega_2^2 = c_{66}(k_x^2 + k_y^2) + \frac{c_{44}}{d^2}\sin^2(k_z d). \tag{10b}$$

Obviously these equations correspond exactly to the set of equations (2a) and (2b), which have been derived from a "thin plate" model.

For the "out of plane" mode of vibration, however, the situation is quite different. The constant frequency contour, given by equation (8b), appears to be more or less disc-shaped, and hence dispersion effects will be important near the xy plane rather than along the z axis. Within the restrictions pointed out above, these effects may be described by a cylinder-shaped MBZ boundary located parallel to the z axis at a radius $\pi/2d_1$, which transforms equation (8b) to

$$\rho\omega_3^2 = \frac{c_{44}}{d_1^2}\sin^2\left[(k_x^2 + k_y^2)^{1/2} d_1\right] + c_{33}\,k_z^2. \tag{11}$$

This equation now appears to be quite different from the corresponding equation (2c), which has been derived from a "thin plate" model. This point will be clarified in the next section.

3.2.4. Bending stiffness

Komatsu's treatment of the bond bending problem of a mono-atomic layer was based upon the assumption that the layer might be considered as a thin elastic plate. The validity of this assumption may be suitably examined by the atomistic model shown in Figure 3.3, which represents a cross-section perpendicular to the layers. The different atoms - denoted by n,m - are arranged in a rectangular array, the spacing between adjacent atoms along the x and z axis being equal to a and d, respectively. The array is assumed to resist variations of both the bond

lengths and bond angles. Only nearest neighbour interactions will be considered. In Figure 3.4 the possible elementary deformations are indicated, together with the corresponding increase in potential energy.

If both the kinetic energy T and the potential energy V are expressed in $u_{n,m}$ and $w_{n,m}$, which denote the atomic displacements along the x and z axis, respectively, the equations of motion may be found by applying Hamilton's principle

$$\delta \int_{t_1}^{t_2} (T-V)\, dt = 0. \tag{12}$$

The result is

$$\begin{aligned} & M \frac{\partial^2 u_{n,m}}{\partial t^2} + \frac{C_a}{a^2} (2u_{n,m} - u_{n,m+1} - u_{n,m-1}) + \frac{4C_\Theta}{d^2} (2u_{n,m} - u_{n+1,m} - u_{n-1,m}) \\ & + (\frac{ad}{\ell^4} C_\ell + \frac{1}{ad} C_\Theta)(w_{n+1,m-1} + w_{n-1,m+1} - w_{n+1,m+1} - w_{n-1,m-1}) \\ & + \frac{a^2}{\ell^4} C_\ell (4u_{n,m} - u_{n+1,m+1} - u_{n-1,m-1} - u_{n+1,m-1} - u_{n-1,m+1}) \\ & + \frac{C_\psi}{d^2} (6u_{n,m} - 4u_{n+1,m} - 4u_{n-1,m} + u_{n+2,m} + u_{n-2,m}) = 0 \ , \end{aligned} \tag{13a}$$

$$\begin{aligned} & M \frac{\partial^2 w_{n,m}}{\partial t^2} + \frac{C_d}{d^2} (2w_{n,m} - w_{n+1,m} - w_{n-1,m}) + \frac{4C_\Theta}{a^2} (2w_{n,m} - w_{n,m+1} - w_{n,m-1}) \\ & + (\frac{ad}{\ell^4} C_\ell + \frac{1}{ad} C_\Theta)(u_{n+1,m-1} + u_{n-1,m+1} - u_{n+1,m+1} - u_{n-1,m-1}) \\ & + \frac{d^2}{\ell^4} C_\ell (4w_{n,m} - w_{n+1,m+1} - w_{n-1,m-1} - w_{n+1,m-1} - w_{n-1,m+1}) \\ & + \frac{C_\phi}{a^2} (6w_{n,m} - 4w_{n,m+1} - 4w_{n,m-1} + w_{n,m+2} + w_{n,m-2}) = 0 \ , \end{aligned} \tag{13b}$$

where M denotes the atomic mass. For long wavelengths the relative differences between the atomic displacements may be replaced by the corresponding derivatives to x and z, and we obtain

$$M\frac{\partial^2 u}{\partial t^2} = (C_a + \frac{2a^4}{\ell^4} C_\ell)\frac{\partial^2 u}{\partial x^2} + (4C_\Theta + \frac{4a^2d^2}{\ell^4} C_\ell)\frac{\partial^2 w}{\partial x \partial z}$$
$$+ (4C_\Theta + \frac{2a^2d^2}{\ell^4} C_\ell)\frac{\partial^2 u}{\partial z^2} + C_\psi d^2(\frac{\partial^4 u}{\partial z^4}), \qquad (14a)$$

$$M\frac{\partial^2 w}{\partial t^2} = (C_d + \frac{2d^4}{\ell^4} C_\ell)\frac{\partial^2 w}{\partial z^2} + (4C_\Theta + \frac{4a^2d^2}{\ell^2} C_\ell)\frac{\partial^2 u}{\partial x \partial z}$$
$$+ (4C_\Theta + \frac{2a^2d^2}{\ell^4} C_\ell)\frac{\partial^2 w}{\partial x^2} + C_\phi a^2(\frac{\partial^4 w}{\partial x^4}). \qquad (14b)$$

As may be inferred from equation (3), continuum elasticity theory yields for the corresponding two-dimensional case

$$\rho\frac{\partial^2 u}{\partial t^2} = c_{11}\frac{\partial^2 u}{\partial x^2} + (c_{13}+c_{44})\frac{\partial^2 w}{\partial x \partial z} + c_{44}\frac{\partial^2 u}{\partial z^2}, \qquad (15a)$$

$$\rho\frac{\partial^2 w}{\partial t^2} = c_{33}\frac{\partial^2 w}{\partial z^2} + (c_{13}+c_{44})\frac{\partial^2 u}{\partial x \partial z} + c_{44}\frac{\partial^2 w}{\partial x^2}. \qquad (15b)$$

It is obvious, that

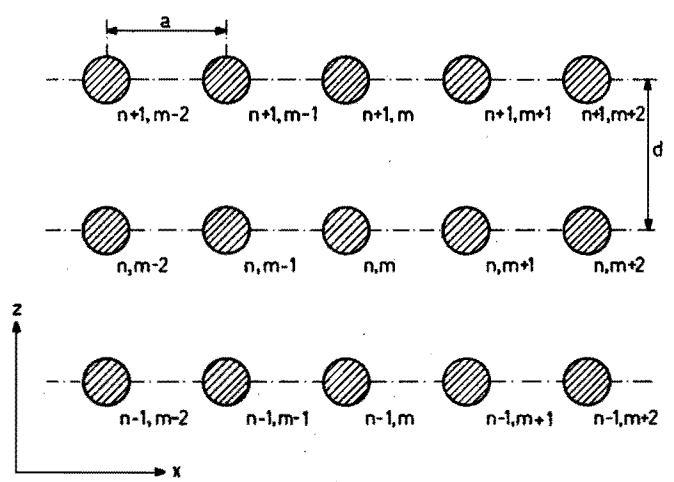

FIG. 3.3. A simple atomistic model used to describe the various interactions in an arbitrary plane perpendicular to the xy layers.

$$c_{11} = \left(C_a + \frac{2a^4}{\ell^4} C_\ell\right) \frac{\rho}{M} , \quad c_{33} = \left(C_d + \frac{2d^4}{\ell^4} C_\ell\right) \frac{\rho}{M} ,$$
$$c_{13} = \frac{2a^2 d^2 \rho}{\ell^4 M} C_\ell , \text{ and } \quad c_{44} = \left(4C_\Theta + \frac{2a^2 d^2}{\ell^4} C_\ell\right) \frac{\rho}{M} , \tag{16}$$

and continuum elasticity theory gives a correct description of the long wavelength limit of the vibrational spectrum. It appears, however, that the stiffness of 180° bonds, represented by C_ψ and C_ϕ, does not enter into the elastic constants. If the corresponding bending constants are extremely large, the influence of the fourth order terms in equation (14) may be important already for acoustic frequencies, although such a drastic effect is likely to occur only for very anisotropic covalent substances like - for instance - graphite and boron nitride. For a description of the vibrational spectrum of these compounds, we may generalize equation (14) to three dimensions, and follow the procedure described in section 3.2.3 to obtain the dispersion relation

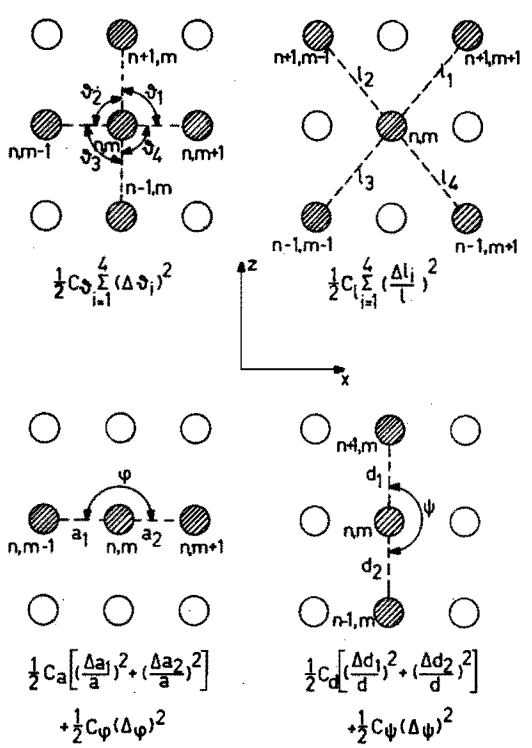

FIG. 3.4.
Some contributions to the increase of the potential energy, arising from variations of the bond angles and bond lengths in the atomistic model presented in Figure 3.3.

$$\rho\omega_3^2 = c_{44}(k_x^2 + k_y^2) + \frac{c_{33}}{d^2}\sin^2(k_z d) + C_\phi' a^2 (k_x^2 + k_y^2)^2. \qquad (17)$$

The prime at C_ϕ is added to avoid confusion with the purely two-dimensional case. Equation (17) appears to be completely analoguous to equation (2c), which has been derived from a thin-plate model, if we put $K^2 = C_\phi' a^2$. Equation (14a) will transform to equation (10a), because for a layered structure the effect of C_ψ is negligible.

3.3. Calculation of the heat capacity

In the diagonal-approximation, the three modes of vibration are decoupled completely, and each mode will account for one third of the total number of degrees of freedom. In the calculation of the molar heat capacity, this number is assumed to amount to $3rN_{AV}$, where N_{AV} is Avogadro's number and r is the number of vibrating units in a formula unit. The total specific heat may be obtained by a summation of the three properly normalized contributions arising from the different modes of vibration.

The dispersion relations (10) and (11) are of two different types, given by

$$\omega^2 = \alpha^2(k_x^2 + k_y^2) + (\beta/d)^2\sin^2(k_z d) \quad \text{with} \quad -\pi/2d \leq k_z \leq \pi/2d, \qquad (18a)$$

$$\omega^2 = (\gamma/d_1)^2\sin^2\left[(k_x^2 + k_y^2)^{1/2} d_1\right] + \delta^2 k_z^2$$

$$\text{with } 0 \leq (k_x^2 + k_y^2)^{1/2} \leq \pi/2d_1. \qquad (18b)$$

In these equations α^2, β^2, γ^2, and δ^2 are combinations of the various elastic constants c_{kl}/ρ. Since the sample size is normally very large compared to atomic dimensions, the distribution of the normal mode frequencies will be independent of the shape of the sample [14, 15]. Therefore we define an uniform density of states in the $\vec{k}$ space, denoted by ρ_k. The different contributions to the heat capacity may then be evaluated rather straightforwardly. Let us consider equation (18a) first.

By differentiating the number of vibrations with $\omega' < \omega$ with respect to ω, the frequency distribution function $g(\omega)$ can be found as

$$g(\omega) = \rho_k \frac{4\pi}{\alpha^2 d} \omega \arcsin(\omega/\omega_c) \quad \text{for } \omega \leq \omega_c, \tag{19a}$$

$$g(\omega) = \rho_k \frac{2\pi^2}{\alpha^2 d} \omega \quad \text{for } \omega \geq \omega_c. \tag{19b}$$

In these expressions ω_c is written for β/d, the frequency at which "truncation" at the MBZ boundary occurs. The frequency distribution function is plotted in Figure 3.5, where ω_m denotes the "cut-off" frequency at which the normalization condition

$$\rho_k \int_0^{\omega_m} g(\omega)\, d\omega = rN_{AV} \tag{20}$$

is satisfied. Substitution of equation (19) in equation (20) yields

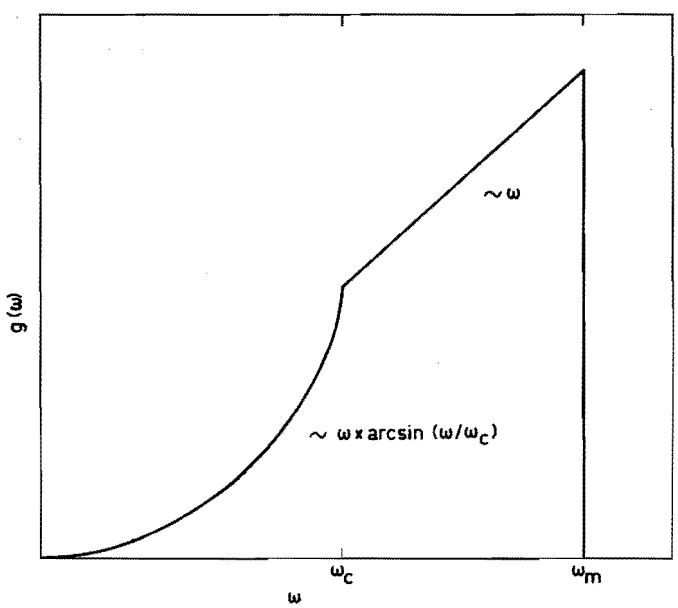

FIG. 3.5. The frequency distribution function g(ω) arising from a mode of vibration, for which dispersion effects near the z axis are dominant.

$$\rho_k \frac{\pi^2}{\alpha_d^2} (\omega_m^2 - \omega_c^2/2) = rN_{AV}, \tag{21}$$

from which it follows that

$$g(\omega) = \frac{8rN_{AV}}{\pi(2\omega_m^2 - \omega_c^2)} \omega \arcsin(\omega/\omega_c) \quad \text{for } \omega \leq \omega_c, \tag{22a}$$

$$g(\omega) = \frac{4rN_{AV}}{2\omega_m^2 - \omega_c^2} \omega \qquad \text{for } \omega \geq \omega_c. \tag{22b}$$

As can be seen from these equations, the frequency distribution function $g(\omega)$ is determined completely by the magnitude of ω_c and ω_m, which will be considered as independent parameters in the calculation of the heat capacity.

In general, the molar heat capacity C(T) may be inferred from a normalized frequency distribution function $g(\omega)$ with the formula

$$C(T) = k_B \int_0^{\omega_m} \frac{g(\omega)\ (\hbar\omega/kT)^2\ e^{\hbar\omega/kT}}{\left(e^{\hbar\omega/kT}-1\right)^2}\, d\omega, \tag{23}$$

where k_B is Boltzmann's constant. If equation (22) is inserted in this expression, we obtain a contribution $F_1(\Theta_m,\Theta_c,T)$ to the heat capacity, given by

$$F_1(\Theta_m,\Theta_c,T) = \frac{r}{3(2\Theta_m^2-\Theta_c^2)}\, x \left[\frac{24RT^2}{\pi} \int_0^{\Theta_c/T} \frac{x^3 e^x}{(e^x-1)^2} \arcsin(xT/\Theta_c)\, dx + 2\Theta_m^2\, D_2(\Theta_m/T) - 2\Theta_c^2\, D_2(\Theta_c/T)\right]. \tag{24}$$

In this expression the usual substitutions

$$x = \hbar\omega/kT\ ,\ \Theta_c = \hbar\omega_c/k\ ,\ \text{and}\ \Theta_m = \hbar\omega_m/k \tag{25}$$

have been made, while $D_2(\Theta/T)$ denotes the two-dimensional Debye function, defined in the Appendix.

Before we proceed with the evaluation of equation (18b), we would like to make some remarks about the interpretation of the numerical values

of ω_c and ω_m. While ω_c has been defined as β/d (cf. equation 19), there is no direct relation between ω_m and the constant α. Although it is not basically important for the calculation of the heat capacity, the value of ω_m may - to a certain extent - be associated with the magnitude of α, which can be seen as follows. If we assume a cylinder-shaped MBZ with height π/d and radius $\pi/2d_1$, the volume of the MBZ amounts to $\pi^4/(4dd_1^2)$, and the corresponding density of states in the $\vec{k}$ space ρ_k is found as

$$\rho_k = 4dd_1^2 rN_{AV}/\pi^4. \tag{26}$$

Of course, from a physical point of view, this assumption is not quite compatible with equation (18a), since in this equation dispersion effects near the xy plane are not taken into account, but in the present derivation of an approximate relation between ω_m and α the resulting error in the cut-off frequency of about a factor $\pi/2$ is of no importance. Substitution of equation (26) in (21) yields the relation

$$\omega_m \approx \frac{\pi}{2}\frac{\alpha}{d_1}\left(1 + \frac{2\beta^2 d_1^2}{\pi^2\alpha^2 d^2}\right)^{1/2}. \tag{27}$$

Given the fact that $\alpha>\beta$ and that d_1 and d are of the same order of magnitude, equation (27) shows that the value of ω_m may be used as an indication of the ratio α/d_1.

Next we will consider equation (18b). Following the same procedure as described above the frequency distribution function $g(\omega)$ may be found as

$$g(\omega) = \frac{16\pi\rho_k}{\alpha d_1^2}\int_o^b \zeta[1-(\omega_c/\omega)^2\sin^2\zeta]^{-1/2}d\zeta, \tag{28}$$

with $\omega_c = \gamma/d_1$, $b = \arcsin(\omega/\omega_c)$ for $\omega \leqslant \omega_c$, and $b = \pi/2$ for $\omega \geqslant \omega_c$. Since an analytical evaluation of the integral in this equation is not possible, the frequency distribution function has been computed numerically, and the result is plotted in Figure 3.6. The dashed curve denotes the limit for $\omega \to \infty$, in which case equation (28) reduces to

$$g(\omega) = \frac{16\pi\rho_k}{\alpha d_1^2}\int_o^{\pi/2} \zeta d\zeta = \frac{2\pi^3\rho_k}{\alpha d_1^2}. \tag{29}$$

In order to obtain a rather simple and manageable expression for the heat capacity, involving only linear combinations of Debye functions, similar to equation (24), equation (28) will be used for $\omega < 2\omega_c$, and the limiting behaviour (29) in the frequency range $\omega \geqslant 2\omega_c$. This approximation may produce an error of ~ 1 % in the magnitude of the heat capacity, but this can be practically compensated by a small readjustment of the parameters ω_c and ω_m. For $\omega > \omega_c$ the number of vibrations $I(\omega)$ with $\omega' < \omega$ is equal to

$$I(\omega) = \frac{16\pi\rho_k\omega_c}{\alpha d_1^2} \int_0^{\pi/2} \zeta[(\omega/\omega_c)^2 - \sin^2\zeta]^{1/2} d\zeta \qquad (30)$$

and hence the normalization condition (20) yields

$$\frac{16\pi\rho_k}{\alpha d_1^2} \left[\omega_s \int_0^{\pi/2} \frac{\zeta}{2} (4-\sin^2\zeta)^{1/2} d\zeta + \frac{\pi^2}{8} (\omega_m - \omega_s)\right] = rN_{AV}, \qquad (31)$$

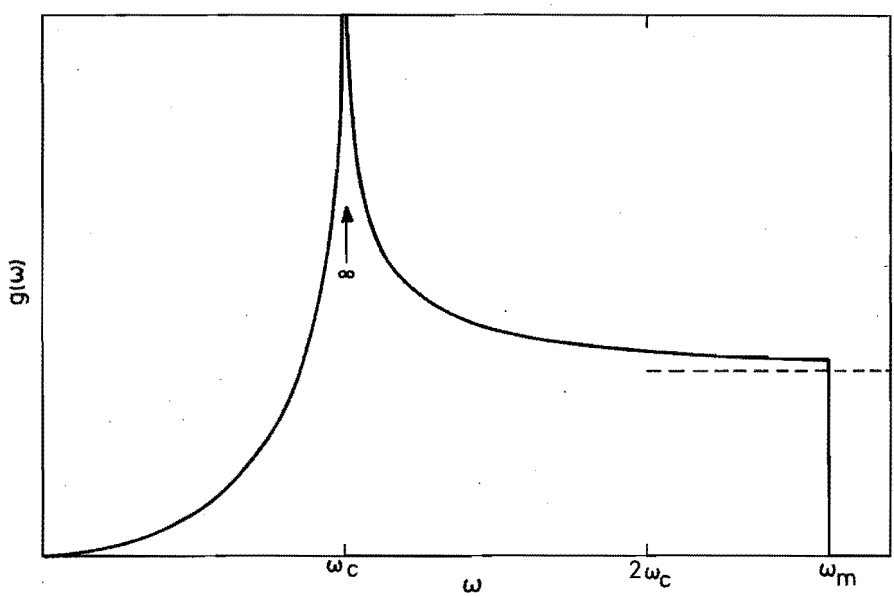

FIG. 3.6. The frequency distribution function g(ω) arising from the mode of vibration, for which dispersion effects near the xy plane are dominant. The dashed curve denotes the limiting behaviour for $\omega \to \infty$.

in which expression ω_s has been substituted for $2\omega_c$. If we denote the integral in equation (31) by I_1, the frequency distribution function

$$g(\omega) = \frac{8rN_{AV}}{\pi^2\omega_m - (\pi^2 - 8I_1)\omega_s} \int_0^b \zeta[1-(\omega_s/2\omega)^2 \sin^2\zeta]^{-1/2} d\zeta, \qquad (32a)$$

with $b = \arcsin(2\omega/\omega_s)$ for $\omega \leqslant \omega_s/2$ and $b = \pi/2$ for $\omega_s/2 \leqslant \omega \leqslant \omega_s$,

$$g(\omega) = \frac{8rN_{AV}}{\pi^2\omega_m - (\pi^2 - 8I_1)\omega_s} \times \frac{\pi^2}{8} \quad \text{for } \omega \geqslant \omega_s \qquad (32b)$$

is obtained. Again, $g(\omega)$ is completely determined by the magnitude of ω_s and ω_m. The same arguments that were applied in the evaluation of equation (18a) may be used to show that the value of ω_m may now be associated with the ratio δ/d. If equation (32) is substituted in equation (23), we obtain a contribution $F_2(\Theta_m, \Theta_s, T)$ to the heat capacity, given by

$$F_2(\Theta_m, \Theta_s, T) = \frac{r}{3[\pi^2\Theta_m - (\pi^2 - 8I_1)\Theta_s]} \times$$

$$[8I_1\Theta_s\, G_2(T/\Theta_s) + \pi^2\Theta_m\, D_1(\Theta_m/T) - \pi^2\Theta_s\, D_1(\Theta_s/T)]. \qquad (33)$$

$D_1(\Theta/T)$ denotes the one-dimensional Debye function, defined in the Appendix, where the function $G_2(T/\Theta)$ will be treated also.

3.4. Layered structures

As has been pointed out in the foregoing section, the lattice heat capacity $C_L(T)$ may be found by a summation of the three contributions arising from the different modes of vibration. This summation may be written as

$$C_L(T) = F_1(\Theta_\ell, \Theta_c, T) + F_1(\Theta_t, \Theta_c, T) + F_2(\Theta_o, \Theta_s, T) \; . \qquad (34)$$

In this expression Θ_ℓ, Θ_t, and Θ_o are associated with the cut-off frequencies of the "longitudinal in plane", the "transverse in plane", and the "out of plane" mode of vibration, respectively. The number of adjustable parameters in equation (34) amounts to 5, but in order to keep this expression manageable in numerical fitting procedures, a further reduction of this number is generally imperative. Fortunately, such a reduction is often possible.

Firstly, the majority of the investigations on low-dimensional magnetic systems have been performed at rather low temperatures, in which case one "average" characteristic temperature may be used to describe the cut-off frequency of both the longitudinal and transverse in plane modes of vibration. If the high temperature region should be described more accurately, one might use the fact that the ratio Θ_ℓ/Θ_t is roughly equal to v_ℓ/v_t, where v_ℓ and v_t denote the propagation velocities of the longitudinal and transverse waves in the xy plane, which are proportional to $\sqrt{c_{11}}$ and $\sqrt{c_{66}}$, respectively. Since for a wide variety of substances [16] the ratio c_{11}/c_{66} appears to range between 3 and 6, the additional condition $\Theta_\ell = a\Theta_t$, with $a \sim 2$, seems rather realistic.

Secondly, when the dimensions of the MBZ in the x,y and z direction are not too different, the problem will be simplified by the fact that "truncation" of the "cigar"-shaped contours in the $\vec{k}$ space occurs at the same frequency as the "truncation" of the "disc"-shaped contour, because for all contours the maximum k-value is proportional to $c_{44}^{-1/2}$. (cf. Figure 3.1.) This yields the additional relation $\Theta_s = 2\Theta_c$, which leaves only three independent parameters.

For extremely anisotropic substances, like graphite, boron nitride, and perhaps $(CH_3NH_3)_2CdCl_4$ [5], a bending modulus K should be included (cf. equation 17). We will, however, not consider this rather special case in the present treatment. For a calculation of the frequency spectrum for the "out of plane" mode of vibration and a discussion of the contribution to the heat capacity, the reader is referred to literature [9, 10, 11].

Finally, we would like to make some remarks about the application of equation (34) to the interpretation of experimental data. Both the integral on the right hand side of equation (24) and the function $G_2(T/\Theta)$, which has been substituted in equation (33), cannot be evaluated analytically. With the aid of a high-speed computer they may be approxi-

mated with a very high degree of accuracy, but, especially when the functions F_1 and F_2 are used in numerical fitting procedures, the time involved with such a procedure is very large, since the various integrals have to be computed for each iteration and for all temperatures that correspond to the data points. Given the fact that even the accuracy of rather elaborate specific heat measurements is generally not better than about one percent, we found it useful to deduce some simple expressions, which describe the various integrals with an accuracy of a few parts in 10^4 for all values of T/Θ. The derivation of these expressions will be given in the Appendix.

As already mentioned in section 3.2.3 the functions F_1 and F_2 are only physically meaningful when the ratio Θ_c/Θ_m and the ratio Θ_s/Θ_m are small compared to unity. If the anisotropy for a particular mode of vibration accidentally appears to be rather small, a description of the corresponding contribution with a properly normalized three-dimensional Debye function is preferred.

3.5. Chainlike structures

In principle, the evaluation of the lattice dynamics of a chainlike structure is completely analoguous to the problem treated in section 2 and 3 of this chapter, if the direction of the chains is chosen along the z axis. Some modifications may arise from the fact that the relative magnitude of the elastic constants may be different from those of a layered structure. For a variety of anisotropic chainlike compounds, however, the shearing constant c_{44} appears to be small compared to c_{11}, c_{66} and c_{33} [16]. Therefore the contours presented in Figure 3.1 can still be considered as representative, except from the fact that the constant c_{33}, which now represents the compressional stiffness of the chains, will generally be larger than c_{11} and c_{66}. As can easily be seen, this has no basic consequence for the description of the dynamical behaviour, given by continuum elasticity theory, and the expressions (10) and (11) are still valid. The dispersion relations denoted by ω_1, ω_2 and ω_3, are now associated with the "out of chain longitudinal", the "out of chain transverse", and the "in chain" mode of vibration, respectively.

In general, the lattice heat capacity of chainlike substances may be described by equation (34) with 5 independent parameters. For these compounds, however, it is not obvious that both Θ_ℓ and Θ_t are high compared to the temperature region in which the expression will be applied, and hence the additional condition $\Theta_\ell = a\Theta_t$ may produce some inaccuracies in the description of the heat capacity. However, if the dimensions of the MBZ are not too different, the number of parameters can be reduced by the relation $\Theta_s = 2\Theta_c$, as has been pointed out in the foregoing section.

To our knowledge, no heat capacity measurements have been reported on substances, which are built up from very covalently bound purely one-dimensional chains. Therefore the bending constant C_ψ (cf. equation 14) has not been included in the present treatment.

3.6. Discussion

It has become common practice to describe both theoretical and experimental results with an apparent Θ_a value, i.e. the value of Θ that should be substituted in a correctly normalized three-dimensional Debye function to describe the predicted or observed magnitude of the specific heat at a certain temperature T [15]. The contributions to the heat capacity F_1 and F_2, obtained in section 3.3, can be described by apparent Θ_a values defined by the equalities

$$\frac{1}{3} D_3(\Theta_a/T) = F_1(\Theta_m,\Theta_c,T) \ , \tag{35a}$$

$$\frac{1}{3} D_3(\Theta_a/T) = F_2(\Theta_m,\Theta_s,T) \ . \tag{35b}$$

The results are presented in Figure 3.7 and 3.8, respectively, where the ratio Θ_a/Θ_m has been normalized to unity at T = 0. In view of the mathematical form of equation (24) and (33), the different curves representing the contributions F_1 and F_2 are characterized by the ratio $(\Theta_c/\Theta_m)^2$ and the ratio Θ_s/Θ_m, respectively. As may be inferred from the derivation given in section 3.3, however, the elastic anisotropy of a substance will actually be reflected by the ratio $(\Theta_c/\Theta_m)^2$ for the modes

of vibration corresponding to a contribution F_1, but by the ratio $(\Theta_s/2\Theta_m)^2$ for the mode of vibration corresponding to a contribution F_2.

One should note that - even for small values of the anisotropy - the present theory predicts a minimum of Θ_a in the temperature region $0.02 < T/\Theta_m < 0.2$. This behaviour has also been observed in a considerable number of experimental investigations. Hence it appears that the most essential shortcoming of the purely elastic Debye model in the description of the low-temperature heat capacity may already be removed by the inclusion of only the most dominant dispersion effects.

The limiting T^3 dependence of the lattice heat capacity appears to occur only at temperatures very low compared to the region in which the "Debye T^3 law" mathematically holds. Therefore conventional techniques to separate the electronic or magnetic contribution from the total

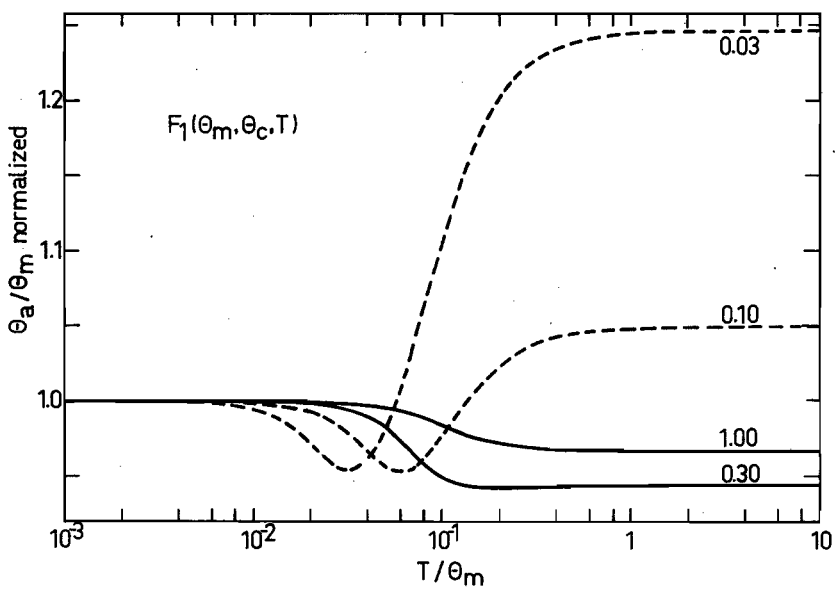

FIG. 3.7. Description of the contribution to the specific heat, arising from a mode of vibration for which dispersion effects near the z axis are dominant, with an apparent Θ_a value. The different curves are characterized by the ratio $(\Theta_c/\Theta_m)^2$, which may be associated with the elastic anisotropy for this mode of vibration.

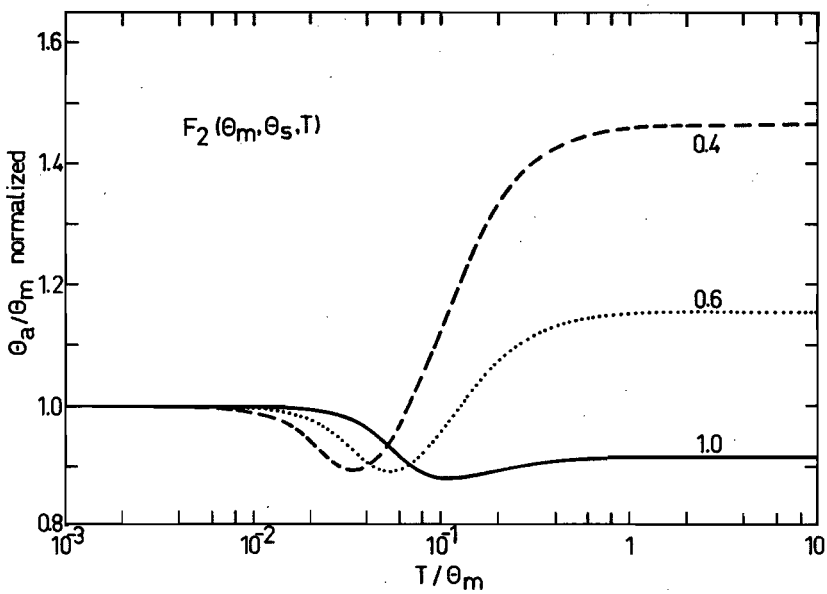

FIG. 3.8. Description of the contribution to the specific heat, arising from the mode of vibration for which dispersion effects near the xy plane are dominant, with an apparent Θ_a value. The different curves are characterized by the ratio Θ_s/Θ_m. The relation of this ratio to the elastic anisotropy for this mode of vibration is pointed out in the text.

specific heat, such as a C/T versus T^2 or a CT^2 versus T^5 plot, respectively, should only be applied with great care if the compound under investigation has a fair amount of anisotropy, since they are based upon a purely T^3 dependence of the lattice heat capacity.

Concluding we would like to make the following remarks.
In this chapter an approximation has been presented, which is intended to provide a rather general description of the lattice heat capacity of both layered and chainlike compounds. The model applied to the description of the lattice vibrations did only take into account the most dominant dynamical characteristics of these particular substances, in order to reduce the number of adjustable parameters as much as possible. Given the succes of some well-known approximations to the heat capacity

of compounds with a small anisotropy [2, 15], we feel that the simplifications made in the course of the treatment will affect the details of the dynamical behaviour rather than the integral properties, such as the heat capacity. Although the effect of some approximations has already been pointed out in the preceeding sections, a proper justification is - of course - only possible by confronting the resulting description with experimental results. We will return to this subject in Chapter V and VI.

REFERENCES CHAPTER III

1. K. Kopinga, P. van der Leeden and W.J.M. de Jonge, accepted for publication in Phys. Rev. B.
2. J.A. Hofmann, A. Paskin, K.J. Tauer and R.J. Weiss, J. Phys. Chem. Solids 1, 45 (1956).
3. V.V. Tarasov, *"New problems in the physics of glass"*, Oldbourne Press, London (1963).
4. K. Kopinga. T. de Neef and W.J.M. de Jonge, Phys. Rev. B11, 2364 (1975).
5. P. Bloembergen and A.R. Miedema, Physica 75, 205 (1974).
6. L.D. Jennings and W.N. Hansen, Phys. Rev. 139A, 1694 (1965).
7. K. Blacklock, H.F. Linebarger, H.W. White, K.H. Lee and S.L. Holt, J. Chem. Phys. 61, 5279 (1975).
8. References can be found, for instance, in K.K. Mani and R. Ramani, Phys. Stat. Sol. 61, 659 (1974), G.F. Newell, J. Chem. Phys. 27, 240 (1957).
9. K. Komatsu and T. Nagamiya, J. Phys. Soc. Japan 6, 438 (1951).
10. K. Komatsu, J. Phys. Soc. Japan 10, 346 (1955).
11. K. Komatsu, J. Phys. Chem. Solids 6, 380 (1958).
12. J.H.M. Stoelinga and P. Wyder, J. Chem. Phys. 61, 478 (1974).
13. J.C. Bowman and J.A. Krumhansl, J. Phys. Chem. Solids 6, 367 (1958).

14. H. Weyl, Math. Ann. 71, 441 (1911).

15. A.A. Maradudin, E.W. Montroll, G.H. Weiss and I.P. Ipatova, *"Theory of the lattice dynamics in the harmonic approximation"*, Academic Press, New York and London (1971).

16. *"Numerical data and functional relationships in science and technology"*, Landolt-Bornstein, Group III, Volume 1,2, Springer-Verlag, Berlin-Heidelberg-New York (1966).

CHAPTER IV

EXPERIMENTAL APPARATUS

4.1. General

The heat capacity measurements were performed with an adiabatic calorimeter, which is schematically shown in Figure 4.1. The sample, usually consisting of ∿ 0.1 mole of polycrystalline material, was sealed inside a cylinder-shaped capsule (1), which was mainly made of copper. The bottom of the sample holder consisted of stainless steel to enable the use of

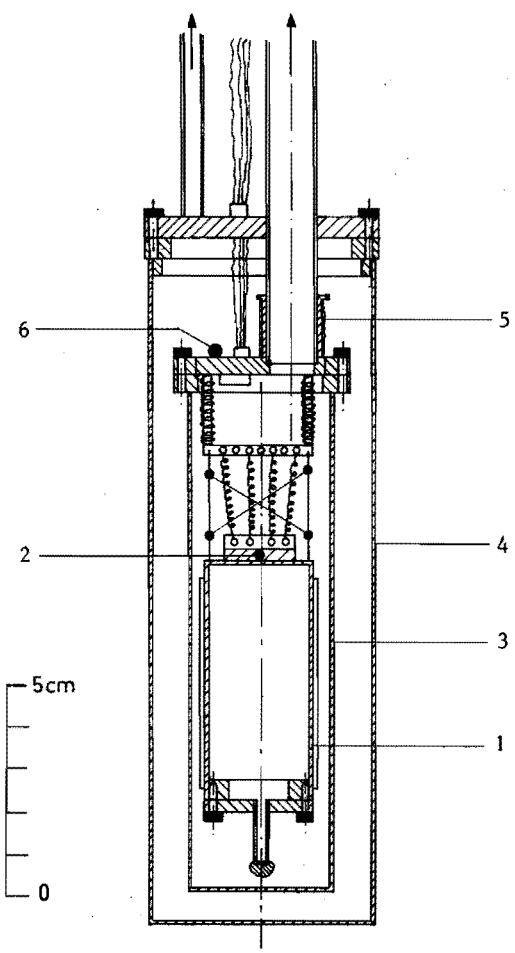

FIG. 4.1. Schematic cross-section of the calorimeter. Some details of the construction are given in the text.

indium O-ring seals. To establish thermal equilibrium within the specimen, a little ^{3}He gas (< 10 Torr at 77 K) was used. Discrete heat inputs could be supplied by means of a heater, made of about 20 m. of manganin wire, which was bifilarily wound around the capsule (R $\sim$ 1000 Ω). To achieve a good heat contact with the capsule, the heater was attached with GE 7031 varnish. During a heating period both the voltage and current supplied to the heater were measured with a digital voltmeter. Temperatures were measured with a "Cryocal" germanium resistance thermometer(2), having a nominal resistance of 1 KΩ at 4.2 K, which was firmly attached to the capsule. The thermometer was incorporated in an a.c. resistance bridge, which will be described in section 4.2.

The sample holder was suspended with silk threads inside a temperature controlled heat screen (3), to which all electrical connections were thermally anchored. The screen was fixed inside a copper can (4), which was placed in liquid ^{4}He. Outer can and screen were sealed with indium O-ring seals and were evacuated with a conventional high vacuum pump assembly. The top flange of the heat screen was linked to the helium bath with a stainless steel tube (ϕ 12 mm), which acted as a heat leak. A 100 Ω manganin heater (5) and a carbon thermometer (6) were employed in the temperature control unit, which will be described in section 4.2. The sample holder could be cooled to low temperatures by means of ^{4}He exchange gas.

4.2. Thermometer resistance bridge and temperature control unit

The basic circuit diagram of the a.c. resistance bridge, which operated at $\sim$ 172 Hz, is shown in Figure 4.2. A lock-in amplifier with input transformer is used as null-detector. To avoid excessive self-heating of the germanium thermometer, the bridge voltage has been chosen as 10 mV RMS, which produces a power dissipation of $\sim 10^{-7}$ W at 4.2 K. The electrical resistance of the thermometer supply leads ($\sim$ 10 Ω) has been compensated by using a three-wire measuring technique. Across the decade resistor a variable capacitor C was connected to balance the out of phase signal due to the capacity of the thermometer leads. The weighed input noise of the null-detector varied between 10^{-8} and 10^{-7} V peak to peak in 1 Hz bandwidth, which corresponds to a bridge resolution of a few parts in 10^6.

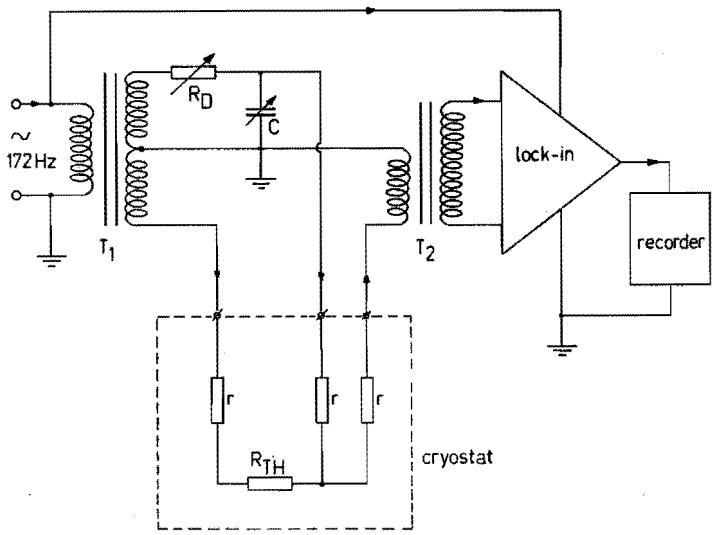

FIG. 4.2. Schematic circuit diagram of the thermometer resistance bridge. The different components are considered in the text.

With the germanium thermometer used in the heat capacity measurements temperatures could be determined with a resolution of $\sim 10^{-5}$ K at 4.2 K and $\sim 10^{-4}$ K at 50 K.

The temperature control unit basically consisted of an a.c. thermometer bridge as described above together with a booster amplifier, which was connected to the recorder output of the lock-in amplifier. The booster was activated only when the bridge voltage was negative, corresponding to screen temperatures lower than the desired value. A maximum power of 2 W could be supplied to the manganin heater on the top flange of the heat screen. About 0.3 W was required to maintain a temperature difference of 50 K between the screen and the helium bath. The amount of feedback was adjusted by means of the gain control of the lock-in amplifier. After changing the temperature setting, the temperature of the heat screen generally stabilized at the desired value within 10-60 seconds. Without any further precautions the temperature was found to be stable within 0.5 mK at 4.2 K and within 10 mK at 50 K for a period of one hour, which was much better than the experimental requirements.

4.3. Calibration and testing

The good temperature stability of the heat screen enabled us to perform an accurate calibration of the sample-holder thermometer against a factory calibrated germanium thermometer, which was used as a temperature-standard. The calibration of this standard-thermometer was based upon the NBS 1965 scale between 2 and 20 K with an accuracy of 5 mK from 2 to 5 K and 10 mK from 5 to 20 K. Above 20 K, the calibration was based upon the NBS 1955 scale with an accuracy of 40 mK from 20 K to 40 K and 100 mK above 40 K. The calibration data of the sample-holder thermometer were fitted to a polynomial of the form

$$[\ln(R)/T]^{1/2} = \sum_n A_n [\ln(R)]^n .$$

Since it was not possible to cover the whole temperature region between 2 K and 50 K with sufficient accuracy by one fit, the data below and above $\sim$ 13 K were fitted separately. The standard-deviation of the fit with n = 9 for the 82 data points in the range 2 - 15 K did amount to 0.03 %. The 56 data between 10 K and 52 K could be fitted with a standard-deviation of 0.02 %. Between 10 K and 15 K, the two fits did overlap within 0.1 %.

For the specific heat measurements a discontinuous heating technique was employed. The temperature increase of sample plus addenda was measured upon an accurately known heat input. Typical heating periods were about 50 - 150 seconds. The error in the determination of the heat input and the variation of the thermometer resistance was typically less than 0.1 %. The heat capacity C_a of the empty capsule was measured in a separate run. The data were described by a polynomial of the form $C_a = \sum_n B_n T^{2n+1}$ with a standard-deviation of 0.37 % for n = 9. The contribution of C_a to the total heat capacity did amount to $\sim$ 25 % at 2 K and 40 % at 50 K.

To check the overall accuracy of the apparatus the heat capacity of $\sim$ 100 grams of 99.999 % spectographic pure copper was measured. The data below 25 K were compared with the copper reference equation of Osborne et al. [1], those above 25 K with the selected values of Furukawa et al. [2]. The overall agreement was very satisfactory. Our data were slightly higher ($\sim$ 1 %) than the values quoted above, which is most likely caused

by the method of preparation of the specimen. The relative deviations for different temperatures varied slowly around their mean value; they showed maxima at 15 K and 45 K and a minimum at $\sim$ 30 K, the difference between maxima and minimum being about 0.8 %. These variations, which are much larger than the scatter in the experimental data, are shown [1] to arise mainly from small systematic errors in the calibration of the thermometer, and therefore may reflect the uncertainty of the heat capacity measurements, which is estimated to be less than $\sim$ 1 %.

REFERENCES CHAPTER IV

1. D.W. Osborne, H.E. Flotow, and F. Schreiner, Rev. Sci. Instr. 38, 159 (1967).

2. G.T. Furukawa, W.G. Saba, and M.L. Reilly, *National Standard Reference Data Series*, N.B.S. 18, Washington (1968).

CHAPTER V

SPECIFIC HEAT OF THE NEARLY ONE-DIMENSIONAL COMPOUNDS TMCC, TMMC AND TMNC

5.1. Introduction

Several investigations [1-4] have shown that at room temperature the series of compounds $(CH_3)_4NMCl_3$, with M = Mn, Ni or Cd, have isomorphous hexagonal structures with space group $P6_3/m$ and two formula units per unit cell. The crystals contain infinite linear chains of face-shared MCl_6 octahedra ($-M-Cl_3-M-Cl_3-$) separated by tetramethylammonium (TM) ions. The crystallographic arrangement is schematically drawn in Figure 5.1. The chains are located parallel to the c axis, the distance between the metal ions within a chain being $\sim$ 3.3 Å. Since the interchain metal

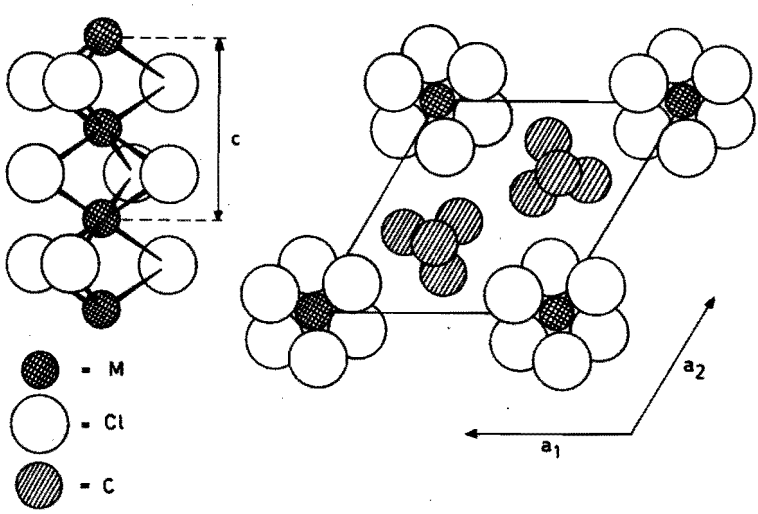

FIG. 5.1. Schematic representation of the room-temperature structure of TMCC, TMMC and TMNC. Linear chains of the form $-M-Cl_3-M-Cl_3-$, shown at the left hand side, are located parallel to the c axis. The chlorine ions are situated on mirror planes at 1/4 and 3/4 along c. The TM ions are located on three-fold axes in an orientationally disordered manner on planes 1/4 and 3/4 along c. (after Peercy et al. [4]).

ion distance amounts to $\sim$ 9 Å, one-dimensional magnetic characteristics may be expected for $(CH_3)_4NMnCl_3$ (TMMC) and $(CH_3)_4NNiCl_3$ (TMNC). TMMC, TMNC and TMCC show a phase transition to a monoclinic structure at T = 126, 171 and 118 K, respectively [4]. This transition, however, produces only a very slight shift of the $M\text{-}Cl_3\text{-}M\text{-}Cl_3$ chains within the a_1a_2 plane, and does not essentially change their internal structure.

Because the elastic properties of these compounds have been found to be strongly anisotropic [4], the low temperature specific heat of the diamagnetic $(CH_3)_4NCdCl_3$ (TMCC) may serve as a good check on the applicability of the description of the lattice heat capacity presented in Chapter III. Furthermore, the heat capacity of TMCC may be used to estimate the lattice contribution to the heat capacity of TMMC and TMNC. This enables us - in principle - to confront the magnetic specific heat of these two compounds with the predictions of some of the model systems outlined in Chapter II.

5.2. *$(CH_3)_4NCdCl_3$ (TMCC)* [5]

Crystals of TMCC were grown by slow evaporation of an aqueous solution of stoichiometric amounts of $CdCl_2$ and $[(CH_3)_4N]Cl$. The starting materials contained less than 0.1 % impurities. The dimensions of the single-crystals were typically in the order of a few millimeters.

Specific heat measurements were performed between 2.5 and 52 K with the experimental apparatus described in Chapter IV. However, due to the relatively high contribution of the sample holder, the uncertainty in the measurements at low temperatures was rather large. Therefore the specimen was measured in a separate run for $1.75 < T < 5$ K with a second calorimeter. This calorimeter was essentially identical to the apparatus described in Chapter IV, but no heat screen was used. Furthermore, the sample holder was entirely made of copper, which resulted in a rather small contribution to the total heat capacity at low temperatures.

Recently, Blacklock et al. [6] have reported specific heat measurements in the temperature range from 1.66 to 17.72 K. Their data agree within 2 % with our results. The data were analyzed by describing them with an "apparent" Debye temperature Θ_a (cf. Chapter III). The effective number of vibrating units in a formula unit was assumed to amount to 9

in the temperature region of interest. The experimental results are represented by dots in Figure 5.2, which reveals a rather pronounced dip in Θ_a at $\sim$ 6 K. Obviously the specific heat of TMCC cannot be described with a three-dimensional Debye model. The fact that the dip occurs at temperatures lower than $\frac{1}{20}\,\Theta_a$, where the Debye function is proportional to T^3, suggests that for T < 6 K higher order terms should be added to describe the heat capacity. Blacklock et al. tried to fit their data with a power series of the form

$$C = aT^3 + bT^5 + cT^7 + \ldots\ldots, \qquad (1)$$

but even this polynomial could not be fitted without large deviations from the experimental data.

In view of these results we may expect that TMCC offers a good opportunity to check the applicability of the theory given in Chapter

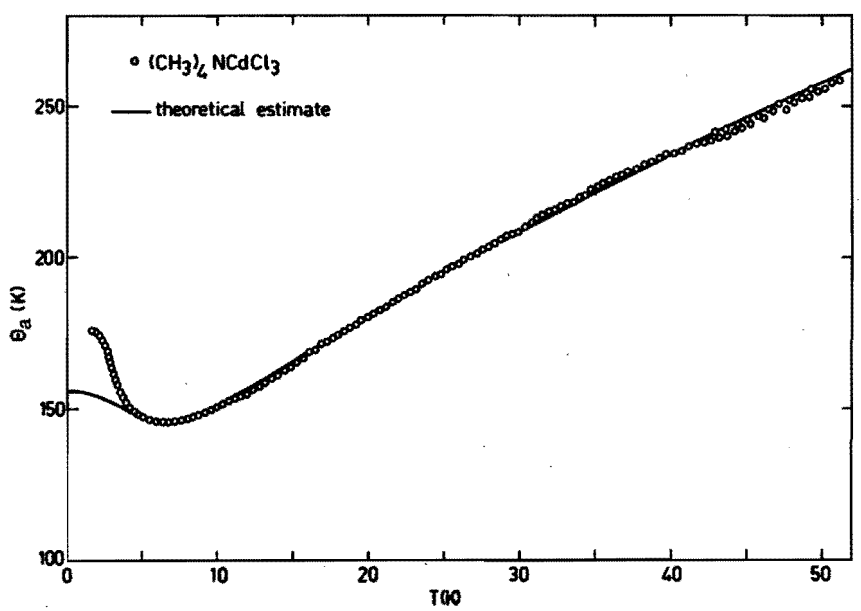

FIG. 5.2. Representation of the specific heat of TMCC by an "apparent" Θ_a value. The circles correspond to the experimental data, the drawn curve denotes the best fit to the data above 4 K.

III. The data between 4 and 52 K, where the experimental uncertainties are expected to be small, were therefore described with the equation

$$C = F_1(\Theta_\ell,\Theta_c,T) + F_1(\Theta_t,\Theta_c,T) + F_2(\Theta_o,\Theta_s,T), \qquad (2)$$

which contains 5 independent parameters. The fitting procedure, however, revealed a strong correlation between the parameters Θ_ℓ,Θ_t and Θ_o, which is caused by the fact that the fit is performed in the - relatively limited - low temperature region. Because especially Θ_o, reflecting the "in chain" stiffness, showed a large standard-deviation, we imposed the additional condition $\Theta_o = 2\,\Theta_\ell$. This condition is consistent with the difference between the compressibilities along the crystallographic a and c axis in TMMC, which has been reported [4] to amount to a factor 4, if we assume that the dimensions of the MBZ are not too different. This assumption yields the additional relation $\Theta_s = 2\Theta_c$ (cf. Chapter III). With these simplifications the experimental data between 4 and 52 K could be described within a few percent. Only a small improvement was achieved by considering Θ_c and Θ_s as independent variables, and hence the expression with three parameters was preferred. The result is

$$\Theta_\ell = 442 \pm 4 \text{ K}$$
$$\Theta_t = 154 \pm 0.6 \text{ K}$$
$$\Theta_c = 36.5 \pm 0.1 \text{ K}.$$

The quoted errorbounds of the Θ-values correspond to their statistical uncertainty, given by the fitting procedure. The actual uncertainty, however, may be a few times larger, because the three parameters still appeared to be somewhat correlated. The fit is shown as a drawn curve in Figure 5.2. In the temperature region, where the fitting procedure has been performed, the agreement is very satisfactory. Only slight deviations, which are about twice the experimental uncertainty, are present.

Below 4 K, however, the theoretical prediction systematically deviates from the experimental data. This deviation cannot be eliminated by a readjustment of the parameter-values. In fact, the observed magnitude of the dip in the experimental Θ_a values cannot be accounted for by the theory presented in Chapter III. It may be shown, however, that the presence of one or more singularities in the frequency spectrum at

moderate ω which have not been included in the general treatment tend to increase the magnitude of the dip in Θ_a, if they involve a rather large number of degrees of freedom. In the present series of isomorphic compounds, these singularities - which are often attributed to low-lying librational states - have indeed been observed [4]. In the low temperature region, however, where they produce significant deviations, the specific heat of TMCC is in the order of 10^{-2} - 10^{-1} J/mol K, which is small compared to the total specific heat of the magnetic isomorphs (10^{-1}-1 J/mol K for TMMC and 1-4 J/mol K for TMNC). Therefore we conclude that the description of the heat capacity of TMCC, given by the simplified form of equation (2), may very probably serve as a good starting point for the description of the lattice contribution of TMMC and TMNC.

Finally we wish to remark that the quality of the fit appeared to be rather insensitive to small variations of the value of r, which reflects the "effective" number of vibrating units in a formula unit. On the other hand, measurements on the isomorphic TMMC by Dietz et al. [7] reveal that even at room temperature the total number of degrees of freedom hardly exceeds 27 N_{AV}, which strongly indicates that the conjectured value (9) is correct.

5.3. $(CH_3)_4NMnCl_3$ (TMMC) [5]

Tetramethylammonium manganese trichloride (TMMC) is considered as one of the best one-dimensional antiferromagnetic compounds known at this moment. The ratio of the inter- to intrachain exchange interactions $|J'/J|$ has been estimated to range between 10^{-3} and 10^{-5} [7]. The intrachain exchange interaction has been found to be highly isotropic, small anisotropy effects have only been observed in susceptibility measurements [8, 9]. Neutron-diffraction experiments [10, 11] have shown that the correlation length and the spin-wave dispersion relation along different directions are consistent with a highly one-dimensional behaviour with S = 5/2, although there exists some discrepancy between the inferred values for the intrachain exchange interaction. Both susceptibility [8] and low-temperature heat capacity [12, 13] measurements indicate that TMMC orders antiferromagnetically at T_c = 0.83 K. An overall picture of the heat capacity has been reported by Dietz et al. [7] at temperatures up to 300 K.

In view of the well-established one-dimensional magnetic behaviour at temperatures down to $\sim$ 1 K and the reported magnitude of the intra-chain interaction (J/k $\sim$ - 7 K), TMMC may - in principle - be used to check the theoretical prediction for the low temperature behaviour of the magnetic heat capacity, presented in Chapter II. For this purpose, measurements were performed between 2 and 50 K on a sample consisting of $\sim$ 0.1 mole of small crystals of TMMC, which were grown by slow evaporation of a solution of stoichiometric amounts of $MnCl_2.4H_2O$ and $[(CH_3)_4N]Cl$. Below 4 K, the data showed a good agreement with the measurements reported by Takeda [12]. The combined data for $0.3 < T < 50$ K are shown in Figure 5.3. Tabulated results for both TMMC and TMCC have been presented in literature [5].

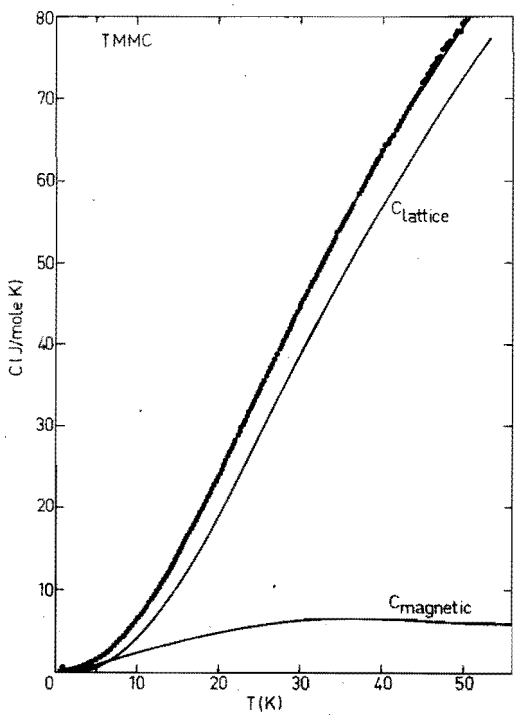

FIG. 5.3. Specific heat of TMMC. The drawn line through the data points represents the best fit to the total heat capacity. The lattice and magnetic contribution are also drawn separately.

In order to obtain experimental information about the magnetic contribution to the specific heat, we have to perform a separation of the magnetic and the lattice contribution. In general, such a separation is performed - at least within a restricted temperature region - by assuming that both the lattice and the magnetic contribution may be properly described by their respective limiting behaviour. In this case such a procedure is rather meaningless, since the limiting low-temperature behaviour of neither the lattice nor the magnetic contribution is known to a sufficient degree of accuracy. Of course, one may speculate on a certain limiting behaviour. Assuming a low-temperature magnetic contribution which varies linearly with temperature, various polynomial forms for the lattice heat capacity have been used. The results, however, were found to be rather inconclusive [5, 7, 13]. Moreover, as stated before, our aim is to confront the experimental data with the theoretical prediction over a rather large temperature region, and for this purpose a procedure as outlined above does not give much information.

A more direct approach to the problem may be found in the subtraction of a suitably scaled heat capacity of a diamagnetic isomorph. The only available compound for this purpose is TMCC, which has, however, the disadvantage that due to the rather large mass difference between the Mn^{++} and Cd^{++} ion, the scaling procedure suggested by Stout and Catalano [14] may introduce serious errors. Moreover it has been shown that the scaling factor is generally slightly temperature-dependent, and hence it may be incorrect to describe the whole region of interest with one single parameter. Despite this, the resulting magnetic heat capacity after subtraction of a scaled heat capacity of TMCC appeared to be rather realistic. The scaling factor was determined as 1.083 by the conditions that $C_M > 0$ in the whole temperature region and that the total evaluated magnetic entropy increase should amount to Rln6. The curve showed a maximum of $\sim$ 6.8 J/mol K at T $\sim$ 40 K, which is in agreement with the predicted behaviour of a Heisenberg S = 5/2 linear chain system with J/k $\sim$ -7.5 K. A more detailed examination, however, revealed rather large systematic deviations.

A more appropriate description of the lattice contribution to the heat capacity of TMMC may probably be possible with the theoretical approximation represented by equation (2).

In view of the good fit of the simplified form of this equation

($\Theta_o = 2\Theta_\ell$, $\Theta_s = 2\Theta_c$) to the heat capacity of TMCC and the isomorphy of TMCC and TMMC, we expect that an identical expression with roughly the same Θ-values will apply to the latter compound. We therefore attempted to fit the total specific heat of TMMC simultaneously varying the three parameters in the expression for the *lattice* specific heat as well as the exchange parameter J in the expression for the *magnetic* specific heat. The magnetic contribution was described with the S = 5/2 antiferromagnetic Heisenberg linear chain model treated in Chapter II. A least-squares fit to the experimental data above $\sim$ 2 K yielded

$$
\begin{aligned}
J/k &= -6.67 \pm 0.02 \text{ K} \\
\Theta_\ell &= 472 \pm 5 \text{ K} \\
\Theta_t &= 169 \pm 1 \text{ K} \\
\Theta_c &= 40.6 \pm 0.3 \text{ K}.
\end{aligned}
$$

The result is shown by drawn curves in Figure 5.3. In Figure 5.4 the relative error of the fit is plotted versus temperature. For comparison, the results for TMCC are plotted in the same figure.

As for TMCC, the quoted errorbounds of the parameter-values correspond

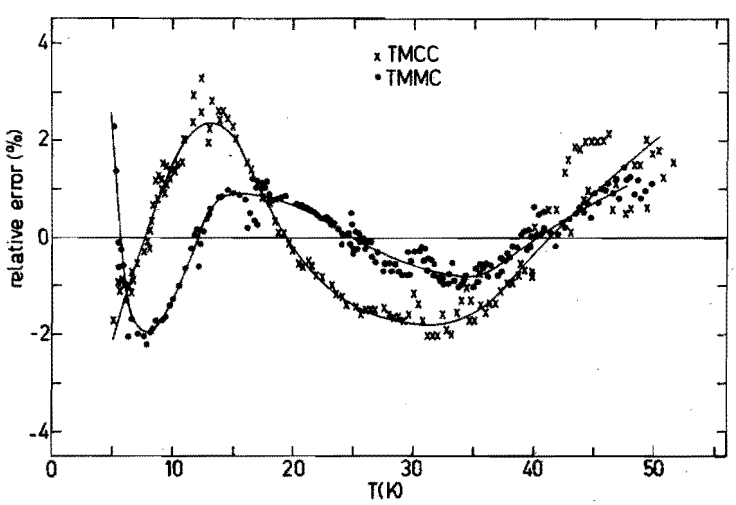

FIG. 5.4. Relative error of the best fit to the experimental specific heat of TMMC and TMCC as a function of temperature.

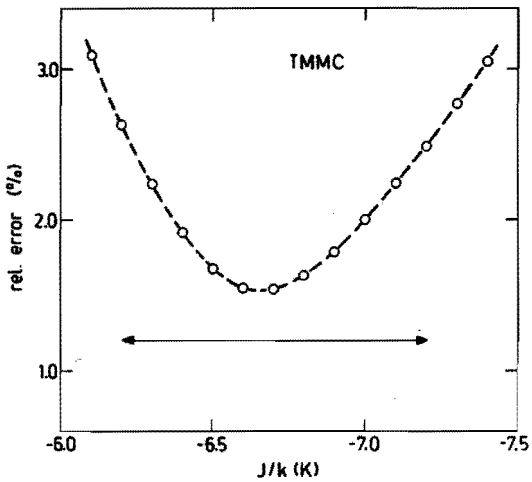

FIG. 5.5.
Standard-deviation of the fit to the specific heat of TMMC versus the value of the intrachain exchange interaction.

to their statistical uncertainty. The actual uncertainty in the determination of the intrachain exchange interaction J/k has been estimated by fitting the theoretical expression to the experimental data for several fixed J/k values. The RMS error of these fits is plotted in Figure 5.5. The uncertainty in the determination of J/k is estimated from this curve as 0.5 K. The value of J/k = -6.7 $\pm$ 0.5 K compares favourably with the values cited in literature, which are obtained from susceptibility, magnetization and neutron-diffraction experiments. A survey of these results is presented in Table 5.1.

TABLE 5.1. Values for the intrachain exchange interaction J/k in TMMC obtained from several experimental techniques.

Technique	J/k (K)	Reference
susceptibility	-6.3	[8]
susceptibility	-6.47 $\pm$ 0.13	[11]
neutron scattering	-7.7 $\pm$ 0.3	[11]
spinwave dispersion	-6.6 $\pm$ 0.15	[11]
specific heat	- 6.7 $\pm$ 0.5	present work

The inferred Θ-values for TMMC appear to be about 9 % higher than those for TMCC, which is consistent with the mass difference between the Cd^{++} and the Mn^{++} ion, if we assume that the binding forces in both compounds are roughly the same. If we consider, however, the change of Θ_ℓ, Θ_t and Θ_o in more detail, there appears to be a small change in their relative ratio, which is most likely caused by a small difference between the elastic anisotropy of TMMC and TMCC. Such a change cannot be accounted for by a simple temperature-independent scaling factor. This may be demonstrated by a description of the inferred lattice contribution of TMMC by a scaled heat capacity of TMCC according to the relation

$$C_{L,TMMC}(T) = C_{TMCC}(T/\alpha). \qquad (3)$$

The result is plotted in Figure 5.6 as a function of temperature. Although the variation of the scaling factor α seems to be rather small, it may give rise to serious systematic deviations in the determination of C_M at higher temperatures, because in that region $C_L >> C_M$.

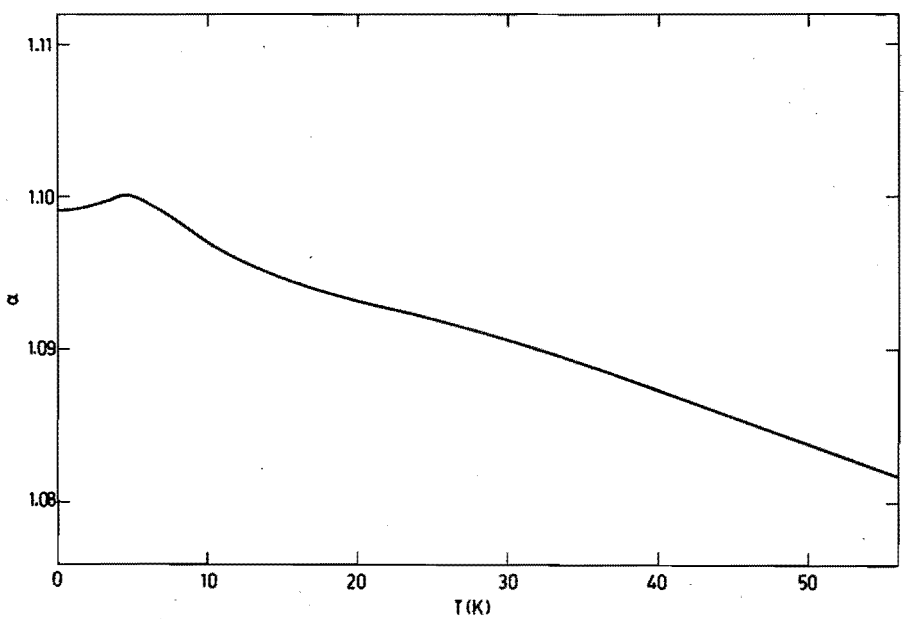

FIG. 5.6. Scaling factor α, defined by the relation $C_{L,TMMC}(T) = C_{L,TMCC}(T/\alpha)$, *as a function of temperature.*

Because of the small ratio $|J'/J|$ and the low three-dimensional ordering temperature, TMMC offers a good opportunity to get experimental evidence on the limiting low-temperature behaviour of an antiferromagnetic S = 5/2 Heisenberg linear chain system. One should note that the prediction for the low-temperature behaviour presented in Chapter II is only based upon a phenomenological description, while conventional spin-wave theory yields somewhat contradictory results. Therefore the temperature region below 7 K will be considered in more detail. At these temperatures, the magnetic heat capacity of TMMC has been approximated by

$$C_{M,TMMC}(T) = C_{EXP,TMMC}(T) - C_{EXP,TMCC}(T/1.09). \qquad (4)$$

We have subtracted a simply scaled heat capacity of TMCC to avoid any interference between magnetic and lattice contribution which might arise from simultaneous fitting procedures. The result is shown in Figure 5.7. The temperature-independent scaling factor was chosen as an average of the values of α for $T < 7$ K obtained from equation (3) (cf. Figure 5.6.) and the factor 1.083 obtained by simple temperature-independent scaling. Because at lower temperatures $C_M > C_L$, we expect that small variations of the scaling factor will not give rise to drastic changes in the curve for C_M. This is confirmed by the fact that below 7 K the curve obtained by equation (4) agrees within 2 % with the result obtained by subtracting the theoretical lattice contribution given above from the experimental data. For comparison, the total specific heat of both TMMC and TMCC is also plotted.

The shaded area represents the estimate for the low-temperature behaviour of a linear antiferromagnetic Heisenberg S = 5/2 system (cf. Chapter II):

$$C_M = -1.15\ kT/J + 0.41\ (kT/J)^2 + 0.08\ (kT/J)^3, \qquad (5)$$

with $J/k = -6.7$ K. The agreement is rather satisfactory. The small systematic deviations are comparable with the estimated inaccuracy of the theoretical prediction, which amounts to ~ 4 %. Moreover, the inferred value for the exchange interaction agrees very well with the value obtained from simultaneous fitting of C_M and C_L between 2 and 50 K. In view of this we conclude that the phenomenological description of the

low-temperature behaviour by equation (5) is in agreement with the experimental evidence, at least within the estimated inaccuracy.

Obviously the approximation of the magnetic heat capacity in this region by a power series of the reduced temperature kT/J is fairly good for S = 5/2. This might have been conjectured already from the fact that the coefficients in equation (5) seem to converge rapidly. The effect of truncation of the series may be examined by adding a fourth term, in which case the coefficients can be obtained from the following boundary

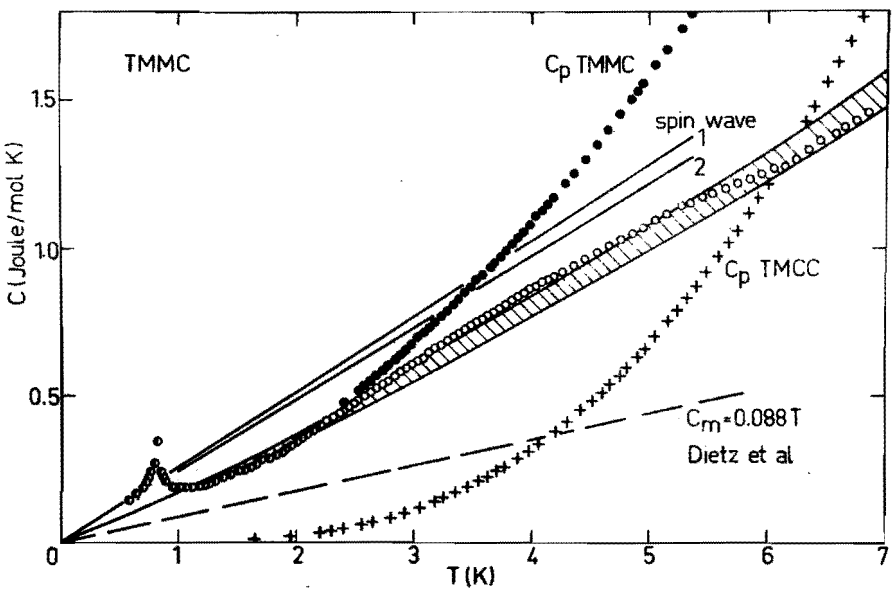

FIG. 5.7. Total specific heat of TMMC and TMCC, denoted by • and +, respectively. The open circles represent $C_{M,TMMC}$ and are obtained from $C_{M,TMMC}(T) = C_{EXP,TMMC}(T) - C_{EXP,TMCC}(T/1.09)$. Below ∿ 2 K the magnetic and the total heat capacity almost coincide. The shaded area is the estimated low-temperature behaviour for C_M in the case of Heisenberg exchange with $J/k = -6.7$ K. The curve denoted by "spinwave 1" represents the prediction from linear spin-wave theory for $J/k = -6.7$ K. The curve marked "spinwave 2" represents the result for C_M obtained from direct integration of the experimental spin-wave dispersion relation given by [7].

conditions. Firstly, we require that the series correctly predicts the heat capacity and derivative with respect to temperature at a "take-over" temperature T* in the region where the results obtained from H.T.E. are still accurate. Secondly, the total evaluated magnetic entropy increase should amount to Rln6, and the series should represent the results obtained by extrapolation of the heat capacity of finite chains as well as possible for $T < T^*$. By these conditions four coefficients are uniquely determined. The result is

$$C_M = -1.10\ kT/J + 0.50\ (kT/J)^2 + 0.13\ (kT/J)^3 + 0.008\ (kT/J)^4. \quad (6)$$

Analogous to the derivation of equation (5) (cf. Chapter II) the error has been estimated by varying T* as $\sim$ 4 %. Comparison of equation (5) and (6) shows that the quoted errorbounds of the phenomenological description are rather realistic, which is supported by the experimental evidence.

The region where C_M may be approximated by a linear term only is greatly obscured by the three-dimensional ordering phenomena. This region, however, does certainly not extend above $\sim$ 2 K, which corresponds to $|kT/J| \sim 0.3$. In view of this we conclude that the results of previous attempts to determine the exchange interaction in TMMC, which did rely on a linear temperature dependence of the magnetic contribution up till T $\sim$ 6 K, should be considered with reservations. For comparison some of these results are plotted in Figure 5.7.

TABLE 5.2. Theoretical and experimental estimates for the coefficient b_o in the expression $C_M/R = b_o T$ representing the limiting behaviour for $T \to 0$ of the heat capacity of an antiferromagnetic Heisenberg linear chain.

Substance	S	theory: spinwave	theory: numerical	experiment
$(CH_3)_4NMnCl_3$	5/2	0.21 [15]	0.14 [26]	0.13, present work
$CuCl_2 \cdot 2HC_5H_5$	1/2	1.05 [15]	0.35 [16]	0.36 [17, 18]

The theoretical prediction for the limiting low-temperature behaviour of the heat capacity of an antiferromagnetic Heisenberg linear chain system has - to our knowledge - only been confronted with experimental evidence for S = 1/2 and S = 5/2. Results are presented in Table 5.2, which demonstrates that conventional spin-wave theory tends to give a better prediction as the spin quantum number increases.

5.4. $(CH_3)_4NNiCl_3$ (TMNC) [19]

In contrast to the behaviour of TMMC, the magnetic interactions in TMNC do not seem to be very well established. The powder susceptibility has been measured for 1.6 - 79 K by Gerstein et al. [20], who reported deviations from a Curie-Weiss behaviour $\chi = C/(T-\Theta)$ with $\Theta = + 4.80 \pm 5.25$ K below 30 K. Their data strongly suggest that the dominant interaction is *ferromagnetic*. Specific heat measurements for $0.64 < T < 27.4$ K performed by Hurley and Gerstein [21] reveal a three-dimensional ordering peak at $T_c \simeq 1.21$ K superimposed on a broad bump with a maximum of 4.5 J/mol K at $T_m \simeq 1.5$ K. The critical entropy amounts to 0.21 R (19 %), which is low compared to the values predicted for various three-dimensional S = 1 models [22]. This suggests a rather low-dimensional character of the magnetic properties, which was already conjectured from the isomorphy with TMMC. In order to account for the magnitude of the heat capacity maximum, Hurley and Gerstein interpreted the data with the spin 1 linear Heisenberg model, but this yielded an *antiferromagnetic* intrachain interaction, which clearly is in disagreement with powder susceptibility measurements.

Single-crystal susceptibility measurements in the liquid hydrogen and helium region were performed by Dupas et al. [23]. They analyzed their data within the framework of a hamiltonian describing a Heisenberg linear chain system with uniaxial single-ion anisotropy

$$H = - 2J \sum_i \vec{S}_i \cdot \vec{S}_{i+1} - D \sum_i \left[S_{iz}^2 - \frac{1}{3} S(S+1) \right] . \qquad (7)$$

This resulted in $J/k = + 1.1$ K and $D/k = - 2.1$ K. The interchain interactions were estimated from $\chi_\perp$ in the ordered state and from a Green's function method [24], which yielded a J'/J value of 3×10^{-2} and 7×10^{-2}, respectively, confirming the conjectured one-dimensional mag-

netic behaviour at high temperatures. In view of this, we thought it worthwhile to analyse the specific heat data of Hurley and Gerstein in more detail, in order to confront them with estimates for the magnetic specific heat resulting from the hamiltonian (7), given in Chapter II. A reliable separation of the magnetic and lattice contribution to the heat capacity in TMNC seems possible, since the lattice heat capacity of the isomorphic TMCC has been determined fairly accurately.

The magnetic contribution C_M was obtained by subtracting the scaled heat capacity of TMCC. The scaling factor, which was assumed to be temperature-independent in the region under consideration, was determined by the conditions $C_M > 0$ and $\partial C_M/\partial T < 0$ for $T > 20$ K. This resul-

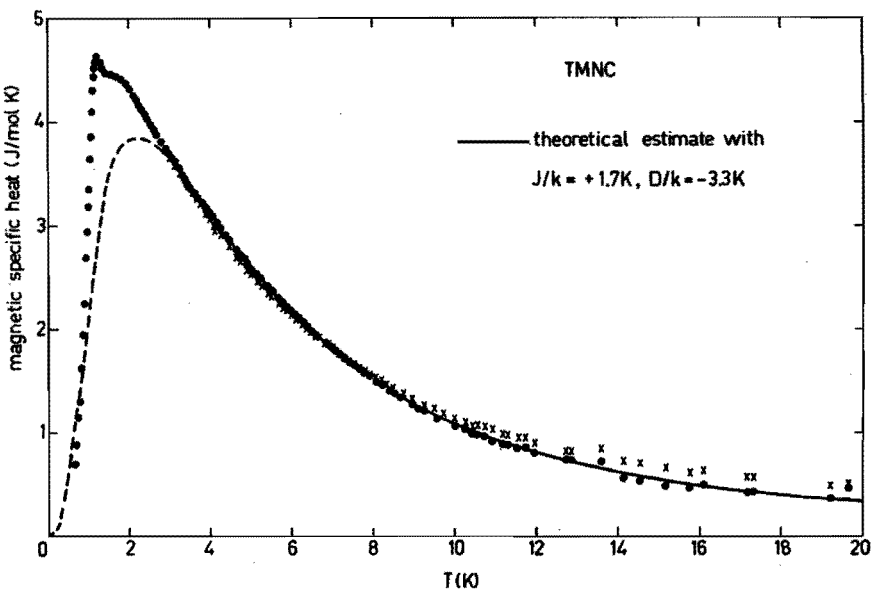

FIG. 5.8. Experimental magnetic specific heat of TMNC. The circles are the data obtained by subtracting a scaled heat capacity of TMCC from the total specific heat. The crosses represent the data obtained by subtracting a scaled lattice heat capacity of TMMC. The drawn curve denotes the best fit, corresponding to J/k = + 1.7 K, D/k = - 3.3 K. The dashed part of the curve indicates the estimated low-temperature behaviour, if no interchain interactions were present (cf. Chapter II).

TABLE 5.3. Values for the intrachain exchange interaction and the single-ion anisotropy in TMNC obtained from different experimental techniques.

Technique	J/k (K)	D/k (K)	Comment
Powder-susceptibility	+1.8 ± 2.0	---	[20] Θ-value 30-80 K
	+1.9	---	[20] Ising S = 1 3-80 K
	+1.0	---	[20] Fisher S = 1 2-80 K
Specific heat	-2.73	---	[21] 6-20 K
Single-crystal susceptibility	+1.1 ± 0.1	-2.1 ± 0.5	[23] 13-20 K
Specific heat	+1.7 ± 0.3	-3.3 ± 0.5	present work 3.5-20 K

ted in a scaling factor 1.230 ± 0.005. The total evaluated magnetic entropy increase, including the extrapolated contribution 0.02 R below T = 0.64 K, did amount to 1.09 R, which corresponds within 1 % to the theoretical value Rln3.

As outlined before, use of a temperature-independent scaling factor may produce some systematic deviations, since the mass difference between the Ni^{++} and the Cd^{++} ion is rather large. In order to check the accuracy of the procedure presented above we determined C_M in a similar way using the inferred lattice contribution of TMMC, which resulted in a scaling factor 1.125 ± 0.005. The magnitude of both scaling factors indicates that the binding forces in the Ni^{++} compound are significantly different from those in the Mn^{++} and Cd^{++} isomorphs. The results of both procedures are plotted in Figure 5.8. Both sets of data are quite consistent; significant differences are found for T > 12 K only.

The data for 3.5 < T < 20 K could be described within the experimental uncertainty with the hamiltonian (7) with J/k = + 1.7 ± 0.3 K, and D/k = - 3.3 ± 0.5 K. The parameters were obtained by a least-squares fit to the experimental C_M data. The best fit is shown as a drawn curve in Figure 5.8. Below T ≈ 3 K the observed magnetic specific heat rises systematically above the theoretical prediction, indicating that interchain interactions in this compound are presumably no longer negligible. This

is supported by the fact that the three-dimensional ordering temperature is comparable to the temperature corresponding to the maximum of C_M predicted for a linear chain model.

The values for J and D obtained from different experimental techniques are listed in Table 5.3. It appears that the present values are somewhat higher than those reported by Dupas et al. [23], which is most likely explained by the fact that their interpretation is based upon a Curie-Weiss behaviour of the susceptibility at liquid hydrogen temperatures. This is inconsistent with earlier measurements of Gerstein et al. [20], which reveal a Curie-Weiss behaviour at temperatures above 30 K only. In general, a $1/\chi$ versus T plot at temperatures low compared to the region in which the Curie-Weiss law $\chi = C/(T-\Theta)$ strictly holds will yield an extrapolated intersection Θ^* on the temperature axis with $\Theta^* < \Theta$. This indicates that the parameter-values obtained from the single-crystal susceptibility measurements are indeed to low.

The intrachain interaction in TMNC is found to be ferromagnetic, whereas this interaction in the isomorphic TMMC is strongly antiferromagnetic. As each magnetic ion is linked with its nearest neighbours within the chain by three chlorine bridges with a bond angle of about 80^o, this behaviour is not inconsistent with the model of Anderson [25], which predicts - for a 90^o bridge - a decreasing importance of the antiferromagnetic contributions to the superexchange going from $3d^5$ to $3d^8$.

REFERENCES CHAPTER V

1. B. Morosin and E.J. Graeber, Acta Crystallogr. 23, 766 (1967).
2. G.D. Stucky, Acta Crystallogr. B24, 330 (1968).
3. B. Morosin, Acta Crystallogr. B28, 2303 (1972).
4. P.S. Peercy, B. Morosin and G.A. Samara, Phys. Rev. B8, 3378 (1973).
5. W.J.M. de Jonge, C.H.W. Swüste, K. Kopinga and K. Takeda, Phys. Rev. B12, 5858 (1975).
6. K. Blacklock, H.F. Linebarger, H.W. White, K.H. Lee and S.L. Holt, J. Chem. Phys. 61, 5279 (1974).

7. R.E. Dietz, L.R. Walker, F.S.L. Hsu, W.H. Haemmerle, B. Vis, C.K. Chau and H. Weinstock, Solid State Comm. 15, 1185 (1974).

8. R. Dingle, M.E. Lines and S.L. Holt, Phys. Rev. 187, 643 (1969).

9. L.R. Walker, R.E. Dietz, K. Andres and S. Darack, Solid State Comm. 11, 593 (1972).

10. R.J. Birgeneau, R. Dingle, M.T. Hutchings, G. Shirane and S.L. Holt, Phys. Rev. Letters 26, 718 (1971).

11. M.T. Hutchings, G. Shirane, R.J. Birgeneau and S.L. Holt, Phys. Rev. B5, 1999 (1972).

12. K. Takeda, Phys. Letters 47A, 335 (1974).

13. B. Vis, C.K. Chau, H. Weinstock and R.E. Dietz, Solid State Comm. 15, 1765 (1974).

14. J. Stout and E. Catalano, J. Chem. Phys. 23, 2013 (1955).

15. R. Kubo, Phys. Rev. 87, 568 (1952).

16. J.C. Bonner and M.E. Fisher, Phys. Rev. 135A, 640 (1964).

17. K. Takeda, S. Matsukawa and T. Haseda, J. Phys. Soc. Japan 30, 1330 (1971).

18. K. Takeda, Y. Yamamoto and T. Haseda, Phys. Lett. 45A, 419 (1973).

19. K. Kopinga, T. de Neef, W.J.M. de Jonge and B.C. Gerstein, Phys. Rev. B13, 3953 (1976).

20. B.C. Gerstein, F.D. Gehring and R.D. Willett, J. Appl. Phys. 43, 1932 (1972)

21. M. Hurley and B.C. Gerstein, J. Chem. Phys. 59, 6667 (1973).

22. C. Domb and A.R. Miedema, "*Progress in Low Temperature Physics*", Vol. IV, North Holland Publishing Co., Amsterdam (1964).

23. C. Dupas and J.P. Renard, J. Chem. Phys. 61, 3871 (1974).

24. T. Oguchi, Phys. Rev. 133, A1098 (1964).

25. P.W. Anderson, "*Solid State Physics*", Vol. 14, Academic Press, New York (1963).

26. T. de Neef, Ph.D. Thesis, Eindhoven (1975).

CHAPTER VI

SOME MAGNETIC PROPERTIES OF $CsMnCl_3.2H_2O$, $\alpha RbMnCl_3.2H_2O$ and $CsMnBr_3.2H_2O$

6.1. Introduction

$CsMnCl_3.2H_2O$ (CMC), $\alpha RbMnCl_3.2H_2O$ (αRMC), and $CsMnBr_3.2H_2O$ (CMB) belong to a series of isomorphic compounds $AMB_3.2H_2O$ with A = Cs,Rb; M = Mn,Fe,Co; and B = Cl,Br. Their crystallographic structure is orthorhombic with space group Pcca and 4 formula units in a chemical unit cell [1, 2]. The A,M and one of the B ions occupy special positions on 2_c, 2_b and 2_c axes, respectively. The unit cell dimensions of the Mn compounds are given in Table 6.1. The crystallographic arrangement is schematically drawn in Figure 6.1. The structure can be considered as built up from *cis*-octahedra of four B ions and two oxygen ions. Neighbouring octahedra in the a direction share one B ion, and form slightly staggered chains along this axis, which are separated in the b direction by layers of A ions. In the c direction the chemical structure is kept together by hydrogen bonds.

The existence of $- M^{++} - B^- - M^{++} - B^-$ - chains in the a direction, where the B^- ions provide a superexchange coupling between the M^{++} spins, will very likely give rise to one-dimensional characteristics in the magnetic behaviour of these compounds. Especially in CMC these characteristics have been the subject of a large number of experimental investigations [3-11]. These studies reveal that above $\sim$ 9 K the magnetic behaviour can be described by a system of isolated chains of S = 5/2 ions with an isotropic antiferromagnetic intrachain exchange interaction J of about 3 K.

TABLE 6.1. The unit cell dimensions of $CsMnCl_3.2H_2O$, $\alpha RbMnCl_3.2H_2O$ and $CsMnBr_3.2H_2O$ at room temperature.

Substance	a (Å)	b (Å)	c (Å)	Reference
$CsMnCl_3.2H_2O$	9.060	7.285	11.455	[1]
$\alpha RbMnCl_3.2H_2O$	9.005	7.005	11.340	[2]
$CsMnBr_3.2H_2O$	9.61	7.49	11.94	[23]

In the next section, we will investigate to what extent the Heisenberg S = 5/2 linear chain model describes the magnetic *heat capacity* of CMC also. In order to perform such an analysis, however, we have to separate the magnetic and the lattice contribution to the total specific heat. It will be shown that the model presented in Chapter III offers a good description of the lattice heat capacity of CMC. An appropriate procedure to separate both contributions to the heat capacity will be outlined.

In CMC relatively small interchain interactions are present, giving rise to a three-dimensional ordering at T_N = 4.89 K. From linear spin-wave theory we may anticipate a drastic influence of these interactions on the magnetic properties below T_N, because in the limit of the *ordered* purely one-dimensional case the density of states would diverge in the origin of the $\vec{k}$ space. Therefore we shall consider the region below T_N in more detail in the second part of the next section.

In the last section the heat capacity of the two other Mn^{++} isomorphs, αRMC and CMB, will be analyzed. Such an analysis serves two different

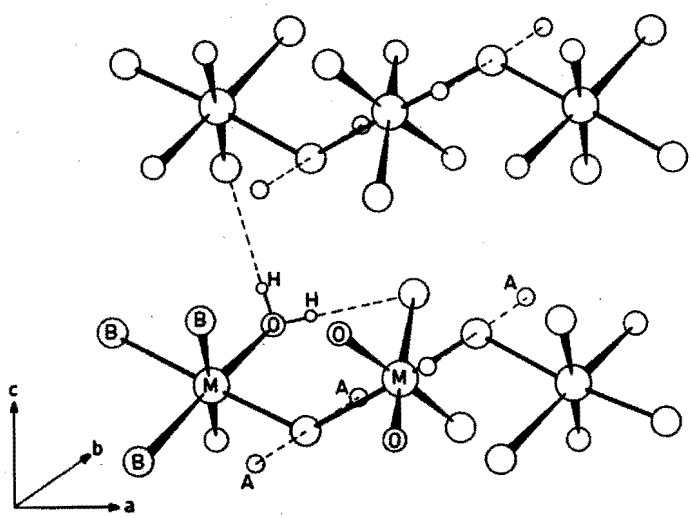

FIG. 6.1. Schematic representation of the crystallographic structure of $AMB_3 \cdot 2H_2O$. Only one set of hydrogens and hydrogen bonds is shown.

purposes. Firstly, these isomorphs involve rather different atomic masses, and hence the lattice contribution to the heat capacity may be fairly different from that of CMC. This may yield additional information about the reliability of the theoretical model for the lattice heat capacity. Secondly, by comparison of the magnetic behaviour of these compounds the influence of the intermediate alkali ion as well as the halide ions on the various magnetic interactions may be studied.

6.2. $CsMnCl_3.2H_2O$ (CMC) [9,12]

6.2.1. Introduction

As already mentioned, the magnetic properties of CMC have been the subject of a large number of experimental investigations. The intrachain interaction has been determined from susceptibility [3], neutron diffraction [5], and EPR [6, 7] studies. The magnetic space group in the ordered state has been determined from NMR experiments as $P_{2b}c'ca'$ [4]. The interchain interactions have been estimated by a Green's function method [4], and have been found experimentally from neutron-diffraction [5], EPR lineshape [7] and NMR [13] studies. Recently a fairly consistent set of interactions has been determined from a spin-wave analysis of the susceptibility in the ordered state [10]. The available experimental evidence indicates that the ratio of the interchain interactions to the intrachain interaction is in the order of 10^{-2} - 10^{-3}.

In view of these extensive investigations it is surprising that no detailed heat capacity measurements have been reported. The main reason for this may be found in the fact that no reliable estimate was available for the relatively large lattice contribution. A direct interpretation of the heat capacity measurements was hampered by the fact that all attempts to grow a diamagnetic isomorph were unsuccessful. Furthermore, an independent determination of the lattice heat capacity by saturating the magnetic system with an external magnetic field was precluded by the magnitude of the intrachain coupling and the temperature region of interest. A description of the lattice contribution with the usual three-dimensional Debye model yielded very unsatisfactory results.

A more appropriate description of the lattice heat capacity may be found by considering the typical chemical structure of these compounds. As already mentioned, the chemical structure in the c direction is kept together by hydrogen bonds. Because the crystals cleave very easily parallel to the ab plane and no other cleavage planes are present, we assert that, from a *lattice dynamical* point of view, these compounds may be considered as systems of loosely coupled layers. Hence we expect that the model presented in Chapter III may provide a fair description of the lattice heat capacity.

Single-crystals of CMC were grown by slow evaporation of an equimolar solution of CsCl and $MnCl_2.4H_2O$. They showed the morphology described by Jensen et al. [1]. A specimen consisting of $\sim$ 38 grams of small crystals (average dimensions 2 x 5 x 5 mm) was measured with the calorimeter described in Chapter IV. The data between 1.1 and 52 K are shown in Figure 6.2. Above the three-dimensional ordering temperature, the total heat

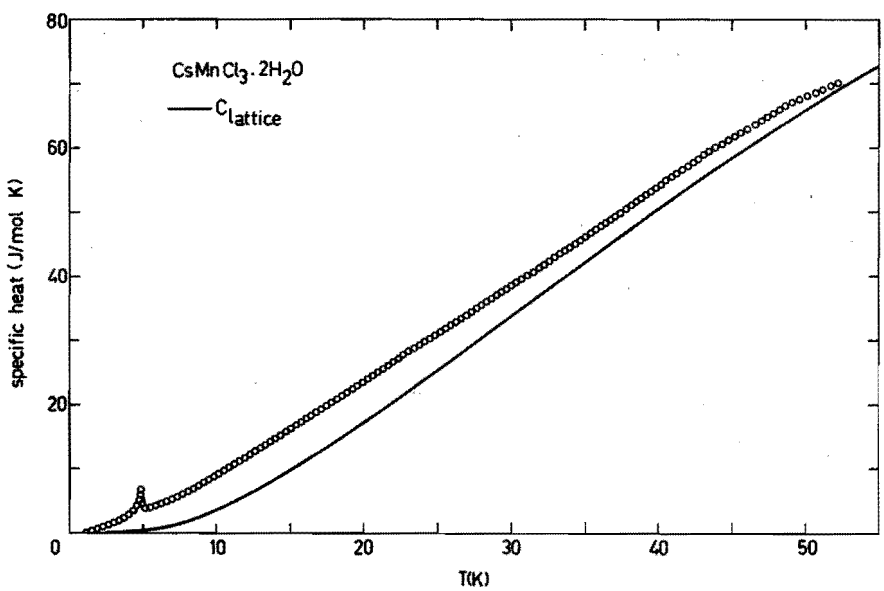

FIG. 6.2. Specific heat of $CsMnCl_3.2H_2O$ versus temperature. The open circles represent the experimental data, the drawn line denotes the lattice contribution obtained from the procedure outlined in section 6.2.2.

capacity gradually increases to $\sim$ 70 J/mol K, indicating that the magnetic heat capacity in the paramagnetic region is completely dominated by the lattice contribution. We will first focus our attention on this region.

6.2.2. Heat capacity in the paramagnetic region

In view of the reported experimental results, the magnetic heat capacity above 9 K has been described by the S = 5/2 antiferromagnetic Heisenberg linear chain model, presented in Chapter II. To reduce the total number of parameters as much as possible, the lattice contribution was represented by the simplified form of the expression for the heat capacity of a layered structure, given in Chapter III:

$$C_L(T) = F_1(2\Theta_t, \Theta_c, T) + F_1(\Theta_t, \Theta_c, T) + F_2(\Theta_o, 2\Theta_c, T). \qquad (1)$$

It was assumed that in the temperature region of interest the H_2O molecules vibrate as a whole and that rotational states are of no importance. This yields a number of 7 vibrating units in a formula unit.

We fitted the data above 9 K simultaneously varying the three parameters in the expression for the lattice specific heat as well as the parameter J/k in the expression for the magnetic specific heat. This yielded

$$J/k = -2.85 \pm 0.02 \text{ K}$$
$$\Theta_t = 287 \pm 1.0 \text{ K}$$
$$\Theta_o = 204 \pm 1.5 \text{ K}$$
$$\Theta_c = 56.0 \pm 0.5 \text{ K}.$$

The quoted errorbounds correspond to the uncertainty of the parameter-values assuming that the deviations are statistical in nature. The actual uncertainty, however, may be larger. Since we are primarily interested in the value of the exchange interaction J/k, we performed several fits in which this parameter was fixed at a certain value. The RMS error of these fits is plotted in Figure 6.3 as a function of J/k. From this curve no reliable upperbound for $|J/k|$ can be determined. Therefore the possible

uncertainty was estimated independently by considering the total magnetic entropy gain associated with these fits. Below 1.1 K, the entropy increase was estimated by approximating the heat capacity down to T = 0 with the relation $C_M = \alpha T^{\beta}$. α and β were obtained from a double-logarithmic plot of the data between 1.1 and 1.5 K. The extrapolated fraction did amount to $\sim$ 0.5 %. For 1.1 < T < 52 K, the entropy gain was calculated by numerical integration of $(C_{EXP}-C_{L,CALC})/T$, while the increase above 52 K was determined from the high temperature series expansion for an antiferromagnetic S = 5/2 Heisenberg linear chain system. For the various fits, this fraction typically did amount to $\sim$ 10 %. Since the magnetic heat capacity below 9 K has been obtained by subtracting an extrapolated lattice contribution, we estimate that the error in the calculation of $S_\infty - S_o$ may be $\sim$ 3 %. Given a spinvalue of 5/2, the value of $S_\infty - S_o$ should amount to Rln6 within this uncertainty. This condition was found to be satisfied

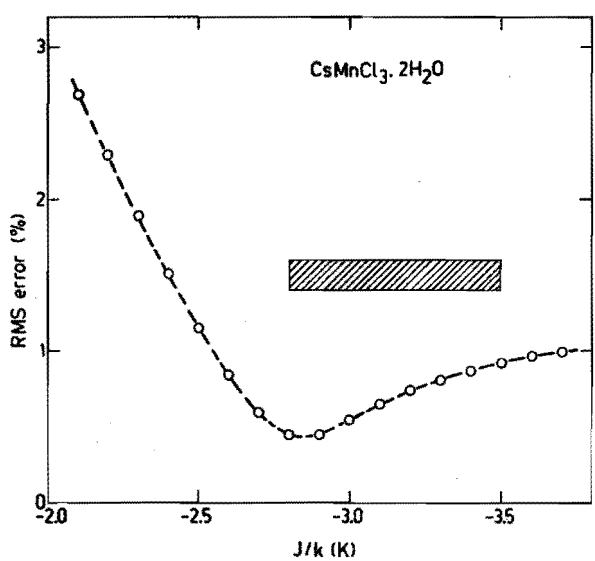

FIG. 6.3. RMS error of fits of the theoretical expression to the experimental specific heat of $CsMnCl_3.2H_2O$ between 9 and 52 K for fixed values of J/k. The shaded bar denotes the region in which the total magnetic entropy gain amounts to Rln6 within the experimental uncertainty.

TABLE 6.2. Values for the intrachain exchange interaction J/k in $CsMnCl_3.2H_2O$ obtained from several experimental techniques. Except for the heat capacity results no errorbounds were reported.

Technique		J/k (K)	Reference
I	Paramagnetic susceptibility	-3.12	[3]
II	I + quantumcorrections	-3.00	[3]
III	Perpendicular susceptibility below T_N	-3.39	[8]
IV	Spin-wave analysis of X below T_N	-3.2	[10]
V	Neutron scattering	-3.53	[5]
VI	Electron paramagnetic resonance	-3.57	[6]
VII	Specific heat	-3.3 ± 0.3	[9]
VIII	Specific heat	$-3.0 \begin{smallmatrix} +0.2 \\ -0.4 \end{smallmatrix}$	present work

for $-2.8 > J/k > -3.5$ K, which is represented by the shaded bar in Figure 6.3. The intrachain interaction is estimated from a weighed average of both procedures presented in this figure as $J/k = -3.0 \begin{smallmatrix} +0.2 \\ -0.4 \end{smallmatrix}$ K. This value is in good agreement with the reported experimental results obtained from susceptibility, neutron-diffraction and EPR linewidth studies. For comparison, a survey of these results is presented in Table 6.2.

The theoretical lattice contribution $C_{L,CALC}$ corresponding to $J/k = -3.0$ K is shown as a solid line in Figure 6.2. The experimental magnetic heat capacity $C_{EXP}-C_{L,CALC}$ is represented by the open circles in Figure 6.4, while the drawn curve denotes the theoretical estimate for a S = 5/2 Heisenberg linear chain with $J/k = -3.0$ K. The errorbars reflect the uncertainty in the experimental determination of the *total* heat capacity ($\sim$ 1 %). The agreement is very satisfactory. The small systematic variations of the experimental data around the theoretical curve above 12 K show a striking resemblance to the deviations, which were observed in the

results of the measurements on pure copper (cf. Chapter IV). Therefore these variations will reflect a systematic experimental error rather than any inadequacy of the theoretical description. Below 7 K, the experimental data begin to deviate significantly from the theoretical curve, which indicates that in this region the interchain interactions are presumably no longer negligible. The ordering phenomena will be discussed in some detail in Chapter VIII.

The question may arise, to what extent the inferred value of the intrachain exchange coupling depends on the particular expression for the lattice contribution used in the separation procedure. In principle, this problem may be examined by simultaneous fits of the lattice and the magnetic heat capacity to the experimental data for various expressions for the lattice contribution. Because the physical relevance of a number of

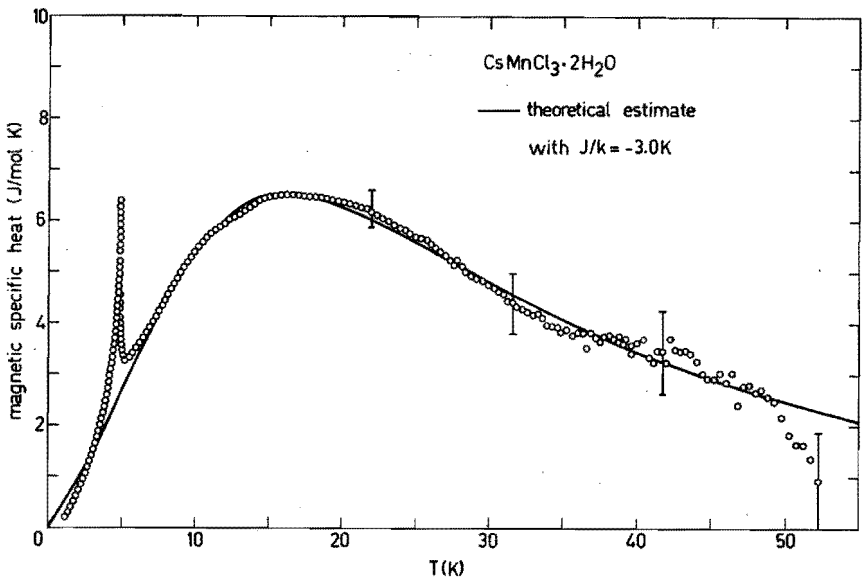

FIG. 6.4. Magnetic heat capacity of $CsMnCl_3.2H_2O$. The open circles correspond to the experimental data minus the calculated lattice contribution, the errorbars reflect the experimental uncertainty in the determination of the total heat capacity. The drawn curve denotes the theoretical estimate for a $S = 5/2$ Heisenberg linear chain system with $J/k = -3.0$ K.

*TABLE 6.3. Values for the intrachain exchange interaction J/k in $CsMnCl_3.2H_2O$ obtained from simultaneous fits of the lattice and magnetic heat capacity to the experimental data. The column headed "C_L" gives the model with which the lattice heat capacity has been described. In the cases marked *) both systematic deviations and correlations between the description of the lattice and the magnetic heat capacity have been taken into account.*

C_L	J/k (K)	RMS error
$7D_3(\Theta_3)$	-2.8 ± 0.7	$\sim$ 30 %
$7D_2(\Theta_2)$	-2.95 ± 0.25	$\sim$ 10 %
$7[\frac{2}{3} D_2(\Theta_2') + \frac{1}{3} D_2(\Theta_2'')]$	-3.32 ± 0.02	$\sim$ 1 %
Tarasov, modified	-3.3 ± 0.3*)	0.4 - 1 %
pseudo-elastic	$-3.0 \begin{smallmatrix}+0.2\\-0.4\end{smallmatrix}$*)	0.4 - 0.8 %

these expressions has already been considered before [9], we will confine ourselves to a summary of the results, which is presented in Table 6.3. It appears that, although some of these fits show very large systematic deviations from the experimental data, the resulting values for J/k are within 10 % equal to the value obtained from the present analysis. Hence we conclude that, given the characteristic properties of CMC, a fairly accurate determination of the intrachain exchange interaction has been possible. From the measurements in the paramagnetic region, however, no estimate for the magnitude of the interchain interactions could be deduced. Since we anticipate a drastic influence of these interactions on the magnetic properties below T_N, we will consider the ordered state in the next part of this section.

6.2.3. Spin-wave analysis of the ordered state

Because the magnetic structure of CMC in the ordered state is well-established [4, 5], the calculation of the spin-wave spectrum is rather straightforward, if only nearest-neighbour interactions are taken into account. The magnetic structure is schematically drawn in Figure 6.5. The intrachain interaction along the a axis is denoted by J_1; J_2 and J_3 represent the interchain interactions along the c and b axis, respectively. It is evident that all interactions are antiferromagnetic, and that neighbouring spins belong to different sublattices. The system will therefore be described with the hamiltonian

$$H = -2 \sum_{\ell,m} J_{\ell m} \vec{S}_\ell . \vec{S}_m - g\mu_B H_A \left(\sum_\ell S_\ell^z - \sum_m S_m^z \right), \qquad (2)$$

where H_A denotes the anisotropy-field arising from - relatively small - dipolar and crystal-field effects. The indices ℓ,m refer to spins located on the + and - sublattice, respectively. Within the Holstein-Primakoff

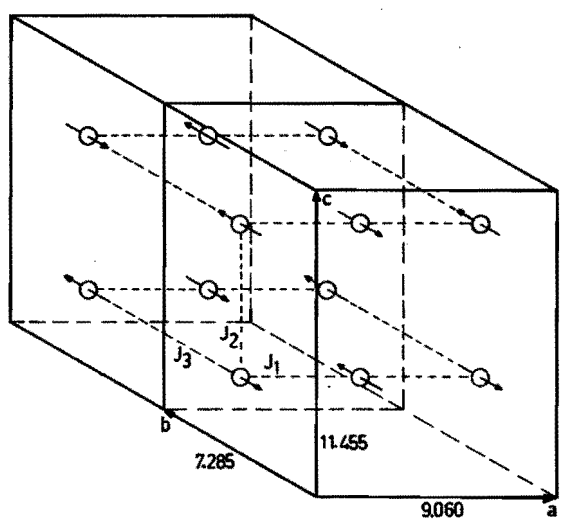

FIG. 6.5. The spin array of $CsMnCl_3.2H_2O$ in the ordered state. The drawn figure corresponds to the magnetic unit cell. J_1 denotes the intrachain interaction along the a axis, J_2 and J_3 are interchain interactions.

formalism [14], this hamiltonian can be written as

$$H = 2 \sum_{\ell,m} J_{\ell m}[S^2 - S(a_\ell^* a_\ell + b_m^* b_m + a_\ell^* b_m^* + a_\ell b_m)]$$

$$- g\mu_B H_A[\sum_{\ell} (S - a_\ell^* a_\ell) + \sum_{m} (S - b_m^* b_m)]. \qquad (3)$$

a_ℓ^*, a_ℓ and b_m^*, b_m represent creation and annihilation operators acting on spins at + and - lattice sites, respectively. All terms of higher order than quadratic in these operators are neglected (unrenormalized spin-wave theory). The next step in the derivation is the introduction of the Fourier transforms of the creation and annihilation operators and the diagonalization of the hamiltonian by a suitably chosen canonical transformation [15, 16]. The result is

$$E_{n,p} = NS(S+1) \sum_{h} J(\vec{r}_h) - g\mu_B N H_A (S+\tfrac{1}{2})$$

$$+ \sum_{k} (n+\tfrac{1}{2})\varepsilon(\vec{k}) + \sum_{k} (p+\tfrac{1}{2})\varepsilon(\vec{k}) \qquad (4)$$

$$n,p = 0,1,2,.....$$

In this expression N denotes the total number of spins, and $\vec{k} = \frac{2\pi}{\lambda}\vec{e}_k$, a wave vector in the direction of the unit propagation vector $\vec{e}_k$. The following substitutions have been made:

$$\vec{r}_h = \vec{r}_\ell - \vec{r}_m \quad , \quad \varepsilon(\vec{k}) = \{\varepsilon_m^2 - [b(\vec{k})]^2\}^{1/2}$$

$$\varepsilon_m = -2S \sum_{h} J(\vec{r}_h) + g\mu_B H_A \quad , \quad b(\vec{k}) = -2S \sum_{h} J(\vec{r}_h) e^{i\vec{k}.\vec{r}_h} . \qquad (5)$$

ε_m corresponds to the maximum energy of the spin-wave spectrum, which is twofold degenerate in zero applied field. If the slight zig-zag of the chains in the a direction is ignored, the contribution of the exchange interactions can be evaluated as

$$\sum_{h} J(\vec{r}_h) = 2(J_1 + J_2 + J_3)$$

$$\sum_{h} J(\vec{r}_h) e^{i\vec{k}.\vec{r}_h} = 2[J_1 \cos(k_a a/2) + J_2 \cos(k_c c/2) + J_3 \cos(k_b b)]. \qquad (6)$$

Usually, the density function N(ε) is calculated from the small-k approximation of the dispersion relation [17]. In this pseudo one-dimensional system, however, this approximation has been shown to give very unsatisfactory results [11]. Therefore the density fuction was calculated by the root sampling method. A large number of energies were generated by solving the dispersion relation (5) for a large number of uniformly distributed points within the first Brillouin zone, and the real spectrum was approximated by a normalized histogram. The sampling was performed according to the procedure described in [11]. In Figure 6.6 the density function is shown for some representative values of the exchange interactions. ε_o denotes the minimum energy of the spin-wave spectrum, corresponding to $\vec{k} = 0$. As anticipated above, the low-energy part of the spectrum appears to be very sensitive to the ratio J_2/J_1. Therefore we expect that the magnitude of the

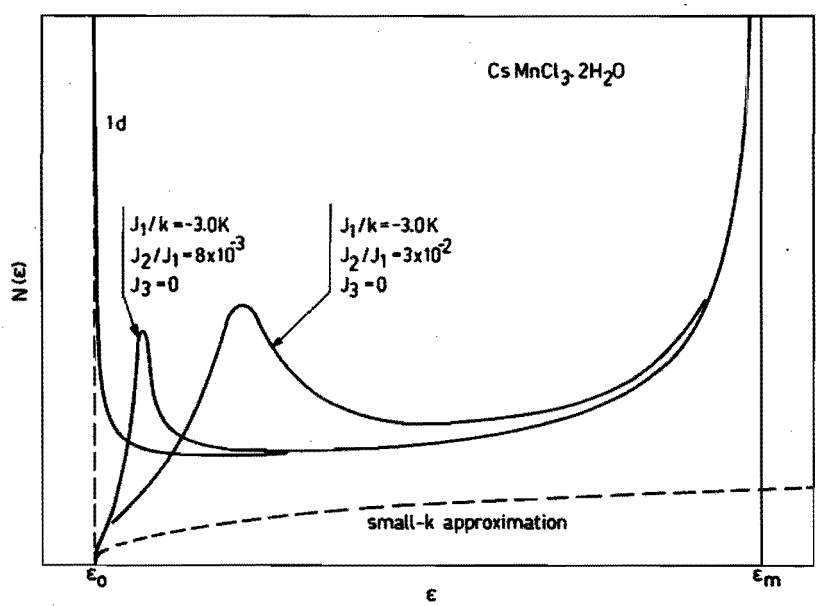

FIG. 6.6. Magnon density of states N(ε) versus ε calculated for $CsMnCl_3 \cdot 2H_2O$ for different sets of exchange constants. The curve marked "1d" denotes the purely one-dimensional limit ($J_2 = J_3 = 0$). The dashed curve reflects the small-k approximation for a representative set of exchange constants.

interchain coupling may be estimated from the thermodynamic properties at low temperatures.

Firstly we will consider the magnetic specific heat, which is related to the normalized spectrum $N(\varepsilon)$ by

$$C_M(T) = k \int_{\varepsilon_o}^{\varepsilon_m} (\varepsilon/kT)^2 e^{\varepsilon/kT} [e^{\varepsilon/kT}-1]^{-2} N(\varepsilon) d\varepsilon, \qquad (7)$$

since the spin-waves described by equation (4) and (5) can be considered as decoupled Bose-oscillators. The integral may be solved numerically. In an actual calculation, one should note that the lower bound of the spin-wave energy spectrum (ε_o) is found to be temperature-dependent. In CMC, ε_o has been determined experimentally from neutron-diffraction experiments [5]. The observed temperature-dependence could be described by assuming a renormalization of ε_o proportional to the sublattice magnetization (ε_o = 2.2 K at 1.5 K, 1.7 K at 4.2 K). In the present calculations, this variation of ε_o has been taken into account explicitly by adjusting the value of H_A (cf. equation 5). In Figure 6.7 some results are plotted. The open circles correspond to the experimental data corrected for the lattice contribution. Because in this temperature region the lattice heat capacity amounts to less than 6 % of the total specific heat, the data in Figure 6.7 will reflect the magnetic contribution fairly accurately. The drawn curve corresponds to the best fit of equation (7) to these data. Since the theoretical prediction at these temperatures was found to depend on $|J_2 + J_3|$ rather than on J_2 and J_3 separately, and several experimental studies indicate that $|J_3| \ll |J_2|$, the problem has been simplified by putting J_3 equal to zero. The result obtained from the set of exchange constants J_1/k = - 3.2 K, $|J_2/J_1| = 7 \times 10^{-3}$, J_3 = 1/5 J_2, determined by Iwashita and Uryû from their fit of linear spin wave theory to the low-temperature susceptibility [10], is represented by the dashed curve marked "Iw". For comparison the predictions from some purely one-dimensional models are also given. The curve marked "$1d_{sw}$" represents the estimate from linear spin-wave theory given by Kubo [16] for J/k = - 3.0 K, the curve marked "$1d_{num}$" corresponds to the low-temperature behaviour of a S = 5/2 Heisenberg antiferromagnetic linear chain system, presented in Chapter II. The large deviation of these one-dimensional predictions from the actual behaviour clearly demonstrates the drastic influence of the interchain interactions. Three-dimensional linear spin-wave theory appears to give a

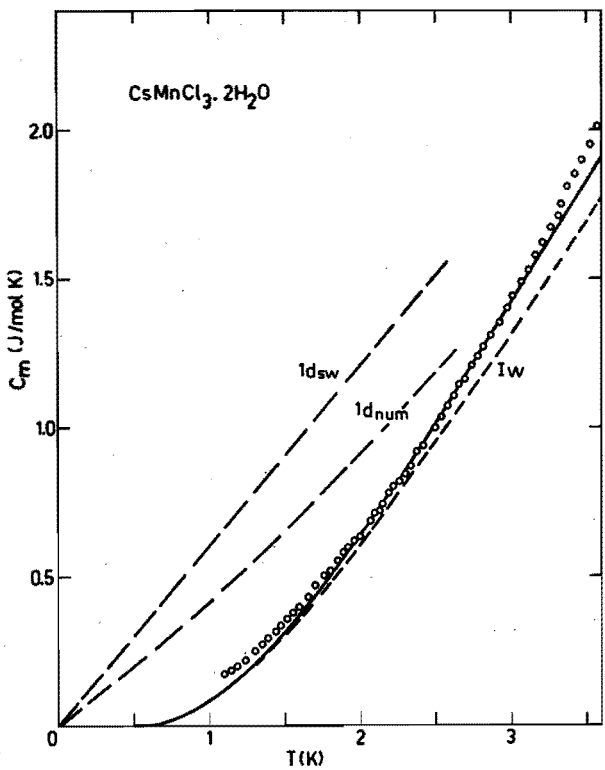

FIG. 6.7. Magnetic heat capacity of $CsMnCl_3.2H_2O$ at low temperatures. The open circles correspond to the experimental data corrected for the lattice contribution. The drawn curve denotes the best fit of the spin-wave prediction to the experimental results. This fit corresponds to the set of exchange interactions $J_1/k = -3.0$ K, $J_2/J_1 = 8 \times 10^{-3}$, $J_3 = 0$. The dashed curve marked "Iw" represents the result obtained from the set of interactions $J_1/k = -3.2$ K, $J_2/J_1 = 7 \times 10^{-3}$, $J_3/J_2 = 0.2$ reported by [10]. The curve marked "$1d_{sw}$" reflects the prediction from purely one-dimensional spin-wave theory. The low-temperature behaviour of the $S = 5/2$ linear chain model presented in Chapter II is denoted by "$1d_{num}$".

TABLE 6.4. Values for the intrachain exchange interaction J_1 and the interchain interactions J_2 and J_3 for $CsMnCl_3.2H_2O$, $\alpha RbMnCl_3.2H_2O$ and $CsMnBr_3.2H_2O$. The last column gives the fraction of the total magnetic entropy increase removed below the ordering temperature.

$CsMnCl_3.2H_2O$		
Neutron diffraction [5]	$J_1/k = -3.53$ K, $\lvert J_2+J_3\rvert = 7\times10^{-3}\lvert J_1\rvert$	
ESR lineshape [7]	between $\lvert J_2\rvert = \lvert J_3\rvert = 2\times10^{-2}\lvert J_1\rvert$ and $\lvert J_2\rvert = 100\lvert J_3\rvert = 2.6\times10^{-2}\lvert J_1\rvert$	
Paramagnetic NMR [13]	$\lvert J_2\rvert = 3.5\times10^{-2}\lvert J_1\rvert \gg \lvert J_3\rvert$	
Proton spin-lattice relaxation [11]	$\lvert J_2\rvert = 5\times10^{-2}\lvert J_1\rvert$, $J_3 \approx 0$	
Oguchi's formula [24]	$\lvert J_2\rvert = \lvert J_3\rvert = 8\times10^{-3}\lvert J_1\rvert$	
Susceptibility below T_N [10]	$J_1/k = -3.2$ K, $\lvert J_2\rvert = 6\times10^{-3}\lvert J_1\rvert = 5\lvert J_3\rvert$	
Specific heat	$J_1/k = -3.0$ K, $\lvert J_2+J_3\rvert = 8\times10^{-3}\lvert J_1\rvert$	$S_{crit} = 13.9$ %
$\alpha RbMnCl_3.2H_2O$		
Susceptibility [26] below T_N	$J_1/k = -2.9$ K	
Specific heat + Oguchi's formula	$J_1/k = -3.0$ K, $\lvert J_2\rvert = \lvert J_3\rvert = 7\times10^{-3}\lvert J_1\rvert$	$S_{crit} = 13.6$ %
$CsMnBr_3.2H_2O$		
Susceptibility [26] above T_N	$J_1/k = -3.2$ K	
below T_N	$J_1/k = -3.0$ K	
Specific heat + Oguchi's formula	$J_1/k = -2.6$ K, $\lvert J_2\rvert = \lvert J_3\rvert = 1.4\times10^{-2}\lvert J_1\rvert$	$S_{crit} = 20.9$ %

fair description of the data up till $\sim$ 3 K, which corresponds to 0.6 T_N. The intra- and interchain interactions $J_1/k = -3.0$ K, $\lvert J_2/J_1\rvert = 8\times10^{-3}$, $J_3 \simeq 0$, which yielded the best fit with the experimental results, compare favourably with the values cited in literature. A survey of these results is given in Table 6.4.

Inspection of Figure 6.7 shows that at the lowest temperatures, where three-dimensional linear spin-wave theory is expected to give the best description, the observed heat capacity systematically rises above the theoretical prediction. Partly this deviation arises from the high temperature tail of the nuclear Schottky anomaly of the Mn^{++} ions caused by the hyperfine coupling $\vec{I}\vec{A}\vec{S}$ in the magnetically ordered state. If we assume $\lvert A\rvert/k = 0.012$ K, a value which can be considered as representative

for Mn^{++} ions in an octahedral environment [18], we arrive at a nuclear contribution to the heat capacity of about 0.02 J/mol K at 1 K, which accounts for ∿ 30 % of the observed deviation. The remaining discrepancy may presumably be removed by the introduction of small non-uniaxial terms in the anisotropy. Susceptibility measurements have indicated the existence of such terms [8].

Next we will consider the magnetic ground state energy E_g. At T = 0 equation (4) reduces to:

$$E_g = 2NS(S+1)(J_1+J_2+J_3) - g\mu_B H_A N(S+\tfrac{1}{2}) + \frac{1}{2}\int_{\varepsilon_o}^{\varepsilon_m} N(\varepsilon)d\varepsilon. \qquad (8)$$

Due to the zero-point motion of the spins, E_g is different from the "naive" ground-state energy $2NS^2(J_1+J_2+J_3)$ corresponding to a completely antiparallel alignment of the magnetic moments. This antiparallel alignment, however, is not an eigenstate of the hamiltonian (1). Since it has been shown [16] that the inclusion of fourth order terms in the spin-wave hamiltonian produces an increase of only 0.5 % in E_g for an S = 5/2 antiferromagnetic linear chain, equation (8) will very likely offer a good estimate of the actual ground state energy of CMC. Substitution of H_A and the set of exchange constants found above in this equation yields E_g = - 357 J/mol. If we assert that the dominant contribution to E_g will arise from the large intrachain interaction this value may be confronted with the rigorous bounds given by Anderson [19]

$$NzJS^2 > E_g > NzJS^2(1+1/zS), \qquad (9)$$

where z denotes the number of nearest neighbours. For z = 2, S = 5/2 and J/k = - 3.0 K this equation yields - 312 > E_g > - 374 J/mol, which comprises the value calculated above. Of course, the ground-state energy may be calculated directly from the experimental data by integrating the C_M versus T curve. Following a procedure similar to the method used in the calculation of the magnetic entropy gain we find E_g = - 361 J/mol, which is in excellent agreement with the prediction from linear spin-wave theory.

The magnitude of the sublattice magnetization (M_s) may be found by considering the difference of $\vec{M}_+$ and $\vec{M}_-$, which represent the magnetization of the + and - sublattice, respectively, as a thermodynamic quantity. Since

in zero applied field $\vec{M}_+ = -\vec{M}_-$, the sublattice magnetization $\vec{M}_s$ can be written as $\vec{M}_s = \frac{1}{2}(\vec{M}_+ - \vec{M}_-)$. The magnitude of $\vec{M}_s$ may be obtained by differentiating the energy, given by equation (4), with respect to the conjugate thermodynamic variable of $\vec{M}_+ - \vec{M}_-$. This variable is usually called the staggered field $\vec{H}_{st}$, which points along the preferred direction of spin alignment, being positive at the + lattice sites and negative at the - lattice sites. Since for an antiferromagnetic array the anisotropy field $\vec{H}_A$ has a staggered character also, H_{st} enters in the hamiltonian (1) in the same way as H_A, and hence it may simply be added to H_A in the final solution (4-5). The sublattice magnetization M_s may be obtained from this modified solution directly as

$$M_s = -\frac{1}{2}(\partial E/\partial H_{st})_{H_{st}=0}, \tag{10}$$

where E denotes the thermal average of $E_{n,p}$. The result is

$$M_s = \frac{N}{2}g\mu_B\left[S + \frac{1}{2} - \frac{1}{N}\int_{\varepsilon_o}^{\varepsilon_m}\frac{\varepsilon_m N(\varepsilon)}{2\varepsilon}d\varepsilon - \frac{1}{N}\int_{\varepsilon_o}^{\varepsilon_m}\frac{\varepsilon_m N(\varepsilon)}{\varepsilon(e^{\varepsilon/kT}-1)}d\varepsilon\right], \tag{11}$$

which is - in fact - equivalent to the expression given by Kubo [16]. At T = 0 the sublattice magnetization is different from the saturation value $\frac{N}{2}g\mu_B S$ by a factor

$$\frac{\Delta S}{S} = \frac{1}{2S} - \frac{1}{NS}\int_{\varepsilon_o}^{\varepsilon_m}\frac{\varepsilon_m N(\varepsilon)}{2\varepsilon}d\varepsilon, \tag{12}$$

usually called the zero-point spin reduction.

The actual behaviour of the sublattice magnetization M_s has been determined from nuclear magnetic resonance measurements on the hydrogen nuclei, hereafter referred to as proton-resonance. From the variation of the proton absorption frequency as a function of temperature the *relative* behaviour of M_s may be inferred. In order to obtain an estimate of the *absolute* value of M_s, the observed local fields at the proton sites can be compared with the calculated internal fields originating from the magnetic dipole moments on the Mn^{++} ions. Whether such a dipole sum really reflects the actual local magnetic fields at the proton sites depends on a number of conditions, which have been pointed out by De Jonge and Swüste [20], and may be summa-

rized as follows. Firstly, the direction of the magnetic dipole moments (or the sublattice magnetization) has to be known exactly. In CMC this is given by symmetry as the b axis. Secondly, the hydrogen positions should be known with a sufficient degree of accuracy. Furthermore, the hyperfine interaction of the hydrogen nuclei with the Mn^{++} spins should be small compared to the dipolar interaction. Although the hyperfine contribution cannot be calculated straightforwardly, it seems to be relatively small in this type of Mn^{++} compounds [20, 21]. If we confront the calculated dipole sums at the proton sites, corresponding to the magnetic space group $P_{2b}c'ca'$, with the experimentally determined internal fields, a magnetic moment of 4.0 μ_B on the Mn^{++} ions is required to fit the experimental fields extra-

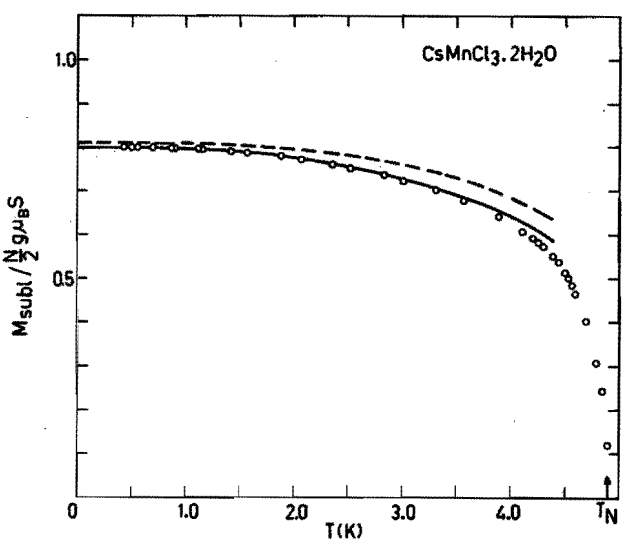

FIG. 6.8. Sublattice magnetization of $CsMnCl_3.2H_2O$. The open circles denote the experimental behaviour deduced from proton NMR measurements. The dashed curve represents the spin-wave prediction corresponding to the set of exchange constants $J_1/k = -3.0$ K. $J_2/J_1 = 8 \times 10^{-3}$, $J_3 = 0$ inferred from the heat capacity measurements, as well as the prediction corresponding to the set of exchange constants given by [10]. The drawn curve is obtained by a readjustment of the interchain interaction J_2 to 4×10^{-3} J_1.

polated to T = 0. Given the small uncertainty of both the hydrogen positions and the hyperfine contribution, we conclude that in CMC a zero-point spin reduction of 20 $\pm$ 4 % is present. The corresponding temperature dependence of the absolute value of the sublattice magnetization is given by open circles in Figure 6.8. The dashed curve in this figure is obtained from equation (11) by substitution of the values for the exchange interactions $J_1/k = -3.0$ K, $|J_2/J_1| = 8 \times 10^{-3}$, $J_3 = 0$ found from the analysis of the heat capacity. The prediction resulting from the set of exchange constants $J_1/k = -3.2$ K, $|J_2/J_1| = 7 \times 10^{-3}$, $J_3 = 1/5\ J_2$ reported by Iwashita and Uryû [10] almost coincides with this curve, and has not been shown separately. The drawn curve corresponds to the best fit of equation (11) to the experimental data, given a fixed value of J_1 and the observed temperature-dependence of ε_o. The ratio $|J_2/J_1| = 4 \times 10^{-3}$ resulting from this fit is considerably smaller than the value 8×10^{-3} obtained from the low-temperature specific heat. The calculated spin reduction, however, is in excellent agreement with the experimental evidence.

In view of the results of the present analysis of both heat capacity and sublattice magnetization as well as the interpretation of the susceptibility in the ordered state [10], we would like to conclude that linear spin-wave theory offers a fair description of the magnetic behaviour of CMC in the ordered state. Unlike the purely three-dimensional case, where considerable renormalization effects occur as T_N is approached, the validity range of the linear spin-wave approximation in this pseudo one-dimensional case extends up till 0.6 T_N. The only renormalization effect that has been considered in the present treatment is the observed temperature-dependence of the energy gap ε_o. The fact that no other renormalization effects have been taken into account does not seriously impair the description of the thermodynamic properties, as can be seen as follows. Firstly, for spin-waves propagating in the direction of the chains, Skalyo et al. [5] have shown that energy renormalization at the zone boundary is only detectable far above T_N, and hence ε_m may safely be considered as being constant in the temperature region below T_N. Moreover, the calculation of the magnetic properties at these temperatures involves mainly the density of states for low values of ε. For spin-waves propagating perpendicular to the chain direction, an energy renormalization of 10 % was observed at the zone boundary. This would give rise to a small shift of the bump in the low-energy part of the spin-wave spectrum. As can be seen from

Figure 6.6, however, such a shift may - to a certain extent - be compensated by a readjustment of the value of $(J_2 + J_3)/J_1$. This probably explains the slightly different sets of exchange constants used to describe the behaviour of the various magnetic properties. Since these differences are not very significant, we are tempted to conclude that linear spin-wave theory may provide very realistic estimates for both the intra- and interchain interaction in pseudo one-dimensional magnetic systems.

6.3. αRbMnCl$_3$.2H$_2$O (αRMC) and CsMnBr$_3$.2H$_2$O (CMB)

The magnetic properties of αRMC and CMB have been studied less extensively than those of the isomorphic CMC. αRMC has been found to order antiferromagnetically at T_N = 4.56 K [22] with the same magnetic space group as CMC, i.e. $P_{2b}c'ca'$ [20, 23], while CMB orders antiferromagnetically at T_N = 5.75 K [22] with magnetic space group Pc'c'a' [24]. From the corresponding magnetic arrays it is obvious that in CMB the interchain interaction J_3 along the crystallographic b direction is positive, in contrast to both αRMC and CMC.

In principle, the influence of the intermediate alkali ion as well as the halide ions on the various magnetic interactions may be studied by comparing the magnetic properties of CMC, αRMC and CMB. On the other hand, the lattice heat capacity of these compounds will probably be considerably different, because the mass difference between the Cs^+ and Rb^+ ions or, alternatively, the Cl^- and Br^- ions is rather large. Therefore an analysis of this series of compounds may serve as a check on the applicability of the description of the lattice heat capacity presented in Chapter III to this particular chemical structure.

Single-crystals of αRMC were grown by cooling a saturated solution of $MnCl_2.4H_2O$ and RbCl in molar ratio 5:1 in 8M HCl from 50 to 5°C. The crystallized mixture of α and β modification transforms gradually into the α modification after a few weeks at 5°C. The crystals were more or less needle-shaped with average dimensions of 10 x 1 x 1 mm. Single-crystals of CMB were grown by slow evaporation of a saturated solution of $MnBr_2.4H_2O$ and CsBr in molar ratio of 6:1 at room temperature. The crystals were rather large (typical dimensions 3 x 8 x 15 mm) and showed roughly the same morphology as CMC [1]. Calorimetric measurements were performed on both

αRMC and CMB with the experimental apparatus, described in Chapter IV. The data between 1.1 and 52 K are shown in Figure 6.9 and 6.10 for αRMC and CMB, respectively. The total heat capacity in the paramagnetic region varies in a similar way as the experimental data on CMC. The heat capacity of CMB, however, appears to be considerably larger than that of the two chlorine isomorphs. The small lambda anomalies at T = 4.56 K for αRMC and T = 5.75 K for CMB are associated with the respective three-dimensional ordering temperatures.

The separation of the magnetic and the lattice contribution to the heat capacity has been achieved by analysing the data between 9 and 52 K according to the procedure described in the preceeding section. The intra-chain interaction in αRMC amounts to $J/k = -3.0 \begin{smallmatrix} +0.2 \\ -0.4 \end{smallmatrix}$ K, the corresponding interaction in CMB is found as $J/k = -2.6 \begin{smallmatrix} +0.2 \\ -0.6 \end{smallmatrix}$ K. Due to the relatively high lattice contribution, the uncertainty in the value of J/k in CMB is somewhat larger than that in both chlorine isomorphs. The lattice contribution in αRMC is represented by Θ_t = 254 K, Θ_o = 232 K, Θ_c = 63 K; for

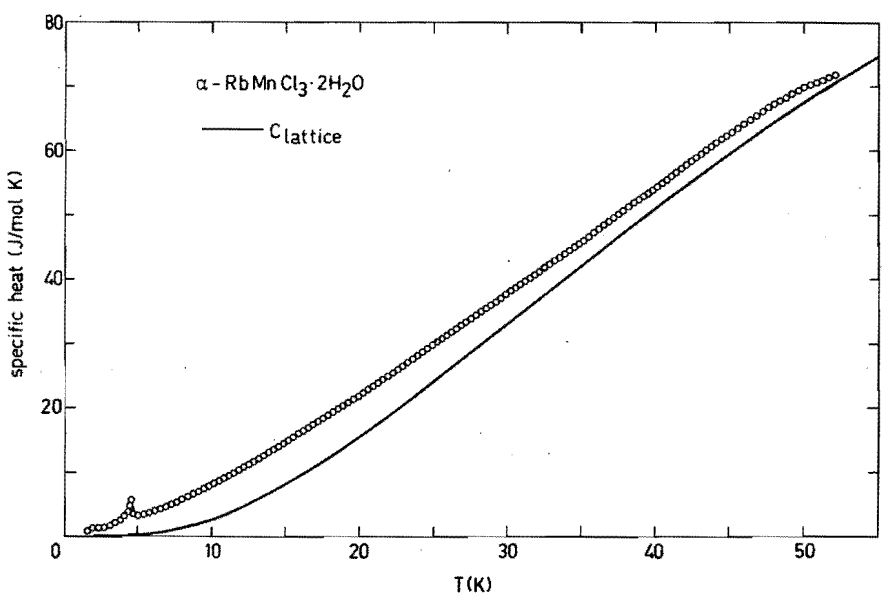

FIG. 6.9. Specific heat of αRbMnCl$_3$.2H$_2$O versus temperature. The open circles represent the experimental data, the drawn curve denotes the lattice contribution given in section 6.3.

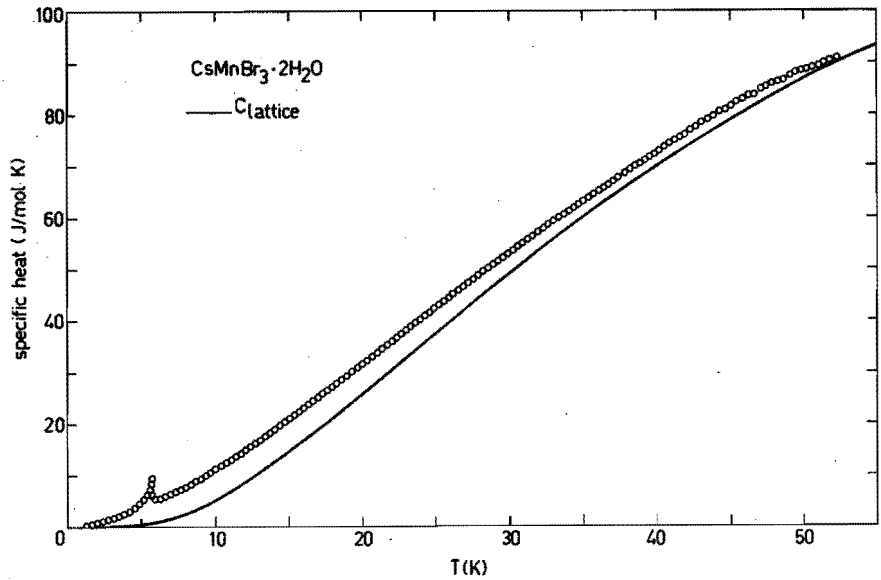

FIG. 6.10. Specific heat of $CsMnBr_3.2H_2O$ versus temperature. The open circles represent the experimental data, the drawn curve denotes the lattice contribution given in section 6.3.

CMB the parameters Θ_t = 204 K, Θ_o = 165 K, Θ_c = 52 K are obtained. If these values are compared with the values Θ_t = 277 K, Θ_o = 219 K, Θ_c = 53 K obtained for CMC from the fit with J/k = - 3.0 K, it appears that apart from a change of the parameters with a constant fraction, which might arise from the difference of the atomic masses, the relative ratio of the Θ values varies considerably. This indicates that the substitution of Cs by Rb or Cl by Br has a rather drastic effect on the elastic anisotropy, and hence the lattice specific heats of these compounds cannot be related to each other by a simple temperature-independent scaling factor.

The magnetic heat capacity, obtained by subtracting the calculated lattice contribution from the experimental data, is shown by open circles in Figure 6.11 and 6.12 for αRMC and CMB, respectively. The drawn curves represent the corresponding theoretical estimate for an S = 5/2 antiferromagnetic Heisenberg linear chain, given in Chapter II. The errorbars reflect the uncertainty in the experimental determination of the *total* heat capacity ($\sim$ 1 %). The variations of the experimental data above 12 K

around the theoretical prediction mainly reflect a systematic experimental error, as has been pointed out in the preceeding section. The magnetic heat capacity of αRMC appears to be basically identical to that of CMC, except for the three-dimensional ordering, which occurs at slightly lower temperatures. The small peak at 2.19 K is due to a small fraction (1-2 %) of $\beta RbMnCl_3.2H_2O$. Unfortunately, this peak precludes a determination of the interchain interactions from the magnetic heat capacity at low temperatures by linear spin-wave theory. Therefore these interactions have been estimated using the expression based upon Green's function theory given by Oguchi [25]:

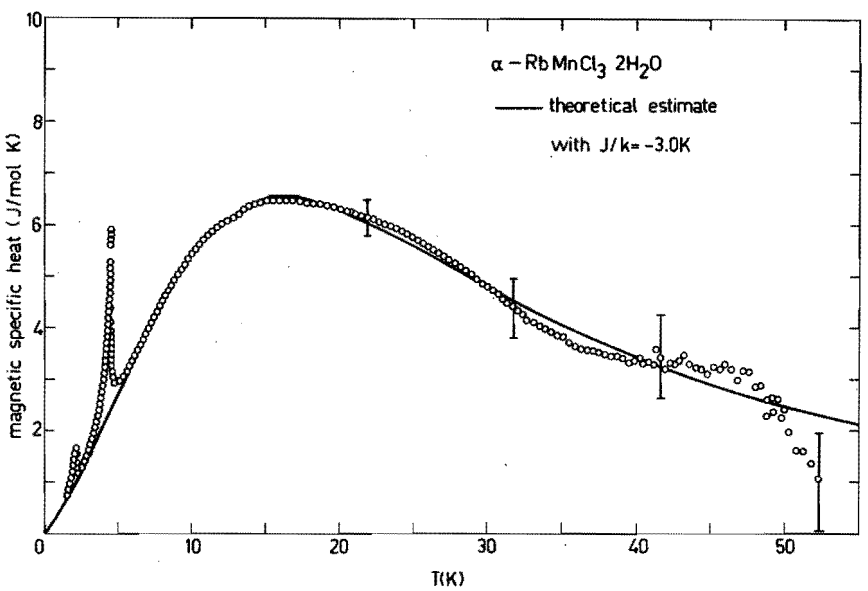

FIG. 6.11. Magnetic heat capacity of $\alpha RbMnCl_3.2H_2O$. The open circles correspond to the experimental data minus the calculated lattice contribution, the errorbars reflect the experimental uncertainty in the determination of the total heat capacity. The drawn curve denotes the theoretical estimate for a S = 5/2 Heisenberg linear chain system with J/k = – 3.0 K. The anomaly at 2.19 K is due to a small fraction of $\beta RbMnCl_3.2H_2O$.

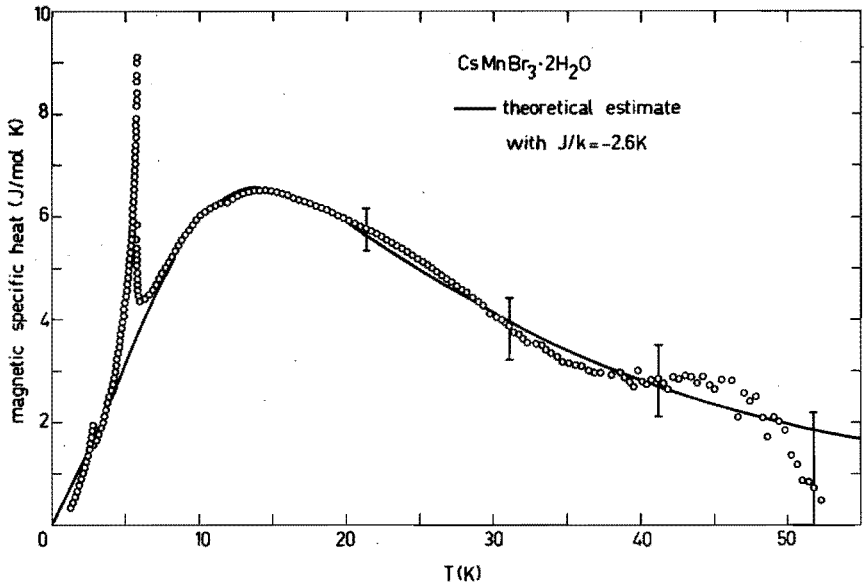

FIG. 6.12. Magnetic heat capacity of $CsMnBr_3.2H_2O$. The open circles correspond to the experimental data minus the calculated lattice contribution, the errorbars reflect the experimental uncertainty in the determination of the total heat capacity. The drawn curve denotes the theoretical estimate for a S = 5/2 Heisenberg linear chain system with J/k = - 2.6 K. The anomaly at 2.8 K is due to a small fraction of $Cs_2MnBr_4.2H_2O$.

$$\frac{kT_N}{|J|} = \frac{4S(S+1)}{3I(J'/J)} \quad , \text{ with} \tag{13}$$

$$I(J'/J) = \frac{1}{\pi^3} \int_0^{\pi}\int\int \frac{dq_a dq_b dq_c}{(1-\cos q_a) + |J'/J|(1-\cos q_b) + |J'/J|(1-\cos q_c)} \quad .$$

In this expression J denotes the intrachain interaction, while $|J'| = |J_2| = |J_3|$. Substitution of the values J/k = - 3.0 K and T_N = 4.56 K for αRMC yields $|J'/J| = 7 \times 10^{-3}$. A similar procedure for CMC yields $|J'/J| = 8 \times 10^{-3}$. In CMB, an analysis of the low-temperature

magnetic heat capacity with linear spin-wave theory is hampered by the small peak at 2.8 K, which is due to a small fraction of $Cs_2MnBr_4.2H_2O$ [26]. Substitution of the values J/k = - 2.6 K and T_N = 5.75 K for CMB in equation (13) yields $|J'/J| = 1.4 \times 10^{-2}$.

In view of the results given above, one might be tempted to conclude that the magnitude of the interchain interactions increases going from αRMC via CMC to CMB. We wish to emphasize, however, that the observed changes of the ordering temperature may probably also be explained by a variation of the - relatively small - magnetic anisotropy, which has been reported to increase going from αRMC via CMC to CMB [27]. The influence of anisotropy, which may arise from dipolar or crystal-field effects, is not included in the expression given by Oguchi, and hence the estimated values of $|J'/J|$ should be considered with some reservations. A survey of the results obtained in this chapter, together with some representative values reported in literature, is presented in Table 6.4.

REFERENCES CHAPTER VI

1. S.J. Jensen, P. Andersen and S.E. Rasmussen, Acta Chem. Scand. 16, 1890 (1962).
2. S.J. Jensen, Acta Chem. Scand. 21, 889 (1967).
3. T. Smith and S.A. Friedberg, Phys. Rev. 176, 660 (1968).
4. R.D. Spence, W.J.M. de Jonge, and K.V.S. Rama Rao, J. Chem. Phys. 51, 4694 (1969).
5. J. Skalyo, G. Shirane, S.A. Friedberg, and H. Kobayashi, Phys. Rev. B2, 1310, 4632 (1970).
6. K. Nagata and Y. Tazuke, J. Phys. Soc. Japan 32, 337 (1972).
7. M.J. Hennessy, C.D. McElwee, and P.M. Richards, Phys. Rev. B7, 930 (1973).
8. H. Kobayashi, I. Tsujikawa, and S.A. Friedberg, J. Low-Temp. Phys. 10, 621 (1973).

9. K. Kopinga, T. de Neef and W.J.M. de Jonge, Phys. Rev. B11, 2364 (1975).

10. T. Iwashita and N. Uryû, J. Phys. Soc. Japan 39, 1226 (1975).

11. H. Nishihara, W.J.M. de Jonge and T. de Neef, Phys. Rev. B12, 5325 (1975).

12. W.J.M. de Jonge, C.H.W. Swüste and K. Kopinga, accepted for publication in Phys. Rev. B.

13. F. Ferrieu, Phys. Lett. A49, 253 (1974).

14. T. Holstein and H. Primakoff, Phys. Rev. 58, 1098 (1940).

15. F. Keffer, *Handbuch der Physik*, edited by S. Flügge (Springer, Berlin 1966), Vol. 18, Bd. 2.

16. R. Kubo, Phys. Rev. 87, 568 (1952).

17. T. Moriya, Progr. Theor. Phys. 16, 23 (1956).

18. A. Abragam and B. Bleaney, "*Electron Paramagnetic Resonance of Transitions Ions*", Clarendon Press, Oxford (1970).

19. P.W. Anderson, Phys. Rev. 83, 1260 (1951).

20. W.J.M. de Jonge and C.H.W. Swüste, J. Chem. Phys. 61, 4981 (1974).

21. D. van Ormond, R. de Beer, M. Brouha, and F. de Groot, Z. Naturforsch. A24, 1764 (1969).

22. C.H.W. Swüste, K. Kopinga, W.J.M. de Jonge, J.P.A.M. Hijmans and A.C. Botterman. Proc. Int. Conf. Magn. ICM-73, Moscow (1973).

23. J.P.A.M. Hijmans and W.J.M. de Jonge, Phys. Lett. 43A, 441 (1973).

24. C.H.W. Swüste. Ph.D. Thesis, Eindhoven (1973).

25. T. Oguchi. Phys. Rev. 133, A1098 (1964).

26. H. Forstat, J.N. McElearny and P.T. Bailey, Proc. 11th Int. Conf. Low-Temp. Phys., St. Andrews (1968).

27. A.C. Botterman. Ph.D. Thesis, Eindhoven (1976).

CHAPTER VII

SOME MAGNETIC PROPERTIES OF $CsCoCl_3.2H_2O$ AND $RbFeCl_3.2H_2O$

7.1. Introduction

The preceeding chapter has been devoted to the magnetic properties of the Mn^{++} compounds belonging to the isomorphous series $AMB_3.2H_2O$. In view of the $3d^5$ configuration of the unperturbed ground state of the Mn^{++} ion (L = 0, S = 5/2) the exchange interactions were represented by the Heisenberg model. The substitution of Mn^{++} by Co^{++} or Fe^{++} is expected to result in a large magnetic anisotropy, since the unperturbed ground state of these ions is $3d^7$ and $3d^6$, respectively, and hence spin-orbit coupling and crystal-field effects will have a rather drastic influence. In fact, a large number of investigations on Co^{++} compounds reveal rather pronounced Ising or XY characteristics [1-4].

In the past few years, $CsCoCl_3.2H_2O$ has been the subject of a number of rather detailed investigations [5-7]. The crystal structure has been determined by Thorup and Soling [8] as Pcca, with a = 8.914 Å, b = 7.174 Å, c = 11.360 Å. The chemical unit cell contains four formula units. The structure is isomorphic with $CsMnCl_3.2H_2O$. The magnetic behaviour of $CsCoCl_3.2H_2O$ was explained by Herweijer et al. [6], who combined the results of specific heat, NMR, magnetic susceptibility, magnetization and antiferromagnetic resonance (AFMR) measurements. From this study a magnetic space group $P_{2b}cca'$ was deduced. The magnetic array is schematically drawn in Figure 7.1. The array represents a canted structure with the magnetic moments located in the ac plane, the angle ϕ between the magnetic moments and the c direction being about 10^o. The magnetic interaction in the a direction - which is essentially antiferromagnetic - was found to be large compared to the coupling in the other directions. The interactions along the c and b axis are ferromagnetic and antiferromagnetic, respectively. Due to the canted structure the individual - Co-Cl-Co-Cl - chains in the a direction have a net magnetic moment along a. The proposed magnetic structure has been confirmed by subsequent neutron-diffraction experiments [7].

The magnetic behaviour of $CsCoCl_3.2H_2O$ has been described by a pseudo one-dimensional S = 1/2 Ising-like system, but the estimates

for the magnitude of the various interactions obtained from different experimental techniques were rather inconsistent. The interpretation of the AFMR results as a spin-cluster resonance yielded an intrachain interaction J_a/k of about -8 K, which is much smaller than the value $J_a/k = -36$ K resulting from a preliminary analysis of the heat capacity in the paramagnetic region. As already noticed by Herweijer et al. [6] their interpretation of the AFMR results should be considered with some reservations. Apart from the fact, that the presence of impurities has been shown [9] to affect the calculation of the J_a value by a factor 2, the interpretation assumes that the magnetic eigenstates can be represented exactly by the Ising model, in which case the first excited level corresponds to a reversal of one single spin. As we will point out below, $CsCoCl_3.2H_2O$ can only roughly be described by this model. On the other hand, a straightforward analysis of the heat capacity was hampered by the fact that at that time no reliable estimates for the lattice contribution were available. In view of the good results obtained in the preceeding chapter for the isomorphous manganese compounds we thought it worthwhile to re-examine the heat capacity of $CsCoCl_3.2H_2O$. The results of this analysis will be confronted with recent experimental evidence from neutron-diffraction studies [10]. Section 7.2 will be devoted to this subject.

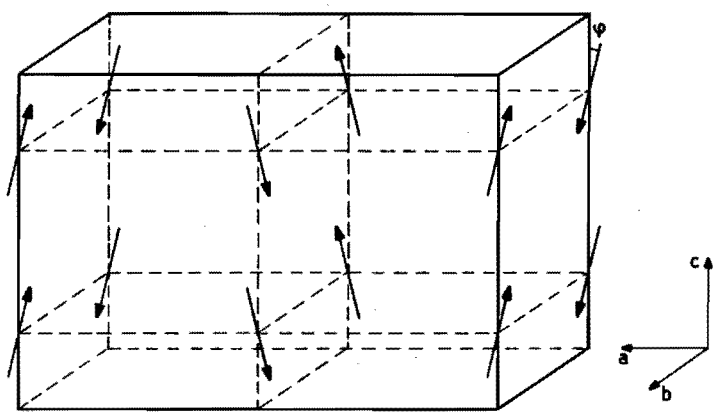

FIG. 7.1. Arrangement of the magnetic moments in antiferromagnetic $CsCoCl_3.2H_2O$. All spins are located in the ac plane.

The magnetic properties of $RbFeCl_3.2H_2O$ have not yet been reported. X-ray diffraction experiments have shown [11] that this compound may be considered as isomorphic with the other members of the present series $AMB_3.2H_2O$. A direct interpretation of the measurements on $RbFeCl_3.2H_2O$ is hindered by the fact that unlike Co^{++} systems, where the magnetic properties at low temperatures may usually be described by an "effective" spinvalue 1/2, the effective spinvalue for Fe^{++} varies from salt to salt [12, 13, 14]. This problem will be considered in section 7.3, where we will present some measurements on this system and propose a model which explains the main features of the observed magnetic behaviour.

7.2. $CsCoCl_3.2H_2O$ (CCC)

Single-crystals of $CsCoCl_3.2H_2O$ were grown by slow evaporation at room temperature from a solution of $CoCl_2.6H_2O$ and CsCl in a molar ratio of 4.8 : 1. The crystals were plate-like and not very well developed in the c direction. Calorimetric measurements were performed between 2 and 52 K on $\sim$ 0.1 mole of small crystals (average dimensions 5 x 5 x 1 mm) with the experimental apparatus described in Chapter IV. The data are shown in Figure 7.2. The small lambda anomaly at 3.4 K is associated with the three-dimensional ordering. Tha data for $4 < T < 25$ K were found to agree within a few percent with the earlier measurements of Herweijer et al. [6].

Although some magnetic properties of $CsCoCl_3.2H_2O$ have been reported to display rather pronounced Ising-like characteristics, this does not necessarily imply that the Ising model will provide a correct description of the magnetic *heat capacity* also. Hence an analysis of the data in the paramagnetic region by a simultaneous fitting procedure as used in the preceeding chapter should only be applied with great care. Therefore we have chosen a somewhat different approach.

As a first attempt, we investigated the overall magnetic heat capacity of $CsCoCl_3.2H_2O$ by subtracting a scaled lattice heat capacity of $CsMnCl_3.2H_2O$ from the experimental data, using a simple temperature-independent scaling factor. Within a wide range of values of the scaling factor, the result showed a broad bump with a maximum at temperatures between 14 and 18 K, which may be attributed to one-dimensional corre-

lation effects. The range of possible values of the scaling factor α was restricted by the condition $C_M > 0$ for $T \leqslant 52$ K to $\alpha \geqslant 1.07$. For these values of α, the magnetic entropy increase below 52 K, including the extrapolated fraction 0.03 R below 2 K, was found to be at least 8 % higher than the theoretical prediction Rln2 for a S = 1/2 system. Therefore we choose the smallest allowed value of the scaling factor, i.e. $\alpha = 1.07$. The resulting data could not be represented properly by any of the S = 1/2 model systems, presented in Chapter II. The best agreement was found by describing the results with a linear chain Ising model, but even this description was rather unsatisfactory. A least-squares fit of the Ising model and the lattice contribution to the experimental data above 9 K, by varying both the exchange parameter J_a and the scaling factor α, yielded $|J_a/k| = 38.6$ K and $\alpha = 1.076$. The result is plotted in Figure 7.3. The open circles are the experimental data minus the lattice contribution, the drawn curve denotes the theoretical

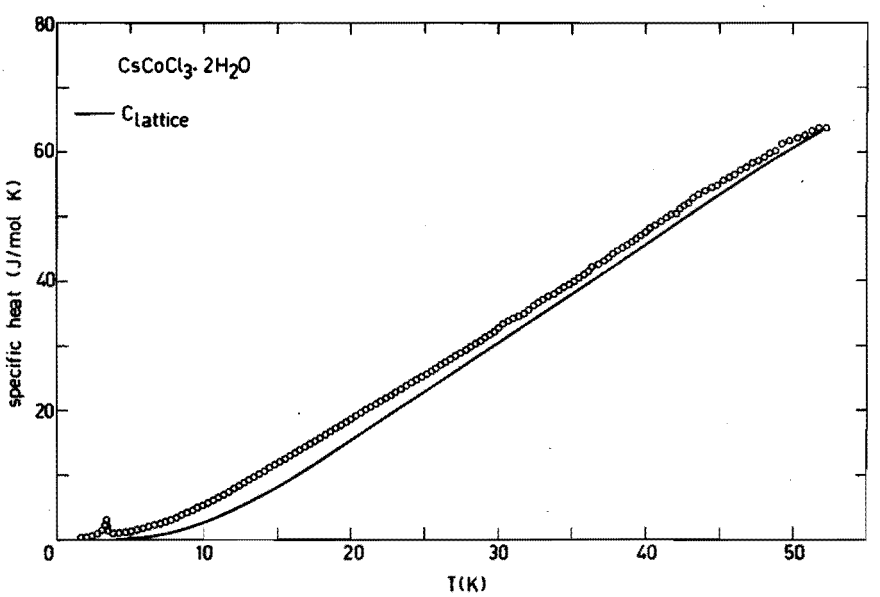

FIG. 7.2. Specific heat of $CsCoCl_3.2H_2O$ versus temperature. The open circles represent the experimental data, the drawn curve denotes the inferred lattice contribution.

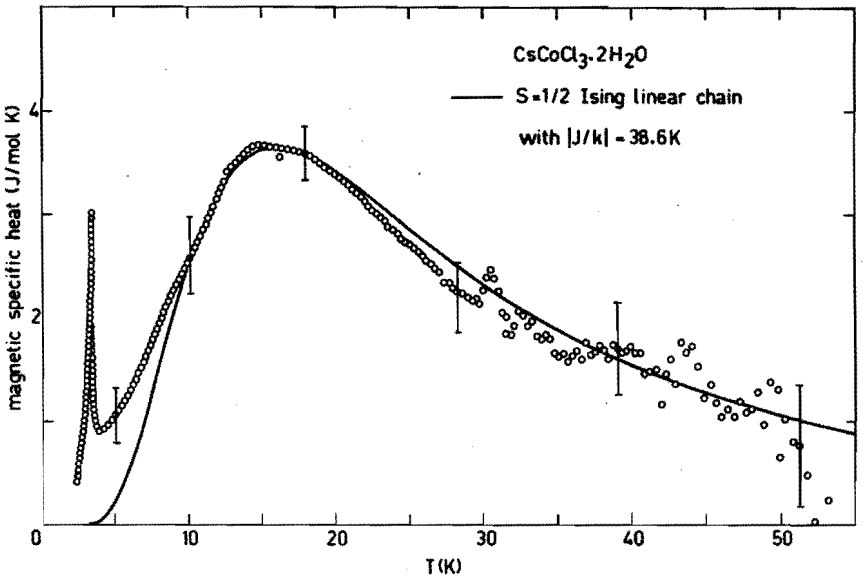

FIG. 7.3. Magnetic heat capacity of $CsCoCl_3.2H_2O$ versus temperature. The open circles are the experimental data minus a scaled lattice heat capacity of $CsMnCl_3.2H_2O$. The errorbars reflect the uncertainty in the evaluation of the lattice heat capacity of the latter compound. The drawn curve denotes the theoretical prediction for an S = 1/2 Ising linear chain system with $|J_d/k| = 38.6$ K.

prediction. The corresponding lattice contribution is plotted as a drawn curve in Figure 7.2.

Before proceeding any further, we would like to make the following remarks. In order to reduce the systematic experimental deviations, the lattice heat capacity C_L of $CsMnCl_3.2H_2O$ above 9 K has been obtained by subtracting the calculated magnetic contribution from the experimental specific heat. Below 9 K, we used the theoretical estimate for C_L, since in this temperature region the magnetic heat capacity of $CsMnCl_3.2H_2O$ has not been fitted to a linear chain model. The resulting lattice heat capacity used in the scaling procedure depends - of course - on the particular choice of the J value in $CsMnCl_3.2H_2O$. This may introduce an additional uncertainty in the determination of the magnetic heat

capacity of $CsCoCl_3.2H_2O$, because in $CsMnCl_3.2H_2O$ the intrachain interaction J may range between -2.8 and -3.3 K (cf. Chapter VI). This uncertainty is reflected by the errorbars in Figure 7.3. Given the small spin quantum number S and the corresponding small magnetic contribution, the relative uncertainty is very large, but, nevertheless, the magnetic contribution above 9 K still seems to be represented most properly by the Ising model. The XY model seems to be ruled out by the experimental data, since it predicts a maximum of the heat capacity in the paramagnetic region with a magnitude of only 2.7 J/mol K (cf. Chapter II).

Although the mass difference between Co^{++} and Mn^{++} is very small, the description of the lattice heat capacity by one temperature-independent scaling factor in the whole temperature region up till 52 K may give rise to some systematic deviations, as the binding forces and hence the elastic constants may change. Therefore the magnetic contribution was evaluated independently by simultaneous fits to the total specific heat using the expression for the lattice contribution

$$C_L = F_1(\Theta_t,\Theta_c,T) + F_1(2\Theta_t,\Theta_c,T) + F_2(\Theta_o,2\Theta_c,T), \qquad (1)$$

in combination with the predictions for the various antiferromagnetic S = 1/2 linear chain model systems, presented in Chapter II. The data in the paramagnetic region could be described - at least roughly - in all these cases; the resulting parameter-values are presented in Table 7.1. At first sight, this procedure seems rather inconclusive, but one should note that only the Θ values resulting from the fit to the Ising model can be approximately scaled to the values Θ_t = 277 K, Θ_o = 219 K, and Θ_c = 53 K obtained for $CsMnCl_3.2H_2O$.

Combining the results of both procedures, we are led to the conclusion that the intrachain interaction in $CsCoCl_3.2H_2O$ is more or less Ising-like with a magnitude of about 40 K. This conclusion is supported by recent measurements of the correlation length in the a direction by means of neutron-scattering experiments [10]. In principle, the intrachain interaction may be calculated from the correlation length if the magnetic model system is known. Due to the finite resolution of the neutron-diffraction experiments, only a lower-bound for J_a could be determined, yielding $|J_a/k| > 25$ K for the Ising model and $|J_a/k| > 150$ K for the Heisenberg model. An estimate for the XY model has not been gi-

TABLE 7.1. Lattice parameters and J_a values for $CsCoCl_3.2H_2O$ obtained from simultaneous fits involving different linear S = 1/2 magnetic model systems. The numbers between brackes denote the relative increase of the lattice parameters compared to the values Θ_t = 277 K, Θ_o = 219 K, Θ_c = 53 K for $CsMnCl_3.2H_2O$.

System	$\|J_a/k\|$	Θ_t	Θ_o	Θ_c
Heisenberg	17 K	293 K (1.058)	242 K (1.105)	51 K (0.962)
Ising	40 K	294 K (1.061)	239 K (1.091)	57 K (1.076)
XY	35 K	278 K (1.004)	277 K (1.265)	43 K (0.811)

ven, but actually this model has been ruled out already by the foregoing analysis of the heat capacity. If we confront the reported lowerbounds for J_a with the corresponding values given in Table 7.1, i.e. $|J_a/k|$ = 40 K for the Ising model and $|J_a/k|$ = 17 K for the Heisenberg model, the conjectured Ising-like character of the intrachain interaction seems to be established.

The magnitude of the interchain interaction in the b direction J_b has been determined by Herweijer et al.[6] from the metamagnetic transition in applied fields along the a axis. They explained this transition by assuming that at a certain critical field H_c all magnetic moments within chains having a net moment opposite to the external field reverse their directions. As may be seen from the magnetic array presented in Figure 7.1, this transition only disturbs the antiferromagnetic coupling J_b between adjacent chains in the b direction. This process has been verified by neutron-diffraction experiments [7]. From the magnitude of H_c an interchain coupling J_b/k = -0.1 K was deduced. The magnitude of the ferromagnetic coupling in the c direction J_c has been estimated from the location of the tricritical point in the magnetic phase-diagram [15, 16] as $J_c/k = 0.2 \pm 0.2$ K [10].

If all interactions in $CsCoCl_3.2H_2O$ could be properly described by the Ising model, a lower bound for T_N might be obtained from the rectangular Ising model presented in Chapter II by putting J_c equal to zero. In that case, however, the interactions J_a/k = -39 K and J_b/k = -0.1 K would produce a two-dimensional ordering already above 6 K. To

obtain an ordering at 3.4 K the interchain coupling would have to be $\sim 10^{-4}$ K, which is ruled out by the experimental evidence. If one assumes that, in contrast to the intrachain interaction, the interchain coupling is Heisenberg-like, the results might be confronted with theories like that of Stout and Chisholm [17], in which the interchain coupling is treated within the molecular-field approximation. These theories, however, are not applicable to cases where $|J'| \ll |J|$. If, on the other hand, the values for J_a and T_N are substituted in Oguchi's formula (cf. Chapter VI), we obtain $|J_b/k| = |J_c/k| = 0.12$ K. Although this method should be considered with some reservations, since J_a is not Heisenberg-like, these values are rather realistic.

The results presented in this section establish the pseudo one-dimensional Ising-like character of $CsCoCl_3.2H_2O$. The ratio of the inter- to intrachain interactions $(|J_b| + J_c)/|J_a| \sim 8 \times 10^{-3}$ indicates that this substance has about the same degree of one-dimensionality as the isomorphic $CsMnCl_3.2H_2O$. The magnetic heat capacity below 9 K is rather high compared to the theoretical prediction, which is also reflected by the value of the evaluated magnetic entropy increase, which is too high by $\sim$ 10 %. This might indicate that the simple S = 1/2 Ising model is a somewhat crude approximation to the thermodynamic properties of $CsCoCl_3.2H_2O$. The result obtained by approximating the lattice contribution to the heat capacity of $CsCoCl_3.2H_2O$ by a simple temperature-independent scaling of the lattice heat capacity of the corresponding manganese isomorph compares favourably with the result of a more general approach. This agreement may serve to justify the analysis of the specific heat of $RbFeCl_3.2H_2O$, which will be presented in the next section.

7.3. $RbFeCl_3.2H_2O$ (RFC)

Single-crystals of $RbFeCl_3.2H_2O$ were grown by slow evaporation at 38 °C from a solution of $FeCl_2.4H_2O$ and RbCl in a molar ratio of 3.2 : 1. To prevent oxidation of the Fe^{++} ions, a few drops of HCl were added to the solution, which was kept in a N_2 atmosphere. The crystals were very pale violet-brown with average dimensions of 2 x 5 x 8 mm and cleaved rather easily parallel to the largest surface, which corresponds to the ab plane. X-ray diffraction experiments showed them to be iso-

morphic with $\alpha RbMnCl_3.2H_2O$ [11]. Calorimetric measurements were performed between 2 and 50 K on $\sim$ 0.1 mole of single-crystals with the experimental apparatus described in Chapter IV. The data are plotted in Figure 7.4. They reveal a rather pronounced λ anomaly at 11.96 K, which is associated with the three-dimensional ordering.

A direct interpretation of the measurements on this compound is hampered by the fact that the actual ground state of the Fe^{++} ions is generally not known. The unperturbed ground state of an Fe^{++} ion is $3d^6$ (L = 2, S = 2). In the presence of an octahedral crystalline field the orbital levels split into a doublet and a triplet, with the triplet lowest [12]. Distortions from octahedral symmetry and spin-orbit coupling split the levels further [12, 13]. The details of the resulting energy spectrum are found to differ considerably from salt to salt.

The number of energy levels per spin N_s involved in the magnetic behaviour in a certain temperature region is usually represented by an effective spin-value, defined by $N_s = 2S + 1$. In principle, the effective spin-value may be estimated directly from the magnetic entropy increase

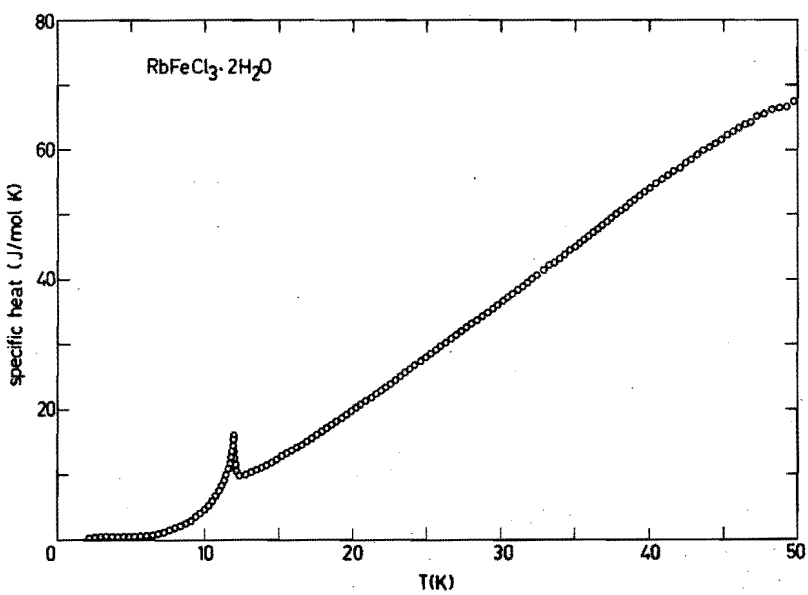

FIG. 7.4. Specific heat of $RbFeCl_3.2H_2O$ versus temperature.

$\Delta S = R\ln(2S + 1)$. In order to perform such a calculation, the magnetic contribution should be separated from the total heat capacity. In this case, however, such a separation cannot be performed straightforwardly, since the magnetic model system representing the most dominant features of the actual behaviour is not known. Therefore we are forced to develop a procedure which avoids - as much as possible - any interference which might arise from a simultaneous determination of the lattice and magnetic contribution.

In view of the results given in the preceeding section, which reveal that the lattice contribution to the heat capacity of $CsCoCl_3.2H_2O$ can be fairly well approximated by a scaled lattice heat capacity of $CsMnCl_3.2H_2O$, we will try to analyse the present data on $RbFeCl_3.2H_2O$ by subtracting a scaled lattice heat capacity of the corresponding isomorph $\alpha RbMnCl_3.2H_2O$. The scaling factor can be roughly estimated as follows. The available experimental evidence on several series of isostructural 3d transition-metal halides indicates a gradual decrease of the lattice heat capacity going from Mn via Fe and Co to Ni. Since the mass differences between these metal ions are rather small, this decrease is caused primarily by a change of the binding forces and hence the various elastic constants. A large number of investigations have been devoted to the series MF_2, resulting in scaling factors 1.08, 1.12, and 1.26 for Mn-Fe, Mn-Co, and Mn-Ni, respectively [18, 19]. The experimental data on other series of isomorphic compounds are less exhaustive, but generally indicate a decreasing influence of the particular kind of metal ion with increasing "dilution" of the system. Among these we mention

$MnCl_2.4H_2O/FeCl_2.4H_2O$	$\alpha = 1.025$ [14, 20]
$CoCl_2.6H_2O/NiCl_2.6H_2O$	$\alpha = 1.018$ [4]

as well as the results obtained in Chapter V and VI

TMMC/TMNC	$\alpha = 1.125$
$CsMnCl_3.2H_2O/CsCoCl_3.2H_2O$	$\alpha = 1.076$.

Given these values of α it seems not unrealistic to assume - as a first attempt - a scaling factor $\alpha = 1.03$ in the present case. The resulting magnetic heat capacity is plotted in Figure 7.5. This figure reveals a rather constant magnitude ($\sim$ 5 J/mol K) of the magnetic heat capacity in the paramagnetic region. The magnetic entropy increase below 50 K is found by numerical integration of the data as 1.013 R, which is slightly lower than the theoretical prediction 1.099 R for a S = 1 system. The critical entropy, i.e. the fraction of entropy removed below the ordering temperature, is found as $\sim$ 0.13 R, corresponding to $\sim$ 12 %. This value suggests a rather pronounced one-dimensional magnetic behaviour.

Measurements of the magnetization in the ordered state revealed two metamagnetic transitions in applied fields along the c axis at 8.1 and 12.4 KOe, respectively [21]. From these measurements an Ising-like anisotropy at low temperatures may be concluded, and hence one might be tempted to describe the magnetic properties in the paramagnetic region by the S = 1 linear chain Ising model or, alternatively, by the S = 1 linear chain model with Heisenberg exchange and a large positive D term, although the Heisenberg character of the exchange within a representation by an effective spin 1 may be somewhat doubtful. The linear S = 1 Ising

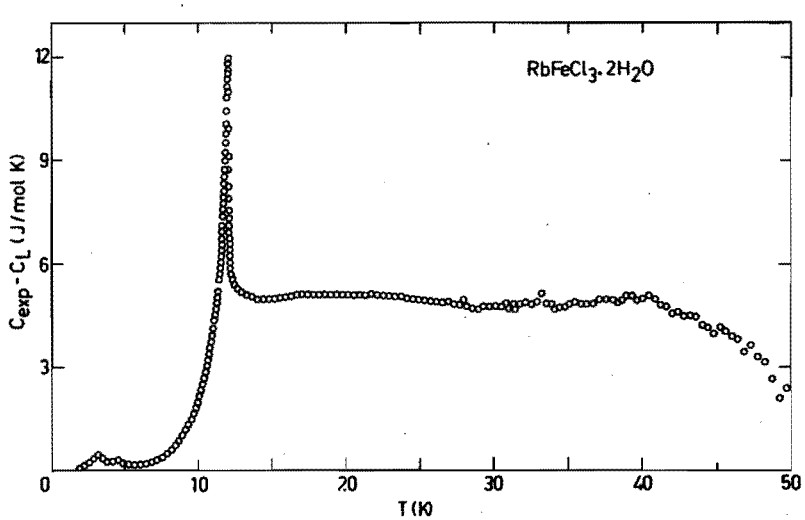

FIG. 7.5. Specific heat of $RbFeCl_3.2H_2O$ minus the lattice heat capacity of $\alpha RbMnCl_3.2H_2O$ scaled by a factor 1.03.

model is ruled out by the experimental evidence, since it predicts a broad bump in the heat capacity with a magnitude of about 7.8 J/mol K [23]. On the other hand, attempts to fit the S = 1 linear chain model with Heisenberg exchange and a positive D term to the experimental data above 13 K, by varying D, J and the scaling factor α, all resulted in a rather poor agreement, but indicated a ratio $|J|/D < 1/8$.

As for positive values of D the single-ion ground state is a doublet, the magnetic properties at low temperatures may according to the spin-hamiltonian formalism be described in first order of $|J|/D$ by the Ising model with an effective spin 1/2. In fact, the hamiltonian

$$H = -2J \sum_i \vec{S}_i \cdot \vec{S}_{i+1} - D[S_{iz}^2 - \frac{1}{3} S(S+1)] \qquad (2)$$

transforms into

$$H_{eff} = -2J_1 \sum_i s_i^z s_{i+1}^z \ , \qquad (3)$$

where $s = 1/2$ and $J_1 = 4J$. Of course, formally this description is only correct for $kT \ll D$ and $|J| \ll D$. It has been shown [23, 24], however, that for small values of $|J|/D$ the heat capacity within the whole temperature region may be fairly well approximated by the heat capacity resulting from the hamiltonian (3), superimposed on a Schottky anomaly, which can be described by the hamiltonian (2) with $J = 0$. This anomaly corresponds to a broad bump in the heat capacity with a maximum of ~ 2 J/mol K for $D > 0$ and ~ 6 J/mol K for $D < 0$ at $kT/|D| \sim 0.4$. Given the small ratio of $|J|/D$ inferred above, we assert that the maximum of the Schottky anomaly will be located at rather high temperatures, and may therefore be partly compensated by a readjustment of the scaling factor. Hence we tried - for what it is worth - to describe the magnetic heat capacity by the S = 1/2 Ising model.

At this stage one should realize that the one-dimensional characteristics of the magnetic heat capacity, involving a broad bump in the paramagnetic region, are somewhat obscured by the three-dimensional ordering, which indicates that significant interchain interactions are present. If we assume, however, that the interactions in the b and c direction are rather different, the heat capacity in the paramagnetic

region should display some characteristics of the two-dimensional rectangular Ising model, which has been presented in Chapter II. We have fitted the heat capacity predicted by this model to the experimental data above 13 K for several values of the scaling factor α. An excellent agreement was found for $\alpha = 0.98$. The result is plotted in Figure 7.6. The open circles denote the experimental data corrected for the lattice contribution. The drawn curve denotes the heat capacity of a S = 1/2 rectangular Ising model with $|J_1/k| = 39$ K, $|J_2/k| = 0.7$ K. The errorbars reflect the uncertainty in the evaluation of the lattice heat capacity of $\alpha RbMnCl_3.2H_2O$, which has been used in the scaling procedure (cf. section 7.2). As may be seen from this figure, the S = 1/2

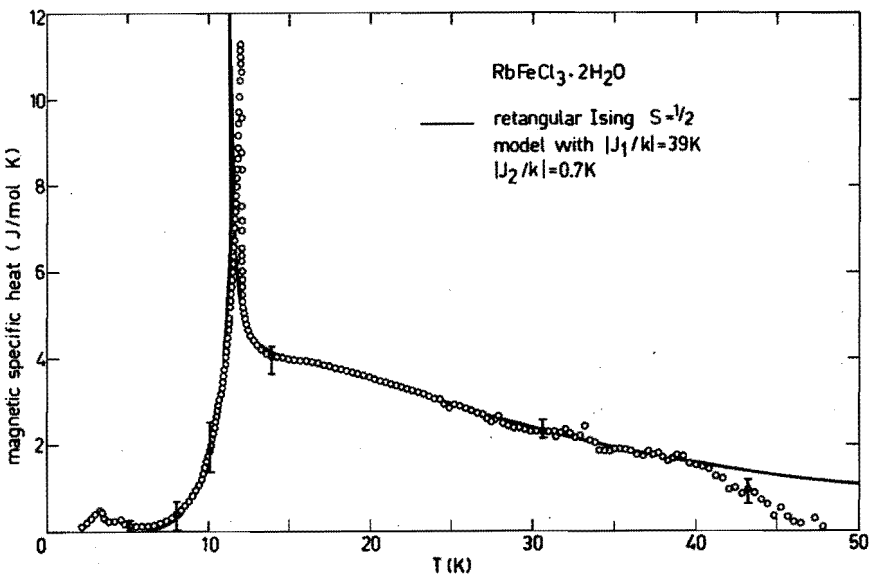

FIG. 7.6. Magnetic heat capacity of $RbFeCl_3.2H_2O$ versus temperature. The open circles are the experimental data minus a scaled lattice heat capacity of $\alpha RbMnCl_3.2H_2O$. The errorbars reflect the uncertainty in the evaluation of the lattice heat capacity of the latter compound. The drawn curve denotes the theoretical prediction for a S = 1/2 rectangular Ising model with $|J_1/k| = 39$ K, $|J_2/k| = 0.7$ K. The small anomalies at 3.3 and 4.6 K are due to sample impurities.

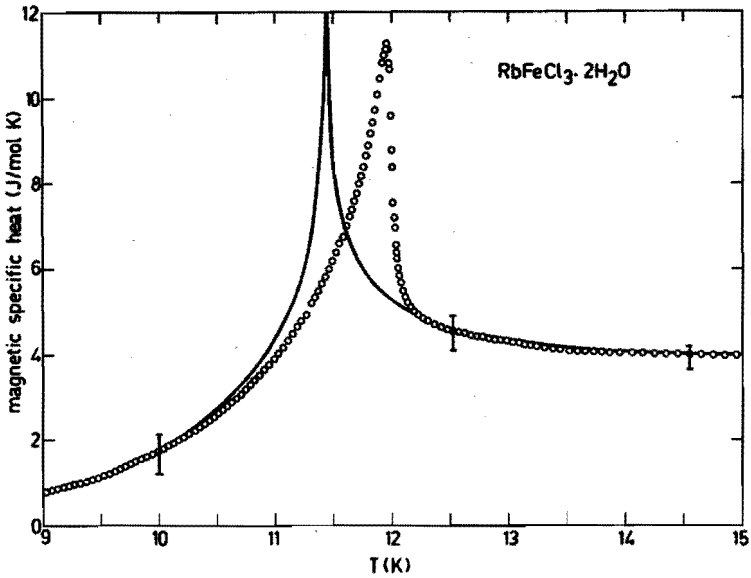

FIG. 7.7. Magnetic heat capacity of $RbFeCl_3.2H_2O$ near the three-dimensional ordering temperature. Details are explained in the caption of Figure 7.6.

rectangular Ising model does not only give a fair description of the *paramagnetic* region, but does also correctly predict the behaviour of the *ordered* state below 10 K. The small anomalies at 3.3 and 4.6 K are due to sample impurities. The behaviour near the ordering temperature is plotted in detail in Figure 7.7. We are tempted to conclude that the second interchain interaction shifts the ordering towards higher temperatures, but produces only a very small effect on the heat capacity below 10 K and above 12.5 K.

If we confront the value $|J_1/k| = 39$ K, obtained from the fit of the Ising model to the heat capacity, with the relation $J_1 = 4J$ and the condition $|J/D| < 1/8$ inferred above, we find that the first excited level in the single-ion energy spectrum should be located more than 80 K above the ground state doublet. One should bear in mind, however, that although the heat capacity at low temperatures can be very well described by the S = 1/2 Ising model, a direct relation with the hamiltonian (2) or (3) would drastically oversimplify the physical

reality. Firstly, NMR [25] and magnetization [21] experiments suggest a *canted* array with the magnetic moments situated in the ac plane, like $CsCoCl_3.2H_2O$, but individual chains having a net moment along c instead of a. Secondly, preliminary measurements of the susceptibility at room temperature [21] can be described with $g \sim 2$ and $S = 2$. These results may indicate that in this substance the orbital degeneracy of the Fe^{++} ground state has been removed completely, which occurs for crystalline fields of sufficiently low symmetry, e.g., rhombic. If this splitting is large compared to the spin-orbit coupling, which is about 100 cm^{-1} [13], we have to deal with a spin-quintet, that may be described with the hamiltonian [13, 14]:

$$H = D[S_z^2 - \tfrac{1}{3} S(S + 1)] + E(S_x^2 - S_y^2) \ , \ S = 2, \tag{4}$$

in combination with exchange interactions. If these interactions are relatively weak, equation (4) yields the single-ion energy levels

$$W_1 = 2D(1 + 3E^2/D^2)^{1/2} \tag{5a}$$

$$W_2 = 2D \tag{5b}$$

$$W_3 = - D + 3E \tag{5c}$$

$$W_4 = - D - 3E \tag{5d}$$

$$W_5 = - 2D(1 + 3E^2/D^2)^{1/2}. \tag{5e}$$

For $D < 0$ and small values of E or, alternatively, for $D > 0$ and $|E| \sim D$ - two situations which are basically identical but correspond to different sets of quantization axes - the resulting energy-level scheme has a quasi-doublet lowest, as is shown in Figure 7.8. As we mentioned above, there is some evidence that the first excited level will be located more than 80 K above the ground state "doublet". Since at room temperature all five levels seem to be populated, the overall width of the level scheme should be considerably smaller than 300 K.

Finally, we would like to make some concluding remarks. The higher excited levels, depicted in Figure 7.8, would give rise to a small gradual increase of the magnetic heat capacity, even below 50 K, which has not been accounted for explicitly in the fitting procedure. As already mentioned above, the resulting error may to a large extent be

compensated by a readjustment of the scaling factor α, which might explain the rather low value 0.98 corresponding to the best fit to the experimental data.

The conjectured magnitude of the zero-field splitting seems somewhat large compared to the splitting of some other ferrous compounds, for instance $FeCl_2.4H_2O$ [14], which would suggest a relatively small splitting of the orbital triplet in RFC [13]. Optical measurements may be necessary to clarify this question.

The present analysis of $RbFeCl_3.2H_2O$ reveals a highly one-dimensional magnetic behaviour. The intrachain interaction has a magnitude of $\sim$ 39 K, which is almost equal to the corresponding interaction in $CsCoCl_3.2H_2O$; the interchain coupling in $RbFeCl_3.2H_2O$ seems larger by a factor 3. Although a description of the lattice contribution to the heat capacity by simple temperature-independent scaling of the lattice heat capacity of an isomorphic compound should generally be considered with some reservations, for these "diluted" systems, where the mass difference of the magnetic ions of both isomorphs is very small and all other constituents are equal, it proves to be a powerful tool in the determination of the characteristic behaviour of the magnetic contribution.

In the analysis given above as well as in the preceeding chapters we assumed that the lattice and magnetic contributions could be linear-

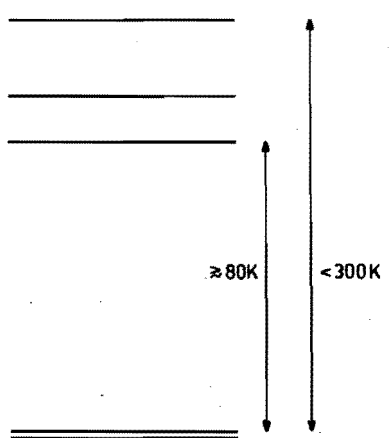

FIG. 7.8.
Proposed energy level scheme of Fe^{++} in $RbFeCl_3.2H_2O$. The level separations are explained in the text.

ly separated. This assumption is very likely correct for the manganese salts, since for these compounds the magnon-phonon interaction energies are rather small [26, 27]. For the Co^{++} and Fe^{++} salts, however, these energies may be substantially larger, because the modulation of the crystal field at the spin sites by the lattice vibrations has a rather direct effect on the "effective" exchange interactions. In fact, optical measurements on $CoCl_2.2H_2O$ and $FeCl_2.2H_2O$ [27, 28, 29] show that a low-lying *optical* phonon ($E_{ph} \sim 30$ cm^{-1}), corresponding to a vibration of the waters of hydration, interacts rather strongly with the magnons.

For CCC and RFC, the "unperturbed" magnon energies will be about twice as high as the magnon energies in $CoCl_2.2H_2O$ and $FeCl_2.2H_2O$, due to the large value of the intrachain interaction ($\sim$ 40 K) in the former two compounds. However, detailed far-infrared optical measurements are necessary to analyse the possible phonon-magnon interaction processes as well as the influence of these effects on the specific heat.

REFERENCES CHAPTER VII

1. T. Moriya, K. Motizuki, J. Kanamori, and T. Nagamiya, J. Phys. Soc. Japan 11, 211 (1956).
2. J.B. Torrance, Jr. and M. Tinkham, Phys. Rev. 187, 595 (1969).
3. D.B. Losee, J.N. McElearny, G.E. Shankle, R.N. Carlin, P.J. Cresswell, and W.T. Robinson. Phys. Rev. B8, 2185 (1973).
4. N. Uryû, J. Skalyo, and S.A. Friedberg, Phys. Rev. 144, 689 (1966).
5. W.J.M. de Jonge, K.V.S. Rama Rao, C.H.W. Swüste, and A.C. Botterman, Physica 51, 620 (1971).
6. A. Herweijer, W.J.M. de Jonge, A.C. Botterman, A.L.M. Bongaarts, and J.A. Cowen, Phys. Rev. B5, 4618 (1972).
7. A.L.M. Bongaarts and B. van Laar, Phys. Rev. B6, 2669 (1972).
8. N. Thorup and H. Soling, Acta Chem. Scand. 23, 2933 (1969).
9. T. de Neef, J. Phys. Soc. Japan 37, 71 (1974).
10. A.L.M. Bongaarts, Ph.D. Thesis, Eindhoven (1975).
11. W.J.M. de Jonge, private communication.

12. A. Abragam and B. Bleaney, "*Electron Paramagnetic Resonance of Transitions Ions*", Clarendon Press, Oxford (1970).

13. M. Tinkham, Proc. Roy. Soc. A236, 535 (1956).

14. J.T. Schriempf and S.A. Friedberg, Phys. Rev. 136, A518 (1964).

15. K. Motizuki, J. Phys. Soc. Japan 14, 759 (1959).

16. J.F. Nagle and J.C. Bonner, J. Chem. Phys. 54, 729 (1971).

17. J.W. Stout and R.C. Chisholm, J. Chem. Phys. 36, 979 (1962).

18. J.W. Stout and E. Catalano, J. Chem. Phys. 23, 2013 (1955).

19. J.A. Hofmann, A. Paskin, K.J. Tauer, and R.J. Weiss, J. Phys. Chem. Solids 1, 45 (1956).

20. S.A. Friedberg and J.D. Wasscher, Physica 19, 1072 (1953).

21. Q.A.G. van Vlimmeren, private communication.

22. M. Suzuki, B. Tsujiyama, and S. Katsura, J. Math. Phys. 8, 124 (1967).

23. T. de Neef, Ph.D. Thesis, Eindhoven (1975).

24. H.W.J. Blöte, Physica 79B, 427 (1975).

25. C.H.W. Swüste, private communication.

26. See, for example, R.L. Comstock, Proc. IEEE 53, 1508 (1965).

27. S.J. Allen and H.J. Guggenheim, Phys. Rev. 166, 530 (1968).

28. J.B. Torrance and M. Tinkham., Phys. Rev. 187, 595 (1969).

29. J.B. Torrance and J.C. Slonczewski, Phys. Rev B5, 4648 (1972).

CHAPTER VIII

THREE-DIMENSIONAL ORDERING OF THE SERIES $AMB_3.2H_2O$

8.1. Introduction

The preceeding two chapters have been devoted mainly to those magnetic characteristics of the series $AMB_3.2H_2O$, which strongly reflect the pseudo one-dimensional magnetic behaviour of these compounds. In this chapter, we shall consider the region near the three-dimensional ordering temperature. Apart from the fact, that this region is very interesting from a theoretical point of view [1], it may - in principle - serve as a source of additional information about the magnetic properties [2-4]. A detailed investigation of the critical behaviour, however, would be beyond the scope of this thesis, and hence it will be studied only briefly.

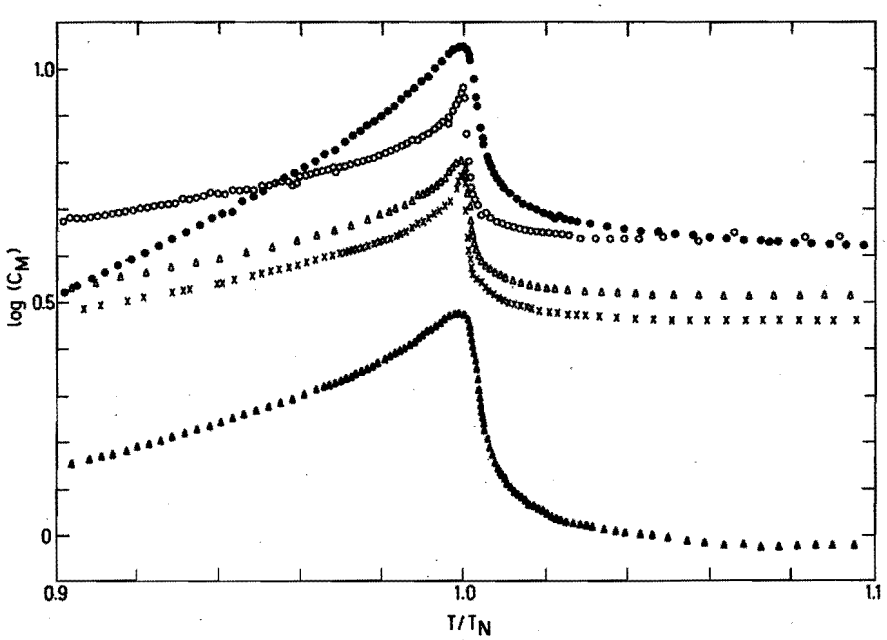

FIG. 8.1. Magnetic specific heat of the compounds $AMB_3.2H_2O$ near the ordering temperature as a function of T/T_N. ● $RbFeCl_3.2H_2O$, ○ $CsMnBr_3.2H_2O$, △ $CsMnCl_3.2H_2O$, × $\alpha RbMnCl_3.2H_2O$, ▲ $CsCoCl_3.2H_2O$.

In Chapter VII we have shown that the magnetic anisotropy of both $CsCoCl_3.2H_2O$ (CCC) and $RbFeCl_3.2H_2O$ (RFC) is very large compared to the anisotropy of the manganese isomorphs. As a first step towards the study of the critical behaviour, we thought it worthwhile to investigate whether this difference is also reflected by the magnetic heat capacity in the neighbourhood of T_N. For this purpose, we plotted log (C_M) versus T/T_N for all five compounds. The results are drawn in Figure 8.1 for $0.9 < T/T_N < 1.1$; the magnetic heat capacity was obtained by subtracting the corresponding lattice contribution from the experimental data. Inspection of this figure shows that two curves, denoted by black circles and black triangles, respectively, have a rather pronounced lambda shape. They can clearly be distinguished from the remaining three curves, which are mutually similar, apart from a small shift in the vertical direction. Since the latter three curves represent the data on the manganese compounds, one is tempted to conclude that the difference in the character of the magnetic interactions is - to a certain extent - reflected by the behaviour in the neighbourhood of T_N. Next, we shall consider the region very close to the ordering temperature.

8.2. The critical behaviour

The properties of magnetic systems in the limit $|T-T_N| \to 0$ have been the subject of a large number of both theoretical and experimental investigations [1]. These studies reveal that for systems with short-range interactions this critical behaviour only depends upon the dimensionality of the lattice and the number of spin-components involved in the magnetic ordering process. The critical behaviour of the magnetic heat capacity just above T_N is customarily characterized by a critical exponent α, defined as

$$-\alpha = \lim_{\varepsilon \to 0} [\ln(C_M)/\ln(\varepsilon)], \text{ with } \varepsilon = T/T_N - 1. \qquad (1)$$

Below the critical temperature, the heat capacity may be characterized in a similar way by a critical exponent α'. Theoretical investigations on some magnetic model systems suggest that α' and α may be equal [1].

For three-dimensional ordering processes, numerical estimates for the value of α have been obtained for several model systems. The results are

$$\begin{array}{lll} \alpha = 1/8 & \text{Ising} & [2] \\ \alpha \sim 0 & \text{XY} & [3] \\ \alpha \sim 0 & \text{Heisenberg} & [4]. \end{array} \qquad (2)$$

Experimental estimates for α as well as α' may - in principle - be obtained by plotting C_M versus $\log|\varepsilon|$ or $\log(C_M)$ versus $\log|\varepsilon|$ in a region close enough to T_N. For all five compounds under investigation these plots revealed a very pronounced curvature of the experimental data, which could not be removed by a physically acceptable readjustment of the value of T_N. This is demonstrated by Figure 8.2 and 8.3, in which the results for $CsMnCl_3.2H_2O$ and $CsCoCl_3.2H_2O$ are presented. The "rounding off" of the data in the region $|\varepsilon| < 10^{-3}$ has been suggested [5, 6] to be due to sample imperfections, although a plausible mechanism to explain the observed order of magnitude has

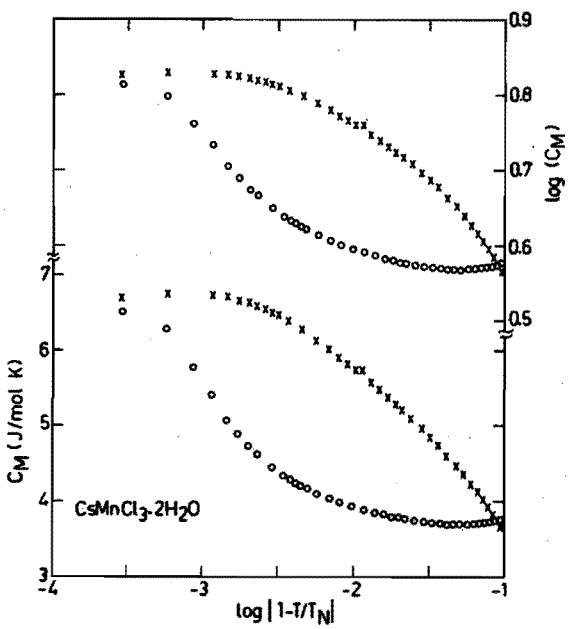

FIG. 8.2.
Plot of C_M and $\log(C_M)$ as a function of $\log|1-T/T_N|$ for $CsMnCl_3.2H_2O$. The open circles represent the data for $T > T_N$, the crosses denote the data for $T < T_N$.

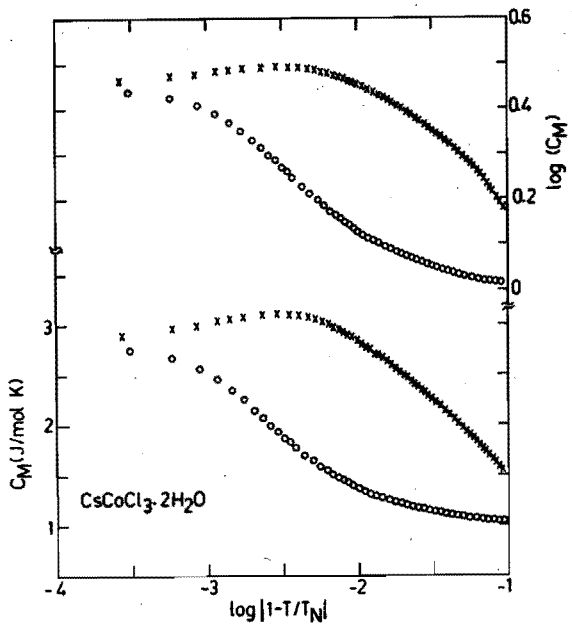

FIG. 8.3.
Plot of C_M and $\log(C_M)$ as a function of $\log|1-T/T_N|$ for $CsCoCl_3.2H_2O$. The open circles represent the data for $T > T_N$, the crosses denote the data for $T < T_N$.

not been reported. The curvature for larger values of $|\varepsilon|$ may be caused by the fact that the critical behaviour of the heat capacity is described by a rather small value of the critical exponent. In this case - a so called "weak divergence" - correction terms on the limiting behaviour $C_M = A\varepsilon^{-\alpha}$, corresponding to equation (1), may be important already for small values of ε.

The relative influence of these correction terms is smaller for a "strong divergence" like the critical behaviour of the magnetic entropy increase, which is given by

$$\lim_{\varepsilon \to 0} \{\ln[S(\varepsilon) - S_{crit}]/\ln(\varepsilon)\} = 1 - \alpha. \qquad (3)$$

In this expression S_{crit} denotes the critical entropy. Both $S(\varepsilon)$ and S_{crit} may be calculated from the experimental data by numerical integration of C_M/T. Estimates of $1 - \alpha$ and $1 - \alpha'$ may be obtained from double-logarithmic plots of $S - S_{crit}$ versus $|\varepsilon|$. In Figure 8.4 the results for the manganese compounds are given. Inspection of this figure shows that the data for $T > T_N$ can be represented very well by straight

lines. The data for $T < T_N$ reveal some curvature, but the results indicate that $\alpha' = \alpha$. The slope (~ 0.90) of the lines representing the data for $T > T_N$ suggests a critical behaviour involving a smaller number of spin-components than 3, a value that would have been expected from the Heisenberg character of the exchange interactions. One should note, however, that in these compounds small dipolar interactions and crystal-field effects are present. Although these "perturbations" are negligible at higher temperatures, they may play an important role in the ordering process close to T_N.

In Figure 8.5 the results for CCC and RFC are presented. The data on

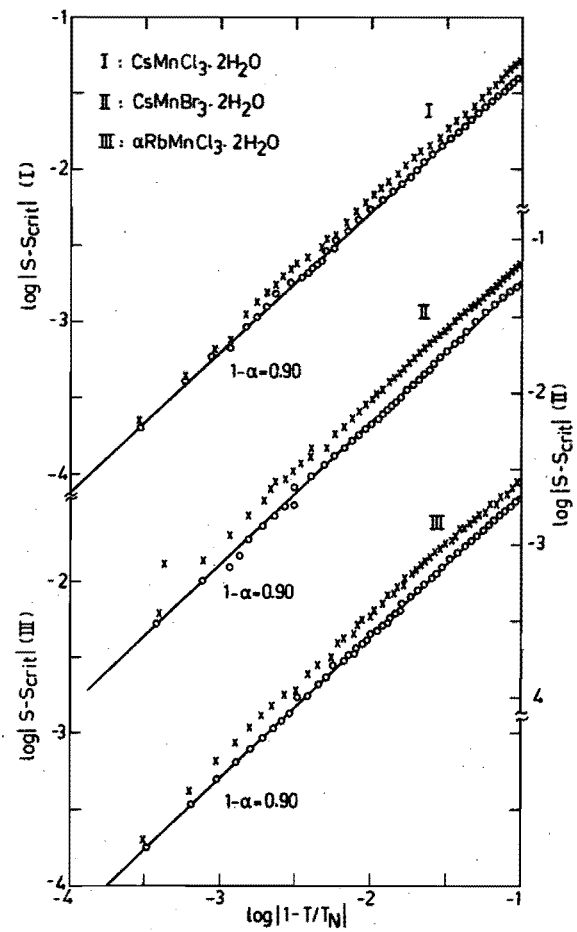

FIG. 8.4. Double-logarithmic plot of the magnetic entropy minus the critical entropy versus $|1-T/T_N|$ for $CsMnCl_3.2H_2O$, $\alpha RbMnCl_3.2H_2O$ and $CsMnBr_3.2H_2O$. The open circles represent the data for $T > T_N$, the crosses are the data for $T < T_N$.

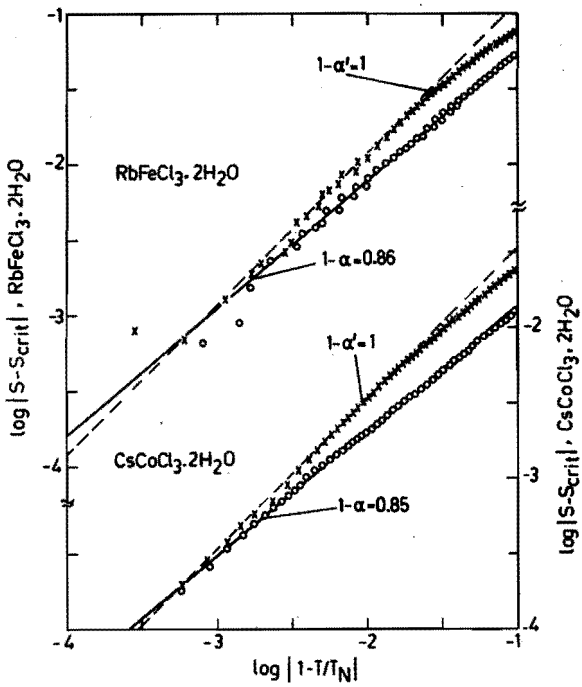

FIG. 8.5. Double-logarithmic plot of the magnetic entropy minus the critical entropy versus $|1-T/T_N|$ for $RbFeCl_3.2H_2O$ and $CsCoCl_3.2H_2O$. The open circles represent the data for $T > T_N$, the crosses are the data for $T < T_N$.

the latter compound show a considerable scatter for $|\varepsilon| < 5 \times 10^{-3}$. This is caused by the fact that at temperatures of about 12 K, corresponding to the ordering temperature of RFC, the experimental resolution is much smaller than in the helium region, due to the lower sensitivity of the thermometer. For both compounds, the data above T_N can be fairly well represented by a straight line with a slope of ~ 0.85. This value is not very different from the value 0.875 corresponding to the three-dimensional Ising model (cf. equation (2)), which is in agreement with the conjectured Ising-like character of the exchange interactions in these compounds. The data below T_N show considerable deviations from a linear behaviour, which cannot be eliminated by a readjustment of the value of T_N. For $10^{-3} < -\varepsilon < 10^{-2}$ the results may locally be described by a straight line with a slope of ~ 1, which is indicated by dashed lines in Figure 8.5. For what it is worth, this value of $1 - \alpha'$ is not inconsistent with the theoretical observation that for $(1 - T/T_N) > 10^{-4}$ the "critical" behaviour of a three-dimensional Ising model may be "virtually" logarithmic [2].

In principle, the divergence of the magnetic entropy increase as a function of T should be similar to the divergence of the induced magnetization M as a function of the applied field H at temperatures not too far below T_N [1]. Detailed information about the behaviour of M(H) is available for CCC, which has been investigated with neutron-diffraction experiments [7]. Some typical results of these experiments are plotted in Figure 8.6, together with our data for the magnetic entropy increase. As can be seen from this figure the overall behaviour of the various sets of data is indeed largely similar. After a gradual increase they have a maximum slope at $T \sim T_N$ or $H \sim H_{crit}$, the increase above the critical point being much smaller. One should note that the data for S/S_{crit} may have some systematic error, because the magnetic entropy increase below 2 K ($\sim$ 0.03 R) is obtained by extrapolating the experimental data down to T = 0. This extrapolated fraction is rather large compared to the value 0.08 R of the critical entropy. Therefore an investigation

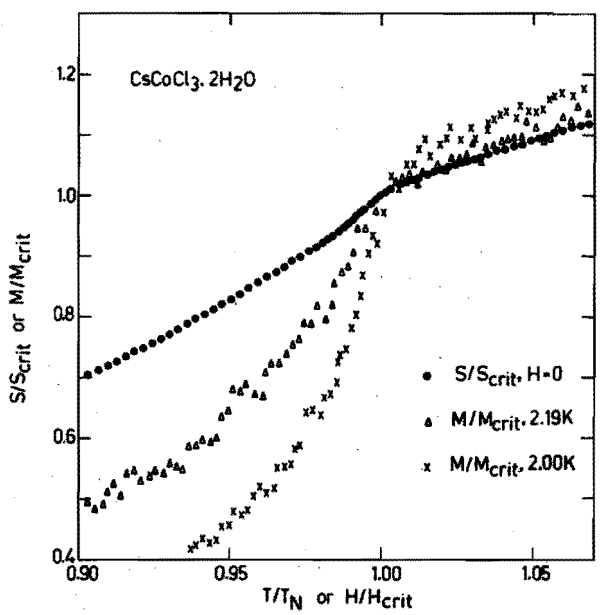

FIG. 8.6. Behaviour of the magnetic entropy S and the induced magnetization M near the antiferromagnetic-paramagnetic phase boundary in $CsCoCl_3.2H_2O$.

whether the various sets of data can be made to overlap by a suitable scaling procedure has to await accurate heat capacity measurements down to very low temperatures.

Concluding we would like to make the following remarks. The results presented in this chapter clearly establish that the ordering process of CCC and RFC differs significantly from that of the manganese isomorphs. A further analysis is necessary to clarify the observed values of the critical exponents. Moreover, some attention should be given to the fact that - in contrast to the magnetic heat capacity - the plots of $S - S_{crit}$ for $T > T_N$ do not show any significant rounding for $\varepsilon < 10^{-3}$. The present study, however, did not intend to consider the critical behaviour in great detail, but the results obtained above seem rather promising.

REFERENCES CHAPTER VIII

1. H.E. Stanley, *"Introduction to phase transitions and critical phenomena"*, Oxford University Press (1971).
2. C. Domb, in *"Phase transitions and critical phenomena"*, Vol. 3, edited by C. Domb and M.S. Green, Academic Press, New York (1973).
3. D.D. Betts, in the same book as reference [2].
4. G.S. Rushbrooke, G.A. Baker, and P.J. Wood, in the same book as reference [2].
5. J. Skalyo and S.A. Friedberg, Phys. Rev. Letters 13, 133 (1964).
6. R.F. Wielinga, Ph.D. Thesis, Leiden (1968).
7. A.L.M. Bongaarts, Ph.D. Thesis, Eindhoven (1975).

APPENDIX

The n-dimensional Debye function is defined as

$$D_n(y) = 3nR/y \int_0^y \frac{x^{n+1} e^x}{(e^x-1)^2}\, dx \ , \qquad (1)$$

where R denotes the molar gas constant.

The integral that appears at the right hand side of equation (III,24) can be evaluated as follows. Let us define a function $G_1(T/\Theta_c)$ as

$$G_1(T/\Theta_c) = \frac{24RT^2}{\pi\Theta_c^2} \int_0^{\Theta_c/T} \frac{x^3 e^x}{(e^x-1)^2} \arcsin(xT/\Theta_c)\, dx \ . \qquad (2)$$

The low-temperature behaviour of $G_1(T/\Theta_c)$ can be found by substituting $\arcsin(xT/\Theta_c) = xT/\Theta_c$, since the integrand goes exponentially to zero for large values of x. The result is

$$G_1(T/\Theta_c) = \frac{8}{3\pi} D_3(\Theta_c/T) \ . \qquad (3)$$

At low temperatures, the function G_1 may also be described by the equation $G_1(T/\Theta_c) = D_3(\Theta/T)$, if we put

$$\Theta = (3\pi/8)^{1/3} \Theta_c \ . \qquad (4)$$

At higher temperatures, the relative difference between the function $G_1(T/\Theta_c)$ and the three-dimensional Debye function $D_3[(3\pi/8)^{1/3}\Theta/T]$ may now be approximated with a function $P_1(T/\Theta_c)$, for example a polynomial series in T/Θ_c. The approximation

$$G_1(T/\Theta_c) = D_3[(\tfrac{3\pi}{8})^{1/3}\Theta_c/T] \times [1-P_1(T/\Theta_c)] \qquad (5)$$

was found to have a relative accuracy better than 2×10^{-4} for $0 < T/\Theta_c < \infty$ with the polynomial series

$$P_1(T/\Theta_c) = \exp\{\sum_{i=0}^{9} B_{1,i} [\ln(T/\Theta_c)]^i\}. \qquad (6)$$

The coefficients $B_{1,i}$, obtained by a least-squares fit of approximation (6), are listed in Table A.1.

The function $G_2(T/\Theta)$, substituted in equation (III, 33), is equal to the heat capacity that is obtained if the frequency distribution function

$$g(\omega) = 3/(\omega_s I_1) \int_0^b \zeta[1-(\omega_s/2\omega)^2 \sin^2\zeta]^{-1/2} d\zeta, \qquad (7)$$

with $b = \arcsin(2\omega/\omega_s)$ for $\omega \leqslant \omega_s/2$ and $b = \pi/2$ for $\omega \geqslant \omega_s/2$, is substituted in equation (III, 23) with $\omega_m = \omega_s$. For $\omega << \omega_s$, equation (7) reduces to

$$g(\omega) = 3/(\omega_s I_1) \int_0^{2\omega/\omega_s} \zeta[1-(\omega_s/2\omega)^2 \zeta^2]^{-1/2} d\zeta = \frac{12\omega^2}{I_1 \omega_s^3} . \qquad (8)$$

The limiting low-temperature behaviour of the heat capacity may now be found as

TABLE A.1. Coefficients $B_{1,i}$ of the polynomial series $P_1(T/\Theta_c)$ that relates the function $G_1(T/\Theta_c)$ to a three-dimensional Debye-function (cf. equation 5).

$T/\Theta_c \leqslant 0.1$	$T/\Theta_c \geqslant 0.1$
$B_{1,0} = +2.43502 \times 10^{+2}$	$B_{1,0} = -5.63143$
$B_{1,1} = +7.11922 \times 10^{+2}$	$B_{1,1} = -1.94211$
$B_{1,2} = +8.66012 \times 10^{+2}$	$B_{1,2} = -5.32241 \times 10^{-2}$
$B_{1,3} = +5.87204 \times 10^{+2}$	$B_{1,3} = +3.39971 \times 10^{-2}$
$B_{1,4} = +2.46622 \times 10^{+2}$	$B_{1,4} = -1.88309 \times 10^{-2}$
$B_{1,5} = +6.70161 \times 10^{+1}$	$B_{1,5} = +7.53021 \times 10^{-3}$
$B_{1,6} = +1.18407 \times 10^{+1}$	$B_{1,6} = -1.48747 \times 10^{-3}$
$B_{1,7} = +1.31640$	$B_{1,7} = -5.64074 \times 10^{-8}$
$B_{1,8} = +8.37847 \times 10^{-2}$	$B_{1,8} = +4.33673 \times 10^{-5}$
$B_{1,9} = +2.33086 \times 10^{-3}$	$B_{1,9} = -4.44569 \times 10^{-6}$

TABLE A.2. Coefficients $B_{2,i}$ of the polynomial series $P_2(T/\Theta_s)$ that relates the function $G_2(T/\Theta_s)$ to a three-dimensional Debye-function (cf. equation 11).

$T/\Theta_s \leqslant 0.03$	$0.03 \leqslant T/\Theta_s \leqslant 0.40$	$0.40 \leqslant T/\Theta_s$
$B_{2,0} = -2.49859 \times 10^{+4}$	$B_{2,0} = -3.00059$	$B_{2,0} = -4.94117$
$B_{2,1} = -7.32324 \times 10^{+4}$	$B_{2,1} = +8.17766$	$B_{2,1} = -2.00101$
$B_{2,2} = -9.28342 \times 10^{+4}$	$B_{2,2} = +2.37706 \times 10^{+1}$	$B_{2,2} = +7.11166 \times 10^{-4}$
$B_{2,3} = -6.70697 \times 10^{+4}$	$B_{2,3} = +3.24892 \times 10^{+1}$	$B_{2,3} = +4.36995 \times 10^{-4}$
$B_{2,4} = -3.05181 \times 10^{+4}$	$B_{2,4} = +2.86322 \times 10^{+1}$	$B_{2,4} = -1.73992 \times 10^{-3}$
$B_{2,5} = -9.08819 \times 10^{+3}$	$B_{2,5} = +1.68368 \times 10^{+1}$	$B_{2,5} = +1.71293 \times 10^{-3}$
$B_{2,6} = -1.77404 \times 10^{+3}$	$B_{2,6} = +6.57270$	$B_{2,6} = -8.19824 \times 10^{-4}$
$B_{2,7} = -2.19161 \times 10^{+2}$	$B_{2,7} = +1.63229$	$B_{2,7} = +2.09085 \times 10^{-4}$
$B_{2,8} = -1.55637 \times 10^{+1}$	$B_{2,8} = +2.31085 \times 10^{-1}$	$B_{2,8} = -2.72743 \times 10^{-5}$
$B_{2,9} = -4.84491 \times 10^{-1}$	$B_{2,9} = +1.40476 \times 10^{-2}$	$B_{2,9} = +1.43144 \times 10^{-6}$

$$G_2(T/\Theta_s) = 4/(3I_1)\, D_3(\Theta_s/T), \tag{9}$$

or, alternatively,

$$G_2(T/\Theta_s) = D_3[(3I_1/4)^{1/3}\Theta_s/T]. \tag{10}$$

Following the same procedure as outlined above the function $G_2(T/\Theta_s)$ can be described with a relative accuracy better than 5×10^{-4} for all temperatures by the approximation

$$G_2(T/\Theta_s) = D_3[(3I_1/4)^{1/3}\Theta_s/T] \times [1 - P_2(T/\Theta_s)]. \tag{11}$$

The magnitude of I_1 has been numerically evaluated as $I_1 = 1.1190677$, while the constants $B_{2,i}$ in the polynomial series $P_2(T/\Theta_s)$, having the same functional form as $P_1(T/\Theta_c)$, are listed in Table A.2.

Given the fact, that for the usual Debye functions various series expansions are available [1], the results given by the relations (5) and (11) are very suitable in numerical fitting procedures, since the derivatives to the different parameters may be calculated very easily.

In this thesis no tabulated results of the heat capacity measurements have been presented. In order to make such tables useful for numerical fitting procedures, they would have to contain a rather large number of experimental data. Detailed results of the measurements, however, are presented elsewhere [2].

REFERENCES

1. M. Abramowitz and I.A. Stegun, "*Handbook of Mathematical Functions*", N.B.S. 55 (1964).

2. K. Kopinga, Internal Report T.H.E. (1976).

SAMENVATTING

Dit proefschrift is gewijd aan de bestudering van de soortelijke warmte van magnetische ketenverbindingen.

Omdat het magnetische gedrag - zelfs van deze verbindingen - doorgaans bijzonder gecompliceerd is, worden de meest karakteristieke kenmerken ervan vergeleken of beschreven met de eigenschappen van een vereenvoudigd magnetisch modelsysteem. Een dergelijk modelsysteem bestaat veelal uit een verzameling geisoleerde ketens of lagen van magnetische ionen. In hoofdstuk II wordt een overzicht gegeven van de voor het onderzoek relevante modelsystemen en wordt de soortelijke warmte ervan behandeld.

Voor de interpretatie van de meetgegevens is een scheiding van de totale soortelijke warmte in een magnetische en een roosterbijdrage noodzakelijk. In hoofdstuk III wordt daartoe een theoretisch model ontwikkeld, waarmee de rooster soortelijke warmte van verbindingen met een gelaagde of keten-structuur op een voor separatie-doeleinden bevredigende wijze kan worden benaderd.

In hoofdstuk IV wordt de gebruikte meetopstelling besproken.
In de daarop volgende hoofdstukken komen de metingen aan de orde die verricht zijn aan een tweetal reeksen isostructurele verbindingen, te weten de reeks $(CH_3)_4NXCl_3$, met X = Cd, Mn, Ni en een aantal stoffen uit de serie $AMB_3.2H_2O$, te weten $CsMnCl_3.2H_2O$, $\alpha RbMnCl_3.2H_2O$, $CsMnBr_3.2H_2O$, $CsCoCl_3.2H_2O$ en $RbFeCl_3.2H_2O$. De verkregen meetgegevens zijn vanuit twee verschillende gezichtshoeken bezien. Enerzijds kon, door vergelijking van de eigenschappen van de verschillende verbindingen het door de modelsystemen voorspelde gedrag aan de praktijk worden getoetst. Anderzijds kon, gedeeltelijk door combinatie met de resultaten verkregen via andere experimentele metingen (kernspinresonantie, AFMR, neutronen-diffractie, magnetisatie en susceptibiliteit) een gedetailleerd inzicht worden verkregen in de aard en grootte van de magnetische wisselwerkingen in deze verbindingen

De reeks $(CH_3)_4NXCl_3$ wordt behandeld in hoofdstuk V. Na een analyse van de rooster soortelijke warmte van de - diamagnetische - Cd verbinding wordt de magnetische soortelijke warmte van de Mn verbinding (TMMC) onderzocht; dit omdat de laatstgenoemde stof als een vrijwel ideale benadering van een zuiver ééndimensionaal magnetisch modelsysteem kan worden beschouwd. Vervolgens worden enkele eigenschappen van de isostructurele Ni

verbinding besproken.

De genoemde Mn verbindingen uit de reeks $AMB_3.2H_2O$ worden behandeld in hoofdstuk VI. Naast een vergelijking van de magnetische eigenschappen van deze verbindingen wordt ingegaan op de invloed van kleine afwijkingen van het zuiver ééndimensionale modelsysteem op het gedrag in zowel de paramagnetische als de geordende toestand.

De eigenschappen van de twee laatstgenoemde verbindingen, $CsCoCl_3.2H_2O$ en $RbFeCl_3.2H_2O$, komen aan de orde in hoofdstuk VII. Deze stoffen onderscheiden zich van de drie mangaan-verbindingen door hun grote magnetische anisotropie.

De invloed van de aard van de magnetische wisselwerkingen in de verbindingen van de reeks $AMB_3.2H_2O$ op het gedrag in de omgeving van de driedimensionale ordeningstemperatuur wordt tenslotte besproken in hoofdstuk VIII.

Het in dit proefschrift beschreven onderzoek is uitgevoerd binnen het kader van het onderzoekprogramma van de groep magnetisme onder leiding van Prof. Dr. P. van der Leeden en Dr. Ir. W.J.M. de Jonge.

Aan het totstandkomen van dit proefschrift hebben velen meegewerkt.

- *Ir. A. Herweijer heeft mij op de hoogte gebracht van de techniek van de soortelijke-warmte metingen.*
- *Verschillende stagiairs en afstudeerders, in het bijzonder de heer A.J.M. Kuipers, hebben een belangrijke bijdrage geleverd aan het verzamelen en verwerken van de meetgegevens.*
- *De technische assistentie werd verleend door de heer A.M.J. Duijmelinck en Ing. J. Millenaar.*
- *De discussies met mijn collega's Dr. Ir. A.L.M. Bongaarts, Ir. J.P.A.M. Hijmans, Dr. Ir. C.H.W. Swüste en Dr. Ir. T. de Neef hebben een zeer positieve invloed gehad op de inhoud van het onderzoek.*
- *Bijzonder veel dank ben ik verschuldigd aan Dr. Ir. W.J.M. de Jonge en Prof. Dr. P. van der Leeden voor hun zeer stimulerende belangstelling en begeleiding.*
- *Mej. M.C.K. Gruijters en Mevr. M.J.H. Doors-Smits ben ik erkentelijk voor het teken- en typwerk.*

LEVENSBERICHT

10-10-1948 Geboren te Eindhoven.

1966 Eindexamen Gymnasium-β, Protestants Lyceum te Eindhoven.

1966 - 1971 Studie aan de Technische Hogeschool te Eindhoven, afdeling der Technische Natuurkunde.
Afstudeerwerk onder leiding van Ir. C.H.W. Swüste in de sectie Physische Analyse Methoden onder leiding van Prof.Dr. P. van der Leeden met als onderwerp "Broomkernspinresonanties in antiferromagnetisch $MnBr_2.4H_2O$".

1971 - 1976 Wetenschappelijk medewerker aan de Technische Hogeschool te Eindhoven in de groep magnetisme onder leiding van Prof.Dr. P. van der Leeden en Dr.Ir. W.J.M. de Jonge.

STELLINGEN

I

De vergelijking van de mate van magnetische ééndimensionaliteit van de ketenverbindingen $CuCl_2.(NC_5H_5)_2$ en $(CH_3)_4NMnCl_3$, zoals die door Takeda et al. aan de hand van de verhouding van de ordeningstemperatuur en de exchange-constante in de ketens wordt gegeven, gaat voorbij aan de feitelijke grootte van de interactie-energie.

K. Takeda, Y. Yamamoto en T. Haseda, Phys. Lett. 45A, 419 (1973).

II

Bij de analyse van de eigenschappen van antiferromagnetische systemen, welke gekarakteriseerd kunnen worden door een effectieve spin 1/2, met behulp van "mean-field" achtige theoriën, verdient een rechtstreekse interpretatie van het gemeten gedrag in termen van anisotrope interactie-tensoren de voorkeur boven de meer gebruikelijke interpretatie in termen van exchange- en anisotropievelden.

M. Date, J. Phys. Soc. Japan 16, 1337 (1961).
K. Kopinga, P.W.M. Borm en W.J.M. de Jonge, Phys. Rev. B10, 4690 (1974).

III

De vermelding in een publicatie, dat een numerieke berekening is uitgevoerd in "double precision", is op zichzelf geen maat voor de doordachtheid, waarmee het betreffende rekenprogramma is opgezet.

D.B. Losee, J.N. McElearny, G.E. Shankle, R.L. Carlin, P.J. Creswell en W.T. Robinson, Phys. Rev. B8, 2185 (1973).

IV

Het specificeren van de electrische belastbaarheid van een luidspreker of luidsprekercombinatie zonder opgave van het rendement - zoals dit door veel fabrikanten en verkooporganisaties wordt gedaan - geeft een onjuiste indruk van de prestaties van een dergelijk systeem. Het verdient derhalve aanbeveling dat dit rendement door consumentenorganisaties in hun beoordeling wordt betrokken.

L.L. Beranek, "*Acoustics*", McGraw-Hill Book Company, New-York (1954).
H.F. Olson, "*Acoustical Engineering*", D. van Nostrand Company, New Jersey (1957).

V

Het uitsluitend toedichten van "vakidiotisme" aan beoefenaren der exacte wetenschappen gaat voorbij aan de sterk vakgerichte of ideologie-bepaalde houding van sommige beoefenaren der niet-exacte wetenschappen; veelal getuigt het ook van een gebrek aan zelfkritiek.

B.A.G.M. Tromp, Intermediair 18, 1 (1976).

VI

Het planten van jonge bomen in een geasfalteerde parkeerplaats in boomspiegels van circa 1 m^2, met de bedoeling om binnen afzienbare tijd schaduw te bieden aan geparkeerde auto's, berust op een misvatting.

J.W. Bakker en M. Uittenbogaard, Groen 10, 306 (1974).
A.E. Kuhlman, Intern rapport L.H. Wageningen (1971).

VII

Het verdient aanbeveling om in gemeenteverordeningen, waarin aan bezitters en/of gebruikers van "geluidswagens" ontheffing wordt verleend van de betreffende artikelen uit de hinderwet, een bepaling op te nemen die verplicht tot stilstand van de geluidswagen, wanneer een gesproken tekst ten gehore wordt gebracht.

VIII

Het is zorgelijk dat het bedrag, dat door sommige jongerensociëteiten in de vorm van subsidies op de activiteiten wordt ontvangen, beduidend lager is dan het bedrag, dat door deze instellingen in de vorm van indirecte belastingen op de barconsumpties aan de overheid wordt afgedragen.

K. Kopinga

Nuenen, 1976.